University of Massachusetts Medical School
eScholarship@UMMS

GSBS Dissertations and Theses | Graduate School of Biomedical Sciences

2014-12-01

rAAV-Mediated Gene Transfer For Study of Pathological Mechanisms and Therapeutic Intervention in Canavan's Disease: A Dissertation

Seemin Seher Ahmed
University of Massachusetts Medical School

Let us know how access to this document benefits you.
Follow this and additional works at: https://escholarship.umassmed.edu/gsbs_diss

Part of the Genetics Commons, Nervous System Diseases Commons, and the Therapeutics Commons

Repository Citation
Ahmed SS. (2014). rAAV-Mediated Gene Transfer For Study of Pathological Mechanisms and Therapeutic Intervention in Canavan's Disease: A Dissertation. GSBS Dissertations and Theses. https://doi.org/10.13028/M25S3R. Retrieved from https://escholarship.umassmed.edu/gsbs_diss/749

This material is brought to you by eScholarship@UMMS. It has been accepted for inclusion in GSBS Dissertations and Theses by an authorized administrator of eScholarship@UMMS. For more information, please contact Lisa.Palmer@umassmed.edu.

rAAV-MEDIATED GENE TRANSFER FOR STUDY OF PATHOLOGICAL MECHANISMS AND THERAPEUTIC INTERVENTION IN CANAVAN'S DISEASE

A Dissertation Presented

By

Seemin Seher Ahmed

Submitted to the Faculty of the
University of Massachusetts Graduate School of Biomedical Sciences, Worcester
In partial fulfillment of the requirements for the degree of

DOCTOR OF PHILOSOPHY

December 1, 2014

Interdisciplinary Graduate Program

rAAV-MEDIATED GENE TRANSFER FOR STUDY OF PATHOLOGICAL MECHANISMS AND THERAPEUTIC INTERVENTION IN CANAVAN'S DISEASE

A Dissertation Presented By

Seemin Seher Ahmed

The signatures of the Dissertation Committee signify completion and approval as to style and content of the Dissertation

_____
Guangping Gao, Ph.D., Thesis Advisor

_____
Anthony Carruthers, Ph.D., Member of Committee

_____
Alonzo Ross, Ph.D., Member of Committee

_____
Miguel Sena-Esteves, Ph.D., Member of Committee

_____
Zuoshang Xu, Ph.D., Member of Committee

The signature of the Chair of the Committee signifies that the written dissertation meets the requirements of the Dissertation Committee

_____
Terence Flotte, Ph.D., Chair of Committee

The signature of the Dean of the Graduate School of Biomedical Sciences signifies that the student has met all graduation requirements of the school

_____
Anthony Carruthers, Ph.D.,
Dean of the Graduate School of Biomedical Sciences

Interdisciplinary Graduate Program
October 21, 2014

Dedication

I would like to dedicate this thesis to my parents Ammi (Hasina) and Abba (Shabbir); my siblings Zeeshan and Zarin, my husband Samyabrata and my daughter Zoya.

ACKNOWLEDGEMENTS

I am extremely grateful to my mentor and thesis advisor Dr Guangping Gao for being an inspiration. His passion for science and hardwork keeps the quest for knowledge exciting. I deeply appreciate his extreme involvement in my progress and constant motivation for getting me to be better at my work and I will be forever in his debt for making me believe in myself and the way I do science. I cannot fathom a more hardworking mentor and I only hope I can become a fraction of the scientist he is.

I want to thank my immediate family for believing in me and standing beside me in all my endeavors. My parents underwent numerous hardships to get me this far and their unwavering belief in me has fueled my passion to strive for the stars. My siblings inspire me to keep improving myself to live up to their expectations. My husband has been the shining star of my life, the sounding board for my troubles and my backbone for any backbreaking struggle. Without him, this journey would have been twice as difficult and half as fun. Finally the love of my life- Zoya, my daughter who is everything I wanted and who makes me realize that I can move the heavens and earth for her and without whose help this thesis would have been completed in half the time. I also want to acknowledge my extended family especially Jana (Safina Rahmat) and Mama (Mohammad Yousuf) for all the love that makes me tick.

A special round of thanks goes to my lab members specially Jun, who taught me a lot and was a shoulder to cry on when the going got tough; Jia, who is my go-to person for fun. I would like to specially thank Qin Su for being my lab mommy. I thank my Gene Therapy Center friends and colleagues who made the lab a fun place to hang out.

My PhD journey would be incomplete without the help and support of all the administrative staff specially Denise and Paula for being there to commiserate when things did not work out and rejoice in times of success.

I cannot thank my parents in law Kanak and Mita Bhaduri enough for being my rock and anchor while I was floundering with an infant. Without them this thesis would have taken twice the time to write. I also want to thank my extended family on both my parents' sides for believing in me. I am grateful to my teacher Dr Swapan Das for nudging me into research. I would also like to thank the huge Indian diaspora in the GSBS and the Worcester County Bengali Association who made life happy and fun.

ABSTRACT

Canavan's Disease is a fatal Central Nervous System disorder caused by genetic defects in the enzyme – aspartoacylase and currently has no effective treatment options. We report additional phenotypes in a stringent preclinical aspartoacylase knockout mouse model. Using this model, we developed a gene therapy strategy with intravenous injections of the aspartoacylase gene packaged in recombinant adeno associated viruses (rAAVs). We first investigated the CNS gene transfer abilities of rAAV vectors that can cross the blood-brain-barrier in neonatal and adult mice and subsequently used different rAAV serotypes such as rAAV9, rAAVrh.8 and rAAVrh.10 for gene replacement therapy. A single intravenous injection rescued lethality, extended survival and corrected several disease phenotypes including motor dysfunctions. For the first time we demonstrated the existence of a therapeutic time window in the mouse model. In order to limit off-target effects of viral delivery we employed a synthetic strategy using microRNA mediated posttranscriptional detargeting to restrict rAAV expression in the CNS. We followed up with another approach to limit peripheral tissue distribution. Strikingly, we demonstrate that intracerebroventricular administration of a 50-fold lower vectors dose can rescue lethality and extend survival but not motor functions. We also study the contributions of several peripheral tissues in a primarily CNS disorder and examine several molecular attributes behind pathogenesis of Canavan's disease using primary neural cell cultures. In summary, this thesis describes the potential of novel rAAV-mediated gene replacement therapy in Canavan's disease and the use of rAAVs as a tool to tease out its pathological mechanism.

TABLE OF CONTENTS

LIST OF TABLES

LIST OF FIGURES

LIST OF ABBREVIATIONS

AAV: Adeno Associated Virus

ABC: Avidin Biotin Complex

ALT: Alanine Aminotransferase

ANOVA: Analysis of Variance

APC: Adenomatous Polyposis Coli

AspNAT: Aspartate N Acetyl Transferase

AST: Aspartate Aminotransferase

BBB: Blood Brain Barrier

CB: Chicken Beta Actin

CD: Canavan Disease

CDC: Complete Differential Count

CFSE: Carboxy Fluorescein Succinimidyl Ester

ChAT: Choline Acetyltransferase

CNS: Central Nervous System

CsCl: Cesium Chloride

CSF: Cerebro Spinal Fluid

DAB: Di-Amidino-Benzidine

DAPI: Di Amidino 2-Phenyl Indole

DNA: Deoxyribonucleic Acid

EB: Evans Blue

ECG: Electrocardiography

eGFP: enhanced Green Fluorescent Protein

ERG: Electroretinography

FACS: Fluorescence-Activated Cell Sorting

GC: Gene Corrected

GFAP: Glial fibrillary Acidic Protein

GPX: Glutathione Peroxidase

GTA: Glyceryl Tri Acetate

H&E: Hematoxylin & Eosin

HPTLC: High Performance Thin Layer Chromatography

Iba1: Ionized calcium binding adaptor molecule 1

ICV: Intra Cerebro Ventricula

IL6: Interleukin 6

iNOS: inducible Nitric Oxide Synthase

IV: Intra Venous

LPS: Lipo Poly Saccharides

MRI: Magnetic Resonance Imaging

miR: micro RNA

MRS: Magnetic Resonance Spectroscopy

MWP: Molecular Water Pump

NAA: N acetyl Aspartic Acid

NAD: Nicotinamide adenine dinucleotide

NADH: Reduced NAD

NMJ: Neuro Muscular Junction

NO: Nitric Oxide

PBS: Phosphate Buffered Saline

PBST: PBS-TritonX-100

PCR: Polymerase Chain Reaction

PRESS: Pont Resolved Spectroscopy Sequence

rAAV: Recombinant AAV

RBG poly A: Rabbit Beta Globin polyA

RNA: Ribonucleic Acid

scAAV: Self complementary AAV

SDS: Sodium Dodecyl Sulphate

SOD: Superoxide Dismutase

ssAAV: Single stranded AAV

TEM: Transmission Electron Microscope

PREFACE

Portions of this dissertation appear in separate publications:

Zhang H, Yang B, Mu X, **Ahmed SS**, Su Q, He R, Wang H, Mueller C, Sena-Esteves M, Brown R, Xu Z, Gao G. (2011). Several rAAV vectors efficiently cross the blood-brain barrier and transduce neurons and astrocytes in the neonatal mouse central nervous system. Molecular Therapy Aug; 19(8):1440-8 [21610699].

Yang B, Li S, Wang H, Guo Y, Gessler DJ, Cao C, Su Q, Kramer J, Zhong L, **Ahmed SS**, Zhang H, He R, Desrosiers RC, Brown R, Xu Z, Gao G. (2014) Global CNS transduction of adult mice by intravenously delivered rAAVrh.8 and rAAVrh.10 and nonhuman primates by rAAVrh.10. Molecular Therapy Jul; 22(7):1299-309. [PMID: 24781136]

Ahmed SS, Gao G. (2014) Making the White Matter Matters: Progress in Understanding Canavan's Disease and Therapeutic Interventions Through Eight Decades [Review accepted at Journal of Inherited Metabolic Diseases Reports; in press]

Ahmed SS, Schattgen S, Sikoglu ME, Su Q, Li J, Hampton TG, Fitzgerald K, Kaspar B, Matalon R, Gao G. CNS-restricted gene delivery using rAAVs rescues lethality but not mobility defects suggesting peripheral tissue involvement and inflammation-mediated pathology in CD mice (manuscript under preparation)

Ahmed SS, Li H, Cao C, Sikoglu EM, Denninger AR, Su Q, Eaton S, Liso Navarro AA, Xie J, Szucs S, Zhang H, Moore C, Kirschner DA, Seyfried TN, Flotte TR, Matalon R, Gao G. (2013) A single intravenous rAAV injection as late as P20 achieves efficacious and sustained CNS Gene therapy in Canavan mice.Molecular Therapy Dec;21(12):2136-47 [PMID: 23817205]

CHAPTER I: INTRODUCTION

The following chapter contains modified parts of the manuscript:

Ahmed SS, Gao G. (2014) Making the White Matter Matters: Progress in Understanding Canavan's Disease and Therapeutic Interventions Through Eight Decades [Review accepted at Journal of Inherited Metabolic Diseases Reports; in press]

The review was written by me and was corrected by Dr Guangping Gao

CHAPTER I: Introduction

Canavan Disease

Canavan disease [CD] is a fatal pediatric leukodystrophy in which the Central Nervous System [CNS] white matter shows progressive spongy degeneration. It results from deficiency of aspartoacylase [N-acetyl-L-aspartoacylasertate amidohydrolase; EC 3.5.1.15] (Matalon et al., 1988), an enzyme required for catabolism of N-acetylaspartate (NAA), the second most abundant amino acid derivative in the CNS.

Clinical Presentation

The first CD patient was reported by Myrtelle Canavan (Canavan, 1931) describing a prominent enlargement of the head and cerebral and cerebellar spongy degeneration as "Schilder's encephalitis periaxialis diffusa" which was later acclaimed as a clinical entity (Van Bogaert L, 1949). Three clinically distinct variants exist (Adachi et al., 1973) namely:

- Congenital form: severe symptoms recognizable in the first few weeks of life,
- Infantile form: most common form where symptoms appear by 6 months of age
- Juvenile form: mildest form in which symptoms manifest by age 4 or 5.

These early reports included a comprehensive description of the clinical and pathological features of the disease and the predilection for its occurrence in Ashkenazi Jews of Eastern European extraction. Currently however a growing number of non-Jewish patients have been identified worldwide (Elpeleg and Shaag, 1999; Mizuguchi et

al., 2009; Stenson PD, 2003; Unalp et al., 2008; Zeng et al., 2006a; Zeng et al., 2006b; Zhang et al., 2010).

Patients show vacuolization in the subcortical white matter (which becomes gelatinous), edema and demyelination and thin delicate meninges. Swollen cortical protoplasmic astrocytes containing membrane-bound cytoplasmic vacuoles, elongated mitochondria with distorted cristae, degraded axonal medullary sheaths and a prominent increase in protoplasmic astrocytes characterize the diseased brain. There also seems to be a significant loss of proteolipid protein and lipids in the white matter (Beaudet, 2001).

Clinical manifestations include weak neck muscles, loss of muscle tone, severe psychomotor and mental retardation, seizures, NAAduria, blindness and megalencephaly.

Characterization of the enzyme: Aspartoacylase

CD was described as an enzyme deficiency disease (Matalon et al., 1988) when NAA-rich patient plasma and urine samples were incubated with normal fibroblasts extracts and subsequently showed increased aspartate levels suggesting a block in NAA catabolism in patients. Intensive genetic studies identified human aspartoacylase cDNA from kidney based on sequence information from bovine aspartoacylase. The gene was localized to 17p13-ter, comprises 6 exons encoding a 313 amino acid long polypeptide chain with a molecular mass of 36kD (Kaul et al., 1993). Aspartoacylase deacetylates NAA (Birnbaum et al., 1952) with a K_m of 8.5 x 10^{-4} mol/L and V_{max} of 43000 nmol/min per mg of protein (Kaul et al., 1991). Isolation of the aspartoacylase cDNA sequence led to identification of causative mutations for CD and hence was a landmark in the field as it made molecular diagnosis and gene therapy of CD possible (Kaul et al., 1994). Currently,

>54 mutations are associated with Canavan disease (Hershfield et al., 2007) with new mutations being identified on a regular basis. Transient transfection of COS cells shows that only some missense mutations in the ASPA gene have negligible aspartoacylase activity (Hershfield et al., 2007).

Genetic analyses have identified two major CD mutations in Ashkenazi Jewish patients namely a missense mutation in codon 285 [exon VI] causing substitution of glutamic acid to alanine. It accounts for 83.6% mutations identified in 104 alleles from 52 unrelated Ashkenazi Jewish patients (Kaul et al., 1994). Another one is a nonsense mutation on codon 231 [exon V] which converts tyrosine to a stop codon, found in 13.4% of the alleles from Jewish patients (Kaul et al., 1994). Among non-Jewish patients, the mutations are more diverse, the most common being a missense mutation substituting alanine for glutamic acid in codon 305. This mutation was observed in 35.7% of the 70 alleles from 35 unrelated non-Jewish patients (Kaul et al., 1994). The diverse mutations associated with CD limit the use of DNA analysis for prenatal diagnosis to known carriers with previously described mutations are among those that are known. Patients seem to follow a similar course of disease irrespective of residual aspartoacylase activity. For instance, children carrying the Tyr231X mutation that has no residual activity cannot be clinically distinguished from those with mutation Glu285Ala that has some residual enzyme activity. Patients homozygous for the most common mutation Ala305Glu, with no residual enzyme activity, have a clinical course similar to patients with the two Jewish mutations (Matalon, 1997). A patient heterozygous for mutations Glyl23Glu, and Ala305Glu was phenotypically a severe Canavan patient in spite of being a double

heterozygote with residual aspartoacylase activity of 26.9% (Matalon, 1997). Interestingly, life expectancy is variable in patients with Canavan disease with the same genotype (Matalon and Michals-Matalon, 1999) . Since aspartoacylase has been structurally resolved (Le Coq et al., 2006), correlation between the location of disease-specific mutations and functional protein domains could allow an insight in mutational analysis. For example, ATRX mutations cause a broad spectrum of X-linked mental retardation syndromes; however, major urogenital abnormalities are associated with truncating mutations at the C-terminal part of the protein (Gibbons and Higgs, 2000). Again, mutations in the plant homeodomain (PHD)-like domain are associated with more severe phenotypes than mutations in the helicase domain (Badens et al., 2006). If the disease-causing mutations are mapped onto functional substructures of proteins, a clearer picture of genotype-phenotype correlations may emerge.

Studies reported cellular localization of aspartoacylase in the white matter of the corpus callosum and cerebellum along with the thalamus (Klugmann et al., 2005). Another study showed that the staining was more intense in large white matter bundles (e.g., corpus callosum, anterior commissure, optic chiasma, corticospinal tract) where oligodendroglia are known to be present in greater density than in grey matter regions (Kirmani et al., 2002). Aspartoacylase was detected by immunohistochemistry in oligodendrocytes and non-reactive microglia but not neurons (Madhavarao et al., 2004). Neurons were largely unstained in the forebrain, although a few large reticular and motor neurons and many ascending and descending neuronal fibers were moderately stained in the brainstem and spinal cord. Most of the staining was confined to the cell body and

proximal processes of oligodendrocytes (Klugmann et al., 2005). Co-localization studies with labeled lectins indicated that aspartoacylase is also present in microglial cells (Madhavarao et al., 2004). Studies showing aspartoacylase activity restricted to the cytoplasm (Kirmani et al., 2002; Klugmann et al., 2003) and the nucleus (Hershfield et al., 2006) have implied a specific subcellular localization, but this remains to be established definitively.

Characterization of the substrate: N acetyl aspartic acid (NAA)

NAA is an abundant [5–10mM] amino acid derivative in the vertebrate CNS with a molecular mass of 175.1 Da. Most neuropsychiatric disorders like schizophrenia show a decrease in NAA levels (Mondino M, 2013), however CD is one of the few diseases along with sickle cell disease (Steen RG, 2005) that show high levels. It averages 5.7 μmol/g of brain in eight mammalian species with a range of 1.6-10.08 μmol/g (Birken and Oldendorf, 1989). NAA is generally absent from the cerebrospinal fluid (CSF) (Tallan et al., 1956) but present in very high amounts in the aneural and avascular lenses (Baslow and Yamada, 1997). Absence of functional aspartoacylase creates a pool of NAA in the brain and also results in NAA aciduria. NAAduria is a reliable and specific biochemical index for CD (Matalon et al., 1988). Additionally CD patients show very high amounts of NAA in their blood and CSF (Matalon et al., 1988).

NAA serves as a marker of neuronal integrity as high levels indicate brain injury and disease; however, the biological function of NAA remains enigmatic. It is metabolically compartmentalized; being exclusively produced in neuronal mitochondria

by L-aspartate N-acetyltransferase (Asp-NAT) [EC 2.3.1.17] (Ariyannur et al., 2010); and metabolized in oligodendrocytes (Madhavarao et al., 2003) by aspartoacylase.

Animal Models

Several animal models have been reported showing symptoms similar to CD notably foxes (Hagen and Bjerkas, 1990; Hagen et al., 1990), goats (Obermaier et al., 1995) dogs (Kleiter et al., 2011; Zachary and O'Brien, 1985) and a naturally occurring mouse (Azzam et al., 1984); however aspartoacylase activity in the latter was not studied. Studies on Canavan disease were initially performed on two rodent models - the naturally existing Tremor rat (Kitada et al., 2000) and an artificially engineered Canavan Mouse (Matalon et al., 2000).

The tremor rat is a naturally occurring mutant isolated from an inbred Kyoto:Wistar colony that has a large deletion (200kb) spanning 4 genes including the aspartoacylase gene, exhibits absence-like seizures and shows spongiform degeneration in the CNS (Kitada et al., 2000). Matalon et al genetically engineered a mouse model (ASPAKO or CD mouse) that had a specific 10bp deletion in exon IV of the aspartoacylase gene (Matalon et al., 2000). Additionally, the phenotype and biochemical characteristics of the homozygous knock-out mice indicate that it is a stringent preclinical model for evaluating gene therapy for congenital CD and for studying the role of NAA and aspartoacylase in the brain.

Newer studies have created two interesting models one with a single point mutation in Nur7 (Traka et al., 2008) and the other - a knock in model (Mersmann et al., 2011) making development of therapeutic modalities much easier. The Nur7 mouse

model shows spongy neurodegeneration, vacuolization and NAA accumulation like patients however myelin rich regions in the brain appear normal (Traka et al., 2008). LacZ knock-in mice have a targeted deletion in aspartoacylase and have a mild phenotype (Mersmann et al., 2011). These mice are not severely affected and have a longer lifespan than the CD mice and could serve as a model for the infantile form of CD (Mersmann et al., 2011).

Theories behind the Molecular Etiology of CD

A comprehensive investigation of aspartoacylase regulation in oligodendrocytes is essential to understand CD pathogenesis because the specific connection between aspartoacylase deficiency and the failure of proper CNS development and myelination remains unclear. Listed here are existing hypotheses that attempt to offer an explanation.

Molecular Water Pump and Osmolyte Imbalance Theory

The adult brain is a major source of metabolic water and uses ~20% of the daily caloric intake. Additionally, the two major CD symptoms- increased CSF pressure and intramyelinic edema, being hallmarks of profound fluid imbalance, suggest the existence of an efficient Molecular Water Pump (MWP) (Baslow, 1999).

The theory propounds that NAA accumulation could result in osmolytic imbalance in the brain since it is similar to taurine (Taylor DL, 1995), an important CNS osmolyte. Furthermore, NAA has two juxtaposed anabolic (neurons) and catabolic (oligodendrocytes) compartments that suggest a mechanical framework for a MWP in the brain. The MWP involves the synthesis and facilitated diffusion of a hydrated intracellular osmolyte [NAA with its ion-dipole and dipole-dipole associated water] down

its gradient. At maturity, intraneuronal NAA concentration is ~10±14mM while the interstitial concentration is only 80-100µm (Sager TN, 1997), indicating a large outward-directed transport gradient. The osmolyte [NAA] is rapidly hydrolyzed [by aspartoacylase to form aspartate and acetate] to maintain tissue-ECF osmotic balance [in the periaxonal space]. The metabolic products are dehydrated as they are once again taken up by an active transport mechanism to complete the cycle (Baslow, 1999).

Presumably, the acetate is taken up by astroglial processes at axon internodes and synapses (Tsacopoulos M, 1996) recycling the hydrolyzed products to produce more NAA [Figure 1.1].

Paranodal seals that connect oligodendrocytes to axons could serve as the site for the NAA inter-compartmental bidirectional cycle (Baslow, 1999). Aspartoacylase deficiency would lead to accumulation of NAA and water and resulting in an increased hydrostatic pressure. This could loosen the tight junctional seals separating interlamellar spaces from the extracellular periaxonal and parenchymatous spaces resulting in intramyelinic edema (Hirano, 1981). Subsequent demyelination could create vacant spaces within the white matter leading to the spongy brain phenotype.

Figure 1.1 Molecular Water Pump Theory. NAA is synthesized within neurons by the Aspartate-N-Acetyl Transferase (AspNAT) creating a large concentration gradient with the interstitial space. NAA and associated dipole water accumulate therein. Under normal conditions, aspartoacylase metabolizes the NAA and removes it. Absence of aspartoacylase results in accumulation of NAA and its associated water causing intramyelinic edema.

Figure 1.1 Molecular Water Pump Theory.

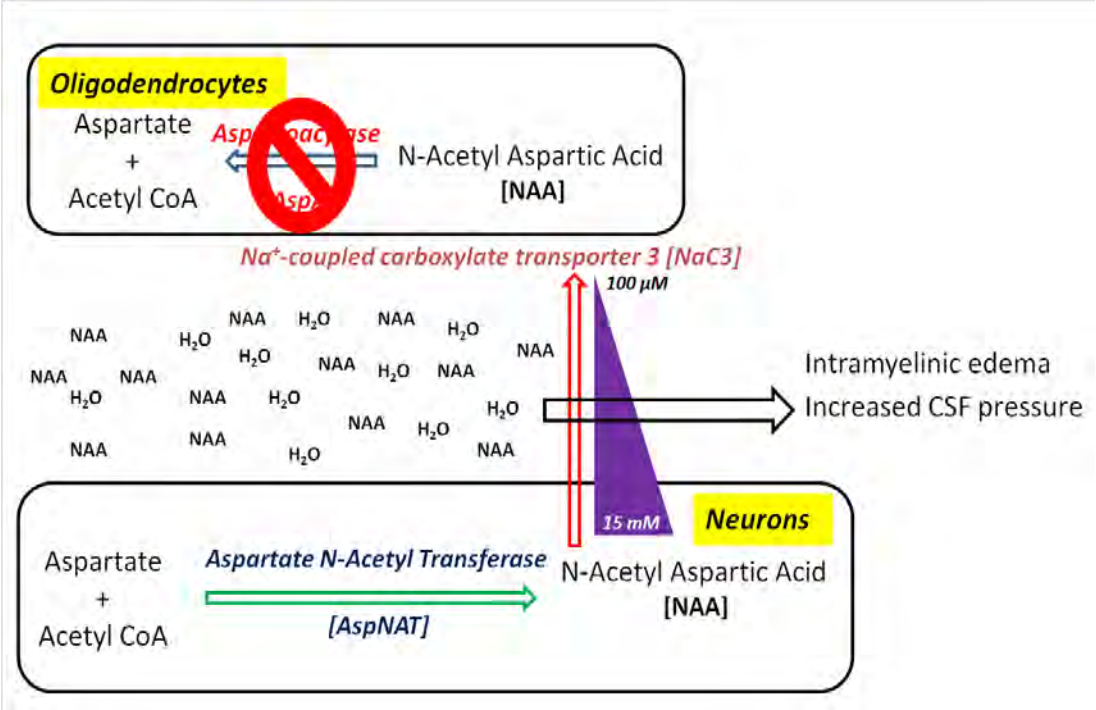

Dysmyelination Theory

NAA-derived acetyl groups were shown to be involved in fatty acid synthesis as acetyl-labeled NAA injection into rats resulted in maximum fatty acid incorporation just before and during myelination (D'Adamo AF Jr, 1968). Later studies indicated that NAA was transferred from the axon to myelin and NAA-derived acetate was incorporated into myelin lipids (Chakraborty et al., 2001).

This theory proposes that deficiency of NAA-derived acetate decreases the synthesis of myelin-associated lipids in CD leading to dysmyelination (Madhavarao et al., 2005) [Figure 1.2]. Additionally, temporal correlations have been shown between developmental increases in aspartoacylase activity and myelination (Bhakoo et al., 2001). Similar to human CD patients, brain acetate levels are reduced by ~80% in CD mice during peak postnatal myelination while myelin lipids such as cerebrosides and sulfatides are reduced (Ahmed SS, 2013; Madhavarao et al., 2005). These data speculate that NAA-derived acetate is essential during postnatal myelination to supply substrate for some proportion of the lipids that make up myelin sheaths in the developing brain.

Studies on the Nur7 KO mouse (Traka et al., 2008) suggest that spongy degeneration is not dependent on disrupted myelin synthesis. Even though Nur7 mice are heterozygous for a null allele of a galacto-lipid synthesizing enzyme which could further reduce brain cerebroside content, they do not show more severe myelin pathology implicating additional mechanisms in the pathophysiology of CD (Madhavarao et al., 2009). Animal models lacking functional aspartoacylase show abundant albeit

Figure 1.2 Dysmyelination Theory. Under normal conditions, aspartoacylase metabolizes NAA to provide acetate for myelin synthesis. Deficiency of aspartoacylase causes inadequate myelin synthesis leaving gaps in the interstitium where normal sheaths would have existed causing vacuolation.

Figure 1.2 Dysmyelination Theory.

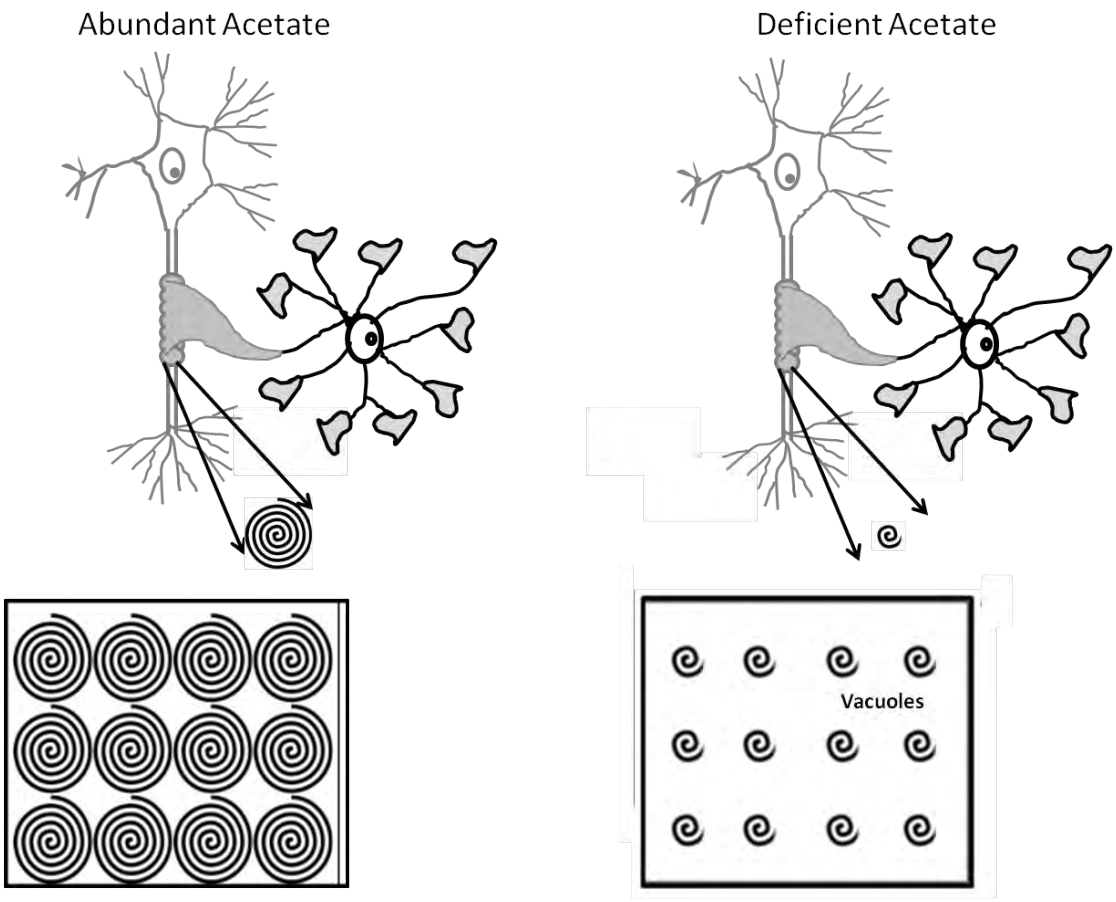

structurally abnormal myelination probably because the initial stages of myelinogenesis have redundant pathways (Wang et al., 2009).

Compromised Epigenetic Regulation of Oligodendrocyte Differentiation

Studies on oligodendrocyte maturation have highlighted the importance of epigenetic control in differentiation (Copray S, 2009). Acetate is derived from NAA in oligodendrocytes (Chakraborty et al., 2001) and this acetate is probably important for histone acetylation reactions that regulate chromatin structure and gene transcription. Dramatic reduction of acetate resulting from aspartoacylase deficiency could impact histone reactions required for epigenetic gene regulation preventing normal differentiation leading to oligodendrocyte cell death and neuronal injury possibly contributing to vacuole formation.

Protein Misfolding Theory

Cells like oligodendrocytes, which have active protein secretory pathways, are sensitive to disorders of protein misfolding. Acetyl CoA is an important substrate for acetylation and deacetylation of nascent polypeptide chains in the endoplasmic reticulum [ER] required for stabilization and correct folding of proteins (Spange S, 2009). Reduced acetyl CoA availability due to aspartoacylase deficiency could negatively impact protein folding and stabilization, targeting proteins for degradation. Oligodendrocytes are highly susceptible to ER stress associated with disruptions in protein synthesis and trafficking (Lin W, 2009). In the CD mouse, a severe loss of myelin basic protein and PLP/DM20

proteolipid proteins has been observed combined with a decrease in myelinated fibers (Kumar et al., 2009).

Oxidative Stress Theory

Intracerebroventricular administration of NAA induces seizures in normal rats, probably by neuronal overexcitation (Akimitsu T, 2000); further, tardive dyskinesia patients also have significantly higher CSF concentrations of NAA like CD patients (Tsai G, 1998). Animal studies show that epileptic seizures result in free radical production and oxidative damage to cellular proteins, lipids and DNA (Bruce AJ, 1995) implicating oxidative stress as one of the possible causes of neurological impairment. Recent work suggests that chronic mitochondrial oxidative stress and resultant dysfunction can render the brain more susceptible to epileptic seizures (Patel, 2004). Hence it seems that there is a role for oxidative stress both as a cause and a consequence of epileptic seizures.

NAA may promote oxidative stress by reducing non-enzymatic antioxidant defenses and stimulating oxidative damage to both lipids and proteins by enhancing reactive species in cerebral cortex [Figure 1.3]. In a study, NAA was found to inhibit the functions of catalase and glutathione peroxidase (GPX) indicating impaired detoxification of hydrogen peroxide but it had no effect on superoxide dismutase [SOD]. Acute administration of NAA also enhanced levels of hydrogen peroxide *in vitro* which could possibly be involved in the progression of the characteristic neurodegeneration in CD (Pederzolli CD, 2007). Though these results could not be extrapolated to humans, they do reveal probable mechanisms since the oxidative stress parameters occurred with concentrations of NAA (~4fold higher) observed in plasma and CSF of patients affected

by CD (Tsai and Coyle., 1995). Based on the supposition that NAA may promote oxidative stress *in vitro* and *in vivo* both by enhancing reactive species and diminishing antioxidant defenses, administration of antioxidants, especially vitamins E and C, could be considered as a potential adjuvant therapy for patients affected by CD (Pederzolli CD, 2007).

A previous study linked NAA accumulation to nitric oxide [NO] toxicity as it upregulates inducible nitric oxide synthase [iNOS] and stimulates neuronal and endothelial nitric oxide synthase (Surendran, 2009). Increased NO levels lead to disturbances in DNA structure and enhance protein interaction (Lee DH, 2007). Discrepancies in the molecular weight of aspartoacylase when prepared using different methods (Kaul et al., 1993) suggest that it may dimerize based on its concentration. It is possible that upregulation of NO synthase as a direct result of NAA accumulation may nitrosylate aspartoacylase causing it to dimerize. This hypothesis proposes that NAA upregulation and aspartoacylase malfunction could be cyclically linked.

Figure 1.3 Oxidative Stress Theory. Accumulation of NAA in the interstitium due to the absence of aspartoacylase gives rise to Reactive Oxygen Species (ROS) that cause inflammation and result in vacuolation and degeneration of white matter.

Figure 1.3 Oxidative Stress Theory.

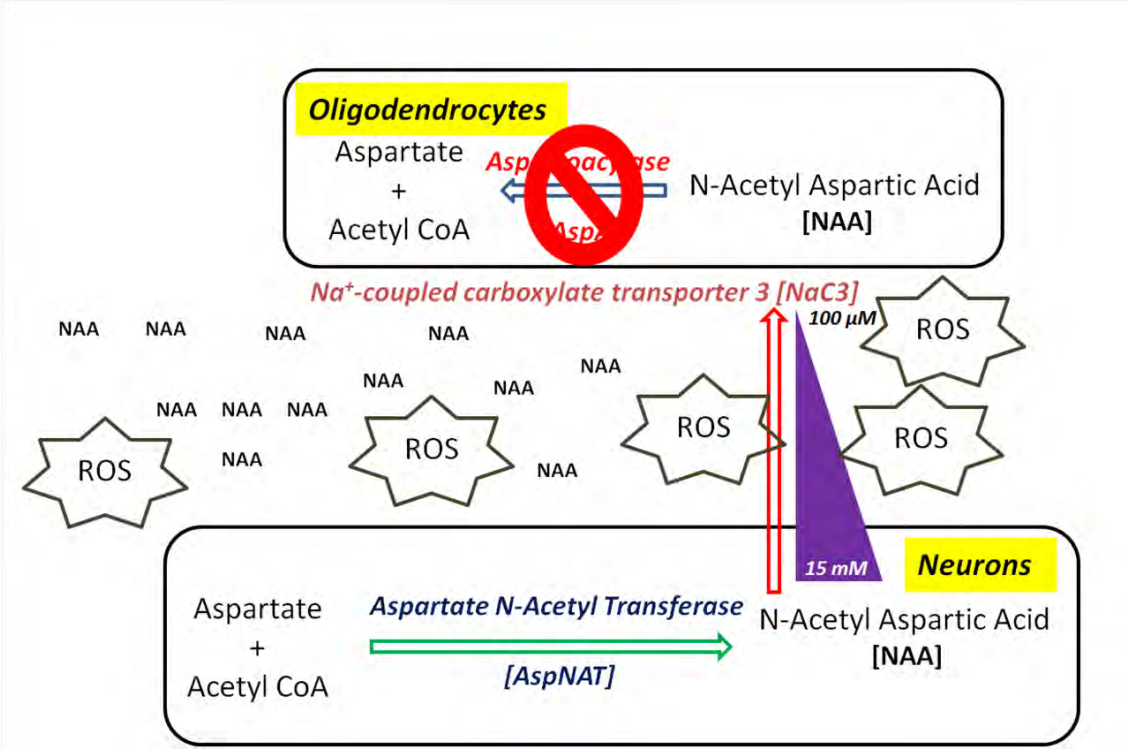

Palliative Measures: Past and present

CD was described as one of the few neurological diseases which manifests increased NAA levels in the brain; most other neurological diseases like schizophrenia show low NAA levels (Mondino M, 2013). Since an increasing number of substances can affect NAA levels in the brain (Baslow and Resnik, 1997); slowing down the anabolic portion of the NAA cycle using pharmaceuticals may allow the existing, albeit enzyme-deficient oligodendrocytes to produce a stable myelin sheath and restore neurological function.

A large number of preclinical proof-of-concept studies have been performed on various CD animal models (described above) making development of therapeutic modalities much easier. Though currently the patients are mostly supported by palliative measures; existing treatment modes focus on different aspects of the disease phenotypes and are described below.

Managing symptoms in the clinic

Most of the palliative measures for patients of Canavan's disease follow the care provided for patients of other pediatric neurodegenerative diseases (Hunt and Burne, 1995). Current palliative measures for Canavan patients with respiratory issues include suction and cough assist machines to clear secretions and mucous from the mouth, throat, nose and upper lobes of the lungs; the Vesta system for airway clearance and oxygen concentrators to provide a continuous flow of oxygen for easy breathing.

Hypotonia being a major Canavan symptom requires positioning equipment which may include foam supports, feeder seats, specialized strollers and bath chairs to

help patients with their positioning needs. Feeding pumps are also used to assist in dispensing liquid nutrients at predetermined rates for feeding. Nebulizers help to administer medication as aerosols for these patients.

Symptomatic treatment of disease

The earliest human clinical trials on CD patients used acetazolamide to reduce water concentration and NAA levels in white matter for a period of 5 months. The drug reduced intracranial pressure, but did not reduce water content or NAA levels (O. Bluml, 1998). A ketogenic diet increased levels of β-hydroxybutyrate in the brain but did not affect the elevated levels of NAA (Novotny EJ Jr, 1999). These treatment strategies were primarily targeted to alleviate edema; however there was little to no benefit for the patients.

In recent years, intraperitoneal injections of lipoic acid (that can cross the blood brain barrier,BBB (Samuel S, 2005)) have also been tried in preclinical studies using tremor rats, the naturally occurring animal model for CD (Pederzolli CD, 2007) based on the fact that NAA induces oxidative stress in the CNS. The encouraging results suggest that this might be a good therapeutic approach for symptomatic treatment.

Addressing the Missing Metabolite by Dietary Supplementation

Dietary supplementation of acetate in newborn patients was proposed as a therapeutic for CD since the primary pathogenesis is postnatal and deficiency of aspartoacylase and acetate are concurrent (Madhavarao et al., 2009). This group reported phenotypic improvements in myelin galactocerebroside content and brain vacuolation and also showed a partial reversion in motor dysfunction in GTA-treated tremor rats over

a course of 4 months (Madhavarao et al., 2009). In conclusion, dietary supplementation may not totally alleviate an inherent genetic metabolic disorder but definitely offers partial symptomatic alleviation. Clinical translation of GTA to human infants showed no significant side effects or toxicity but showed no motor improvement (Segel R, 2011).

A recent study proposed dietary triheptanoin supplementation in Nur7 mice to support fatty acid synthesis and TCA cycles and improve the redox status in diseased animals. It showed phenotypic improvements suggesting that the underlying pathological mechanism of CD may be a combination of several factors (Francis et al., 2013).

Addressing the Elevated Substrate by Neuroprotective Strategies

Neuroprotective strategies may be needed to counteract neurological damage caused by oxidative stress possibly by the accumulated NAA. Intra-peritoneal lithium administration caused a significant drop in brain NAA levels in wild type rats (O'Donnell T, 2000) and tremor rats (Baslow et al., 2002). After 1 year of treatment in patients, NAA levels in both urine and brain were decreased. Patients showed improved alertness and visual tracking; however axial hypotonia and spastic dysplegia were unaffected (Solsona MD, 2012). Pharmacologically, lithium is neuroprotective for dementia patients (Kessing LV, 2008) possibly by reducing expression of pro-apoptotic proteins (Chen RW, 1999) and increasing the levels of anti-apoptotic proteins (Chang YC, 2009).

A complete inhibition or even a significant reduction in NAA production may thus be a viable option in controlling demyelination and improving the quality of life in CD patients. However solely controlling brain NAA levels for CD (Assadi et al., 2010)

may not be a highly effective therapeutic strategy since the NAA system is not universally present in neurons (Baslow, 1997).

Addressing the Enzyme deficiency by Enzyme Replacement

Using enzyme replacement as a therapeutic for neurological disorders has been difficult because of the challenging blood–brain-barrier. Surface lysyl groups of human aspartoacylase were modified through PEGylation to decrease immune response and increase circulation half-life with the intention of treating CD patients (Zano et al., 2010).

Most of these modalities as CD therapeutics showed good tolerance but did not cause any significant improvement in the quality of life in the patients. However, as CD is a monogeneic defect with pathology being most evidently localized in the CNS, it presents an attractive target for gene therapy.

Gene Therapy for Canavan Disease

Gene therapy is a promising area of experimental medicine wherein supplementation or alteration of DNA is used as a therapeutic in organisms to alleviate a genetic disease. The most common approach involves replacement of a non-functional or absent gene by an artificial cassette that would restore functionality of the gene. Therapeutic DNA is packaged into a "vector" that delivers DNA in cells after which the cellular machinery takes over and produces the deficient protein to correct the disease.

Non Viral Gene therapy

Non-viral gene delivery system is a conventional approach for gene therapy; however it is limited by efficiency of gene transfer. Direct injections of plasmids (naked or in complexes) are also inefficient because of limited uptake due to aggregate formation, low rates of diffusion, endotoxin contamination and transient expression necessitating improvements in design (O'Mahony et al., 2013). Therefore, there are ongoing efforts to achieve safe, efficient and specific non-viral vectors which match the efficacy of viruses.

The first clinical trial for CD used a non-viral gene transfer technique with intracerebroventricular injections of a non-aggregating lipid plasmid formulation LPD. This was composed of a recombinant plasmid with a condensing agent [poly-L-lysine or protamine sulfate] and a liposomal formulation [DC-CHOL/DOPE] on two Canavan patients (Leone et al., 2000). The study established that the gene transfer technique worked and was safe but differences in the responses of the patients made it difficult to conclude if the gene therapy was successful.

Viral Gene therapy

Viral vectors have been widely used as gene delivery systems as they can introduce their genetic material into recipient cells. Desired properties of a viral vector include replication deficiency, non-immunogenicity, non-toxicity and the ability to deliver its genetic material to the nucleus of a target cell (Ruitenberg et al., 2002). Gene therapy viral vectors mediating specific delivery into the CNS range in capacity from 4.5kb to 150kb (Davidson and Breakefield, 2003).

Preclinical viral gene therapy studies involved stereotactical adenovirus-mediated delivery of aspartoacylase in tremor rats that showed reduction of seizures (Seki et al., 2002) and AAV2 mediated delivery that showed significant improvement in motor abilities and elevation of aspartoacylase expression (McPhee et al., 2005).

One of the more popular viral vector choices for CD gene therapy is the Adeno associated virus (AAV) that is described in more detail in the next section.

Adeno-Associated Virus (AAV)

Adeno-associated virus (AAV) is one of the smallest nonpathogenic mammalian viruses discovered as a contaminant of adenovirus culture resulting in its name (Mayor et al., 1965). It belongs to the family *Parvoviridae* in the genus *Dependovirus* (as it depends on a helper virus e.g. adenovirus for replication) (Daya and Berns, 2008).

Structure

The wildtype virus is a 4.7kb non-enveloped single stranded DNA (ssDNA) virus reported to be 25nm in diameter with a molecular weight of $1.4x10^6$ Da. It is characterized by 2 open reading frames (ORFs) coding for a total of 7 viral proteins

important for replication and capsid production respectively. The left ORF encodes 4 Rep proteins Rep78, Rep68, Rep52 and Rep40 produced as unspliced and spliced transcripts using the P5 and P19 promoters respectively. They are regulatory proteins that are important in production of single stranded viral DNA for packaging. The right ORF encodes three viral capsid proteins from the P40 promoter namely VP1 (87kD), VP2 (72kD) and VP3 (62kD). 60 viral capsid proteins are produced in a defined ratio that has been variously described as 1:1:10 (Vandenberghe et al., 2009) and 1:1:18 (Opie et al., 2003) to form an icosahedral structure. The 2 ORFs are flanked by 145bp inverted terminal repeats (ITRs) where the first 125 nucleotides being palindromic can fold on themselves to form a T-shaped hairpin. The unpaired 20 bases constitute the D sequence (Wang et al., 1997). The hairpin helps in DNA replication in the presence of a helper virus by serving as a primer for second strand synthesis. The ITRs also contain Rep binding elements and a terminal resolution site that are critical for AAV replication. Additionally, ITRs are essential for AAV genome packaging, transcription, negative regulation under nonpermissive conditions and site-specific integration (Daya and Berns, 2008).

There are several rate determining factors that contribute to efficiency of transduction including entry into the nucleus and uncoating of DNA from the capsid (Sipo et al., 2007; Thomas et al., 2004). However, the most important rate limiting step involves conversion of the single-strand DNA (ssDNA) vector genome into double-stranded DNA (dsDNA) prior to gene expression (Ferrari et al., 1996; Fisher et al., 1996).

This critical step can be entirely circumvented by packaging both strands as a single molecule through the use of self-complementary AAV (scAAV) vectors [Figure 1.4].

scAAV vectors can be packaged like conventional AAV genomes, when the two halves of the ssDNA molecule fold and base pair to form a molecule of half the length (McCarty et al., 2003). In order to enhance vector transduction efficiency and accelerate gene expression, the terminal resolution site (trs) from one end was deleted thus preventing the initiation of replication. These constructs generated single-stranded, inverted repeat genomes, with a wt TR at each end, and a mutated TR in the middle. After uncoating, the viral DNA folds through intramolecular base pairing within the mutant TR, which then proceeds through the genome to form a double-stranded molecule. As conversion from single to double strand does not depend on vector concentration or host cell assisted DNA replication, scAAV vectors result in efficient and fast transgene expression even though this measure further restricts the transgene size in an already small vector.

Figure 1.4 Advantages of self complementary rAAVs over single stranded AAVs. ssAAVs show delayed expression since they require intermolecular hybridization as either a plus or a minus strand is packaged into a capsid. scAAVs on the other hand require intramolecular hybridization that speeds up the time of gene expression.

Figure 1.4 Advantages of self complementary rAAVs over single stranded AAVs.

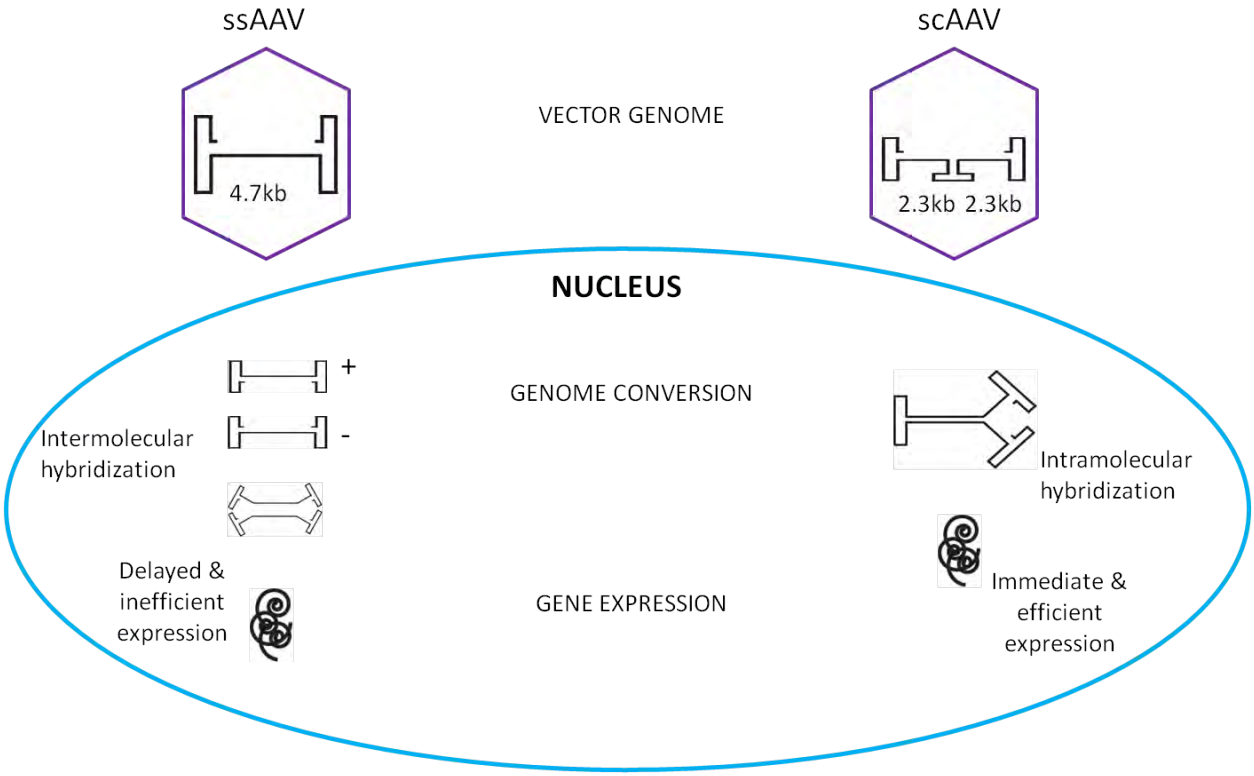

Preclinical Applications

AAVs are almost completely nontoxic after CNS delivery in non-preexposed mammals (Afione et al., 1995; Samulski RJ, 1999) and have sustained gene expression in non-dividing cells (Samulski RJ, 1999). Recombinant AAVs are gutted versions that do not contain any coding sequences from the naturally occurring viruses but carry a complete transcription cassette with the gene of interest flanked by ITRs. rAAVs are a preferred vector of choice for a lot of CNS gene therapy applications as they mediate persistent and safe neuronal transduction (Kaplitt et al., 1994). Such CNS transduction is quite consistent through several species of mammals like mice, cats, dogs and monkeys (Asokan et al., 2012; Cotugno et al., 2011; Foust et al., 2010; Gagliardi and Bunnell, 2009; Gray et al., 2011). Clinical trials using rAAV are ongoing for different neurological diseases (Asokan et al., 2012), and available data suggests that these vectors are capable of mediating long-term stable gene expression in the human brain as well (Hwu et al., 2012; Muramatsu et al., 2010).

AAV2 was the first serotype to be successfully used for gene transfer (Hermonat PL, 1984); however, it is has limited applications in CNS directed therapy since the brain is refractory to systemic delivery of rAAV2. This is due to the presence of the BBB (which physically excludes foreign molecules and microorganisms based on size, charge, and lipid solubility from the blood to the brain) efficiently blocking rAAV entry into the CNS (Zlokovic, 2008) and rendering it incapable of marked therapeutic benefit for global neurological disorders like CD which have no cure to date.

Need for Different Serotypes

AAV2 vectors sparked a widespread interest in the gene therapy field since they were able to effect a persistent transgene expression, apparent lack of pathogenicity and an affinity for multiple organs like the liver (Snyder et al., 1997), eye (Guy et al., 1999), intestine (During et al., 1998) and muscle (Pruchnic et al., 2000). Recombinant AAV2 vectors have been used therapeutically in preclinical studies for a wide variety of diseases (Flotte et al., 1993; Gasmi et al., 2007) and several clinical trials with hundreds of patients have been completed or initiated (Mingozzi and High, 2011). Although the safety and efficacy of AAV2 vectors for *in vivo* gene transfer have been widely acclaimed, research suggests that the transduction efficiency of AAV2 vectors in organ-specific transgene expression leaves a lot to be desired (Nakai et al., 2002; Zabner et al., 2000). Another important consideration is the negative effect of neutralizing antibodies in the serum on AAV transduction efficiency (Janelidze et al., 2014). This alone would jeopardize any application requiring repetitive therapeutic administration. Moreover, since the transduction efficiency of AAV is substantially dependent on capsid structure, it generated a widespread interest in the identification, characterization and isolation of additional AAV capsids. A lot of research is also focused on modifying vector genomes as well as capsid proteins to improve the transduction efficiency of AAV2-based vectors.

AAV capsid determines biodistribution and transduction efficiency in addition to being the focal point of contact between the therapeutic gene and the host (Grimm and Kay, 2003; Grimm et al., 2006). Research has indicated that hybrid vectors generated by cross packaging the genetic backbone of AAV2 with the capsid component of other AAV

serotypes are more efficient than the natural variants in transducing organs and tissues suggesting the need for studying serotype-specific vector distribution (Rabinowitz et al., 2002). A case in point is that AAV4 and 5 target ependymal cells in the CNS at a higher efficiency compared to AAV2 (Davidson and Breakefield, 2003; Davidson et al., 2000). Capsids presumably also affect the interactions of AAVs with anatomical barriers like the BBB (Vandenberghe et al., 2009).

Need for a therapeutic time window

An important issue would be to determine how far along in disease progression can the treatment be administered to patients to achieve substantial therapeutic benefits. Neurometabolic diseases like globoid cell leukodystrophy show favorable outcomes for presymptomatic intervention but not later indicating the existence of a restricted therapeutic time window (Escolar ML, 2005). Similar outcomes were seen in preclinical studies (Ahmed SS, 2013) and follow up study on CD clinical trials (Leone et al., 2012) indicating that future gene therapy interventions should begin before irreversible neuro-structural changes occur underlining importance of rodent studies.

Looking ahead

It has been more than 8 decades since CD was first described in 1931 (Canavan, 1931) and there was little progress in understanding its pathogenesis until it was identified as an aspartoacylase deficiency almost 5 decades later (Matalon et al., 1988). Description of the human aspartoacylase cDNA sequence led to a huge leap in molecular diagnosis for CD patients (Kaul et al., 1993); however, the molecular etiology has remained controversial. To resolve this, strong efforts in modeling CD in animals

significantly broadened avenues to investigate pathological mechanisms. Preclinical studies began with the naturally existing tremor rats and then expanded to include the CD mouse and later the Nur7 and the LacZ knock-in mouse models.

Discovery of rAAV serotypes that can cross the BBB revolutionized the field (Foust et al., 2009; Yang et al., 2014; Zhang et al., 2011); however, an important issue in translation of the intravenous rAAV therapeutic dose from mice to humans is the huge vector manufacturing burden, making treatment costs prohibitive. Codon optimization of the expression cassette would increase expression efficiency and lower therapeutic doses. Moreover delivery of vector to the CSF directly would enhance diffusion in the CNS and lesser spread in peripheral organs. Again surprisingly the kidney expresses high levels of aspartoacylasebut has low NAA levels suggesting additional catalytic functions for aspartoacylase. Thus, alternate approaches may be needed to deal with the pathological consequences of loss in aspartoacylase activity in such peripheral tissues.

Long term studies on rAAV gene therapy- treated patients have documented that it is safe and risk-free. CD is a monogenic genetic disorder with very distinct core clinical features that is amenable for gene therapy. Inclusion of newer CD animal models, continuously expanding viral vector repertoire and less invasive delivery methods for pan-CNS delivery make it likely that gene therapy for CD and other such diseases will advance rapidly in the near future. Efficient translation of the comprehensive data-driven validation of effective therapy in mouse models to humans would push forward the successful development of therapeutics like rAAVs and provide a viable treatment for patients who previously had none.

Focus of this dissertation

This dissertation focuses on developing an efficacious gene therapy for Canavan disease using recombinant AAVs in the aspartoacylase knockout mouse model in a preclinical setting. In Chapter 2, we characterize novel variants of AAVs that can cross the blood brain barrier becoming effective tools for treatment of neurological disorders. An intravascular delivery of these vectors also targets peripheral tissues to cause potential detrimental effects; hence we also describe construction of tissue-specific, endogenous microRNAs (miRNAs) to repress rAAV expression outside the CNS, by engineering perfectly complementary miRNA-binding sites into the rAAV9 genome. In Chapter 3, we show that a single intravenous injection of 3 AAV variants can ameliorate disease symptoms in a *bona fide* mouse model. We also for the first time document that microRNAs can be used to restrict transgene expression in the CNS using AAVs as vectors. Additionally, we define a therapeutic time window for delivery of vectors in CD showing that vector administration as late as P20 can rescue lethality in the animal model. In Chapter 4, we further try to increase efficiency by intracerebroventricular delivery of rAAVs to minimize systemic viral load, potential systemic toxicity, off target expression and lower vector manufacturing burden yet achieve widespread transgene expression. We extensively describe peripheral pathology in the animal model and report for the first time that the immune system may be severely compromised in CD. We also shed light on the role of neural cell types on the disease pathophysiology.

CHAPTER II: CHARACTERIZATION OF AAV VARIANTS THAT CAUSE WIDESPREAD CNS TRANSDUCTION FOLLOWING INTRAVENOUS DELIVERY

The following chapter contains parts of the manuscripts

Zhang H, Yang B, Mu X, Ahmed SS, Su Q, He R, Wang H, Mueller C, Sena-Esteves M, Brown R, Xu Z, Gao G. (2011). Several rAAV vectors efficiently cross the blood-brain barrier and transduce neurons and astrocytes in the neonatal mouse central nervous system. Molecular Therapy Aug; 19(8):1440-8 [PMID: 21610699].

Yang B, Li S, Wang H, Guo Y, Gessler DJ, Cao C, Su Q, Kramer J, Zhong L, Ahmed SS, Zhang H, He R, Desrosiers RC, Brown R, Xu Z, Gao G. (2014) Global CNS transduction of adult mice by intravenously delivered rAAVrh.8 and rAAVrh.10 and nonhuman primates by rAAVrh.10. Molecular Therapy Jul; 22(7):1299-309. [PMID: 24781136]

The studies were a large part of my rotation project and I was involved in perfusing, embedding, sectioning of the mice used. All the staining for mouse tissues was done on these sections.

CHAPTER II: Characterization of AAV variants that cause widespread CNS transduction following intravenous delivery

Introduction

Monogenic neurodegenerative disorders where gene mutations cause loss of function or gain of a deleterious new property/function are ideal candidates for gene therapy. This may be either through the delivery of the normal gene, in the former case, or vehicles that can silence a miscreant gene and protein by RNA interference (Manfredsson and Mandel, 2010; Urbaniak Hunter et al., 2010). Though targeted vector delivery into discrete structures in the central nervous system (CNS) is highly effective for diseases with a localized lesion, or those where localized transgene expression is sufficient to alleviate disease phenotype (Cearley et al., 2008), it comes at a cost of surgical risks and clinical costs. Moreover such an approach is not suitable for global CNS diseases that require more dispersed transduction.

Among non viral and viral vectors, recombinant adeno-associated viruses (rAAVs) have demonstrated a great potential in CNS gene transfer (Davidson and Breakefield, 2003). In human clinical trials, direct injection of AAV vectors gave rise to sustained transgene expression and therapeutic effect (Kaplitt et al., 2007). Emerging self-complementary AAV (scAAV) vectors hold extra advantages over their single strand counterparts due to higher gene delivery efficiency (McCarty, 2008).

An ideal approach to address widespread CNS disorders would harness the vasculature since the brain is a highly vascularized organ. A critical impediment to

widespread CNS gene transfer via the vasculature is the blood–brain barrier (BBB), which is a complex anatomical barrier including endothelial tight junctions, astrocytic end-feet, pericytes, and cellular basement membrane (Bradbury, 1985). The barrier precludes the entry of >98% of small molecule and almost all macromolecules including therapeutic proteins and gene delivery vectors into the CNS (Pardridge, 2002).

In order to overcome the restricted entry of viral particles into the CNS and low transduction efficiency, discovery of new clades of novel primate AAVs with unique tissue/cell tropisms and varying efficiencies of *in vivo* gene transfer is important (Gao et al., 2004; Gao et al., 2002). One of these novel primate serotypes, rAAV9, can achieve robust transduction of neuronal and glial cell types in the CNS of murine neonates following intravenous injections (Foust et al., 2009) and has shown encouraging results in treating a number of CNS diseases that require early life intervention (Falk et al., 2013; Hinderer et al., 2014; Jiang et al., 2006).This is an important breakthrough in CNS gene therapy, although the host-serological response to AAV9 may preclude its widespread use.

There are however other challenges to rAAV-mediated systemic gene delivery to the CNS. The first challenge is to deliver rAAV specifically to the CNS. The viral capsid is the principal determinant for AAV tissue tropism (Vandenberghe et al., 2009), and the liver is the major target for AAV vectors (Nakai et al., 2005). Systemic administration of some rAAV serotypes transduces the liver and other tissues, including the CNS, skeletal muscle and heart (Wang et al., 2005; Zincarelli et al., 2008). Such off-target transduction

raises the spectre of overexpression of transgenes outside the CNS, potentially eliciting toxic responses. The other challenge is to confine transgene expression to the CNS. Historically, CNS-specific promoters have been used for this purpose; however, tissue-specific, strong CNS promoters like the neuron-specific enolase (NSE) and neuron-specific human platelet-derived growth factor-β (PDGF-β) chain are too large to be packaged into the rAAV genome (Hioki et al., 2007).

We first report a survey of nine scAAV vectors for their CNS gene transfer properties after systemic administration in neonatal mice using rAAV9 as a control. We investigated enhanced permeation of the BBB and improved delivery of enhanced green fluorescent protein (EGFP) to the CNS following facial vein injection on P1. Our data document that the ability to cross the BBB in neonatal mice is not restricted to rAAV9. We then characterized highly CNS tropic rAAV(s) with naturally reduced peripheral tissue tropism for systemic gene delivery to the CNS in adult animals. We compared the CNS transduction efficiencies of 12 different rAAVs (rAAV 1, 2, 5, 6, 6.2, 7, 8, 9, rh.8, rh.10, rh.39, and rh.43) in 10-week-old mice following systemic delivery.

Material and Methods

Vector design and construction: The EGFP reporter vector genome uses a hybrid cytomegalovirus enhancer/CB promoter cassette; AAV2 inverted terminal repeats, rabbit beta globin intron, eGFP cDNA and a rabbit globin poly A. The miRNA-regulated EGFP construct was created by inserting three copies each of miR-1 and miR-122 target sites in tandem in the 3′ UTR of EGFP reporter gene as previously described (Xie et al., 2012).

***AAV production*:** All scAAV vectors were produced by trans-encapsidation of rAAV vector genome flanking by inverted terminal repeats from AAV2 with the capsids of different AAVs using the method transient transfection of 293 cells and CsCl gradient sedimentation as described previously (Sun et al., 2010). Vector preparations were titred by quantitative PCR. Purity of vectors was assessed by 4–12% SDS-acrylamide gel electrophoresis and silver staining (Invitrogen, Carlsbad, CA). Morphological integrity of each vector used in the study was examined by transmission electron microscopy of negative stained recombinant AAV virions at Electronic Microscopy Core, University of Massachusetts Medical School, Worcester, MA.

***Animal procedures*:** All animal procedures were approved by the Institutional Animal Care and Use Committees of University of Massachusetts Medical School.

For neonatal injections, wild-type C57BL/6 mice littermates were used. Breeding were conducted using programmatic timing. Pregnant mice were monitored daily from embryonic day 17 to 21 to ensure the newborn pups could be dosed with vectors on P1. Vectors were injected in P1 pups at a concentration of 4×10^{12} genome copies/ml in PBS

(Stoica et al., 2013). Each pup received 4×10^{11} genome copies of different scAAVCBEGFP vectors (rAAV1, rAAV2, rAAV5, rAAV6, rAAV6.2, rAAV7, rAAV9, rAAVrh.10, rAAVrh.39, rAAVrh.43; n = 6–8 mice per group).

For adult injections, 10-week-old C57BL/6 mice (n = 3) with an average body weight of 20 g were treated with rAAV vectors via tail vein injections at a dose of 4×10^{12} GCs/mouse in 100µl PBS.

***Histological processing*:** Mice were anesthetized 21 days postinjection and transcardially perfused with 15 ml of cold phosphate-buffered saline (PBS) followed by 15 ml of fixation solution containing 4% paraformaldehyde (v/v) in PBS. Brain and spinal cord were extracted and postfixed in 4% paraformaldehyde overnight (n = 3). The mouse tissues were cryoprotected in 30% sucrose (w/v) in PBS, embedded in Tissue-Tek OCT compound (Sakura Finetek, Torrance, CA) and frozen in a dry ice/ethanol bath. Serial 40-µm floating sections of the entire brain as well as 3-mm segments from cervical, thoracic, and lumbar regions of the spinal cord were cut with a Cryostat (Thermo Microm HM 550; Thermo Scientific, Walldorf, Germany).

Immunohistochemistry: Brain and spinal cord sections were stained as floating sections in 12-well plates. Sections were washed three times in PBS for 5 minutes each time, and then incubated in blocking solution containing 0.1% Triton-X100 (v/v) (Fisher, Pittsburg, PA) and 10% goat serum (v/v) (Invitrogen, Frederick, MD) for 1 hour at room temperature. Sections were then incubated with primary antibodies diluted in blocking solution at 4 °C overnight. The following day tissue sections were washed twice in 0.05%

Tween-20 (v/v) in PBS (PBST) and once with PBS, with each washing step lasting 10 minutes. Sections were subsequently incubated with appropriate secondary antibodies in blocking buffer for 1 hour at room temperature. Sections were washed again as above. For fluorescent detection, sections were mounted with Vectashield with 4',6-diamidino-2-phenylindole (DAPI; Vector Laboratories, Burlingame, CA) and analyzed using an epifluorescent microscope (Nikon Eclipse Ti; Nikon Instruments, Melville, NY) or a Leica TSC-SP2 AOBS confocal microscope equipped with a ×63 oil lens and a DM-IRE2 inverted microscope.

For avidin biotin complex-3,3′-diaminobenzidine detection, sections were incubated in 0.1% peroxide/PBS and biotin/avidin blocking solution prior to primary antibody incubation to quench endogenous peroxidase and biotin activity. After incubation with a biotinylated secondary antibody, sections were washed and incubated in ABC reagent (PK-6200; VectorLabs) for 30 minutes at room temperature. After a quick wash in PBS, sections were developed with DAB solution (SK-4105; VectorLabs) for 60 seconds followed by three consecutive washes in PBS lasting 5 minutes each. Sections were subsequently dehydrated in a graded ethanol series of 50, 70, 95, and 100%. After two changes of xylene, sections were coverslipped with permount mounting media (Fisher) and left overnight to dry.

The primary antibodies used in this study were as follows: anti-APC (OP80, Calbiochem, Billerica, MA) rabbit anti-GFP (Invitrogen), goat anti-ChAT and mouse anti-NeuN (both from Millipore, Billerica, MA), mouse anti-glial fibrillary acidic protein (Cell Signaling,

Danvers, MA), rat anti-CD34, rabbit anti-CD31 (both from Abcam, Cambridge, MA), mouse anti-Calbindin D-28k (Sigma, St Louis, MO), and mouse anti-tyrosine hydroxylase monoclonal antibody (Millipore). The secondary antibodies used in the study included: DyLight 488 AffiniPure Donkey antirabbit IgG; DyLight 549 AffiniPure Donkey Anti-Goat IgG; DyLight 549 Affinipure Goat antirat IgG; DyLight 594 AffiniPure Goat antimouse IgG (all from Jackson ImmunoResearch, West Grove, PA); goat antirabbit IgG-Alexa fluro 488 and goat antimouse IgG-Alexa fluro 568 (both from Invitrogen).

Semiquantitative analysis of EGFP-positive cells: To provide a semiquantitative measure of the amount and type of cells that were transduced by rAAVs in the CNS, we used a previously described scoring system (Cearley et al., 2008). Briefly, the number of (+) corresponds to the number of EGFP-positive cells where (+) means very few positive cells, (++) some positive cells, (+++) many positive cells, (++++) large areas of positive cells, and (+++++) saturated with positive cells. Regions with no EGFP expression are marked as (−). Mean scores were calculated by averaging plus signs for all brain and all spinal cord areas (n = 3).

Next, we selected 12 subanatomical, functionally important regions in the brain as well as cervical, thoracic, and lumbar sections of the spinal cord for quantitative analysis of images that were taken on a Nikon Eclipse Ti inverted microscope equipped with a Retiga 2000-RV CCD cooled camera. Nikon NIS elements AR software version 3.2 was used for intensity quantification. Prior to quantification, optimal light source intensity and

exposure times were obtained by plotting an intensity/exposure time curve using fluorescence reference slides (Ted Pella, prod. 2273; Ted Pella, Redding, CA). It was found that the intensity and exposure times had linear correlation. In addition, overexposure and extreme underexposure distorts the linear correlation. We have therefore used the maximum intensity (ND1) and a 20ms exposure for all sections to avoid overexposure. For quantification, fixed region of interest was used to quantify the brightest area of any given brain region. A mean intensity (total intensity/size of region of interest) was obtained for each region of all serotypes. Statistical analysis was performed using one-way analysis of variance test for comparison of semiquantitative scores as well as biodistribution data.

Results

Intravenous injection of rAAVs mediated widespread transduction in neonatal mouse CNS

We compared the CNS transduction profiles of the following recombinant AAV vectors encoding EGFP: rAAV1, rAAV2, rAAV5, rAAV6, rAAV6.2, rAAV7, rAAV9, rAAVrh.10, rAAVrh.39, and rhAAVrh.43 21 days post injection in P1 pups. As assessed by the scoring system (Cearley et al., 2008), rAAV9 was indeed among the best performers; seven out of nine other rAAVs tested (rAAV1, rAAV6, rAAV6.2, rAAV7, rAAVrh.10, rAAVrh.39, and rAAVrh.43), but not rAAV2 and rAAV5, also gave rise to widespread EGFP expression in the CNS [Table 2.1]. However, the apparent number of EGFP-positive cells varied between CNS structures in a vector dependent manner. The region with the highest EGFP transduction was the hypothalamus followed by medulla, striatum, hippocampus, cortex, and cerebellum. In contrast, the transduction efficiency in olfactory bulb and thalamus was relatively low [Table 2.1]. We also assessed average EGFP signal intensity/pixel in 12 different CNS regions to derive a more quantitative assessment of gene transfer efficiency of each rAAV [Figure 2.1a]. For the eight rAAV vectors that achieved CNS transduction after intravenous injection, the mean EGFP signal intensity/pixel was relatively low in cortex, habenular nucleus, cornu ammonis, dentate gyrus, thalamus, cerebellum, and olfactory bulb, moderate in choroid plexus and caudate- putamen, but high in hypothalamus, medulla and amygdala [Figure 2.1a]. Next, the average EGFP signal intensity/pixel in the brain (average of 12 regions) for different

Table 2.1 Semi Quantitative evaluation of vector performance. Based on the Cearley system, we established a scoring system to evaluate efficiency of vector transduction (See Materials and Methods).

Scoring: (−) no transduction, (+) very few positive cells, (++) some positive cells, (+++) many positive cells, and (++++) region is almost saturated with EGFP-positive cells. The number of animals (n) is given to the right of the score.

Table 2.1 Semi Quantitative evaluation of vector performance.

	Scores in sub-anatomical regions in neonatal mouse CNS											
Serotypes	Olfactory bulb	Striatum	Hippocampus	Cortex	Thalamus	Hypothalamus	Cerebellum	Medulla	Cervical	Thoracic	Lumbar	Choroid plexus
AAV1	$+_{n=3}$	$++_{n=3}$	$++_{n=3}$	$++_{n=3}$	$+_{n=3}$	$+++_{n=3}$	$+++_{n=3}$	$+++_{n=3}$	$+++_{n=3}$	$+++_{n=3}$	$+_{n=3}$	$+++_{n=3}$
AAV2	$-_{n=3}$	$-_{n=3}$	$+_{n=3}$	$+_{n=3}$	$+_{n=3}$	$+_{n=3}$	$+_{n=3}$	$+_{n=3}$	$+_{n=3}$	$-_{n=3}$	$-_{n=3}$	$++_{n=3}$
AAV5	$-_{n=3}$	$-_{n=3}$	$-_{n=3}$	$+_{n=3}$	$-_{n=3}$	$+_{n=3}$	$-_{n=3}$	$-_{n=3}$	$-_{n=3}$	$-_{n=3}$	$-_{n=3}$	$-_{n=3}$
AAV6	$+_{n=3}$	$+_{n=3}$	$++_{n=3}$	$++_{n=3}$	$+_{n=3}$	$+++_{n=2}$ $++_{n=1}$	$++_{n=3}$	$++_{n=3}$	$++_{n=3}$	$+_{n=3}$	$+_{n=3}$	$+++_{n=3}$
AAV6.2	$-_{n=3}$	$+++_{n=2}$ $++_{n=1}$	$++_{n=3}$	$++_{n=3}$	$+_{n=3}$	$++++_{n=3}$	$++_{n=3}$	$++_{n=3}$	$++_{n=3}$	$++_{n=3}$	$+_{n=3}$	$++++_{n=3}$
AAV7	$+++_{n=1}$ $++_{n=2}$	$+++_{n=3}$	$+++_{n=2}$ $++_{n=1}$	$++_{n=3}$	$+_{n=3}$	$++++_{n=3}$	$+++_{n=1}$ $++_{n=2}$	$++_{n=3}$	$++_{n=3}$	$+_{n=3}$	$+_{n=3}$	$++++_{n=3}$
AAV9	$+++_{n=2}$ $++_{n=1}$	$+++_{n=3}$	$++_{n=3}$	$+++_{n=1}$ $++_{n=2}$	$+_{n=3}$	$++++_{n=1}$ $+++_{n=2}$	$+++_{n=1}$ $++_{n=2}$	$++_{n=3}$	$++++_{n=1}$ $+++_{n=2}$	$++_{n=3}$	$+_{n=3}$	$++++_{n=3}$
rh10	$+++_{n=1}$ $++_{n=2}$	$++++_{n=1}$ $++_{n=2}$	$+++_{n=3}$	$+++_{n=2}$ $++_{n=1}$	$++_{n=2}$ $+_{n=1}$	$++++_{n=3}$	$+++_{n=1}$ $++_{n=2}$	$+++_{n=3}$	$++++_{n=1}$ $+++_{n=2}$	$++_{n=3}$	$+_{n=3}$	$++++_{n=3}$
rh39	$+++_{n=1}$ $++_{n=2}$	$++++_{n=2}$ $+++_{n=1}$	$+++_{n=3}$	$+++_{n=1}$ $++_{n=2}$	$+_{n=3}$	$++++_{n=3}$	$+++_{n=1}$ $++_{n=2}$	$++++_{n=1}$ $+++_{n=2}$	$++++_{n=1}$ $+++_{n=2}$	$+++_{n=3}$	$+_{n=3}$	$++++_{n=3}$
rh43	$++_{n=3}$	$+++_{n=3}$	$+++_{n=3}$	$+++_{n=3}$	$+_{n=3}$	$++++_{n=1}$ $+++_{n=2}$	$++_{n=3}$	$++++_{n=1}$ $+++_{n=2}$	$++++_{n=2}$ $+++_{n=1}$	$+++_{n=3}$	$+_{n=3}$	$++++_{n=3}$

Figure 2.1 Quantification of GFP intensity levels in brain and spinal cord. 4×10^{11} genome copies of ten different rAAV vectors were injected into neonatal P1 pups via the superficial temporal vein. Mice were killed 21 days after injection, and 40 μm brain and spinal cord cryosections were stained with an anti-EGFP antibody for immunofluorescence. (a) EGFP signal intensity/pixel in different brain and spinal cord regions was measured for each rAAV vector. (b) Average EGFP signal intensity/pixel in brain and spinal cord corresponds to the average value across all respective structures analyzed individually in (a). CSP, cervical section of spinal cord; D, dorsal region; EGFP, enhanced green fluorescent protein; LSP, lumbar section of spinal cord; rAAV, recombinant adeno-associated virus; TSP, thoracic section of spinal cord; V, ventral region.

Figure 2.1 Quantification of GFP intensity levels in brain and spinal cord.

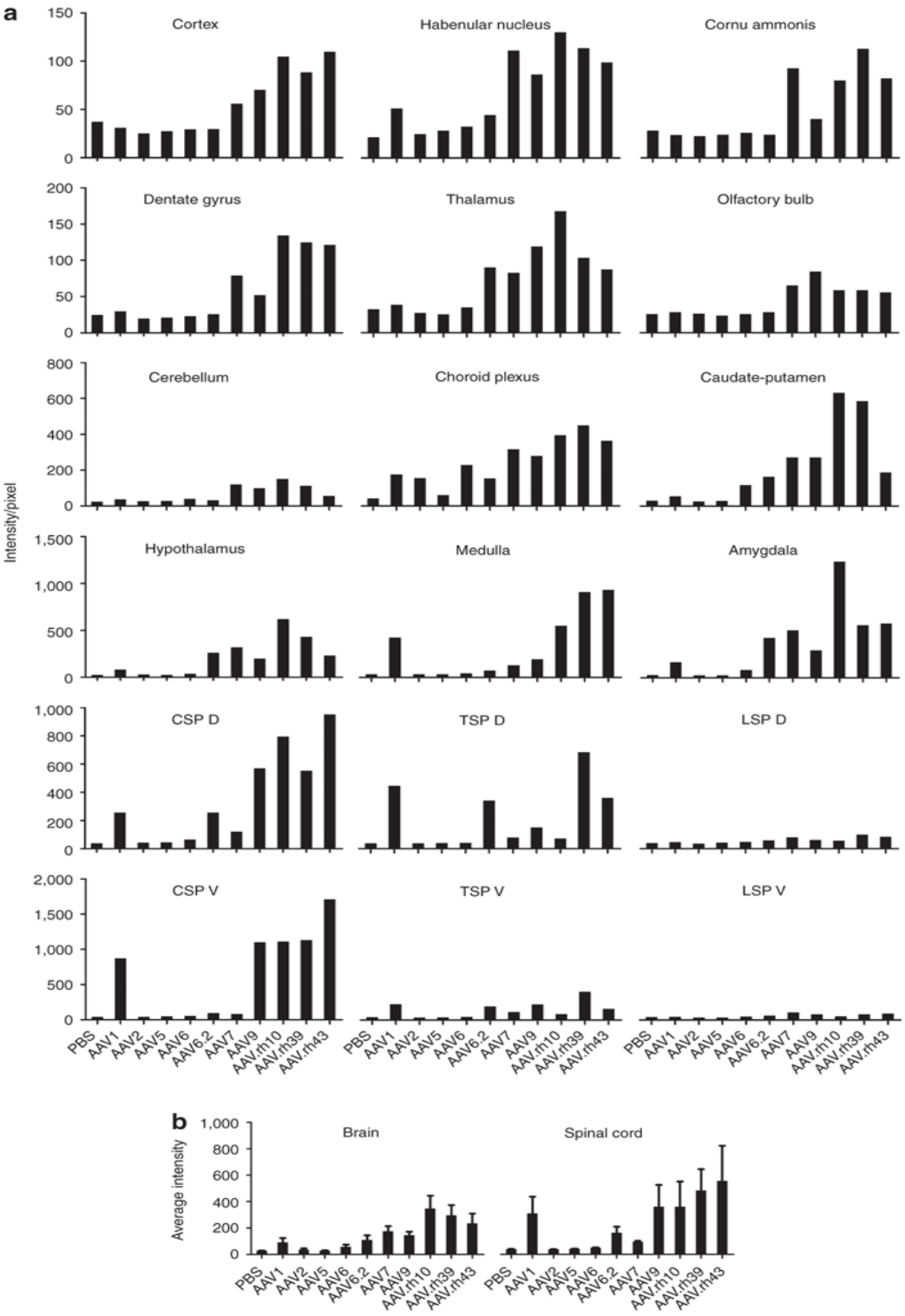

rAAVs were compared [Figure 2.1b]. AAVrh.10, AAVrh.39, and AAVrh.43 stood out for their overall gene transduction efficiency in brain, followed by AAV7, AAV9, and AAV1 [Figure 2.1b].

These eight effective serotypes also mediated EGFP expression throughout the spinal cord, to different degrees. The same quantitative analysis was performed for each rAAV in the cervical, thoracic and lumbar sections of the spinal cord [Figure 2.1a]; the average EGFP signal intensity/pixel of the three sections for different rAAVs were also compared [Figure 2.1b]. Overall, rAAV1, rAAV9, rAAVrh.10, rAAVrh.39, and rAAVrh.43 displayed stronger transduction in the spinal cord with the highest EGFP signal intensity/pixel observed in cervical, followed by thoracic and lumbar sections of the spinal cord [Figure 2.1]. For rAAV2 there were only a few EGFP-positive cells in hippocampus, cortex, and hypothalamus, while none was observed in most CNS regions in AAV5-injected mice except in the hypothalamus.

The following is a more detailed description of our findings. Selection of CNS structures was based on their relevance to neurodegenerative diseases in humans (e.g., striatum in Huntington's disease, hippocampus, and cortex in Alzheimer's disease, cerebellum in spinal-cerebellar ataxias, spinal cord in amyotrophic lateral sclerosis, and spinal cord injury), and distinct transduction profiles by different rAAVs.

Striatum. Previous studies have shown that systemic injection of rAAV9 in neonatal mice yields robust striatal transduction (Foust et al., 2009). In this study, a large number of neurons were also transduced by rAAVrh.10, confirmed by costaining with a neuronal

marker [Figure 2.2]. Other vectors, including rAAVrh.39, rAAVrh.43 and rAAV7, also mediated moderate transduction in striatum. In contrast, rAAV6, rAAV6.2, and rAAV1 resulted in relatively lower EGFP expression in this structure [Figure 2.2].

Hippocampus. Large numbers of EGFP-positive neurons were observed bilaterally in all regions of the hippocampus, namely dentate gyrus, hilus, CA1, CA2, and CA3 for the mice that received intravenous rAAVrh.10, rAAV9, rAAV7, rAAVrh.39, and rAAVrh.43 (ranked by transduction efficiency in this structure, Table 2.1 and Figures 2.1 & 2.2). In addition to the neuronal transduction pattern, we also observed EGFP-positive cells that morphologically resembled astrocytes [Figure 2.2]. This was further confirmed by double staining with antibodies against EGFP and GFAP, an astrocyte marker. For intravenously delivered rAAV1, rAAV6, and rAAV6.2 only a small proportion of EGFP-positive cells in the hippocampus [Figure 2.2].

Cortex. AAV7, AAV9, AAVrh.10, AAVrh.39, and AAVrh.43 vectors achieved moderate EGFP transduction in cortex targeting mainly neurons and astrocytes [Table 2.1 and Figures 2.1 & 2.2]. Prominent EGFP-positive cells were typically observed in the ventrolateral regions of the cortex, including posterior agranular insular cortex, piriform cortex, lateral entorhinal cortex, posterolateral cortical amygdaloid nucleus, and posteromedial cortical amygdaloid nucleus [Figure 2.2]. The cortical transduction efficiency of rAAVrh.10, rAAV9, rAAVrh.39, and rAAVrh.43 was comparable. AAV1, AAV6, and AAV6.2 vectors also transduced cortical cells, albeit at considerably lower levels than the rAAV vectors mentioned above [Figure 2.2].

Figure 2.2 Strong and widespread EGFP expression in mouse brain after neonatal injections. 4×10^{11} genome copies of rAAVs vectors were injected into neonatal postnatal day 1 (P1) pups, and distribution of EGFP expression in the brain was analyzed at 21 days post-injection. 40 micrometer thick cryosections were stained with an anti-EGFP antibody for immunofluorescence. The regions shown are: olfactory bulb, striatum, hippocampus, cortex, hypothalamus, cerebellum, and medulla. Representative sections are shown for each rAAV. Bars = 100 μm. EGFP, enhanced green fluorescent protein; rAAV, recombinant adeno-associated virus.

Figure 2.2 Strong and widespread EGFP expression in mouse brain after neonatal injections.

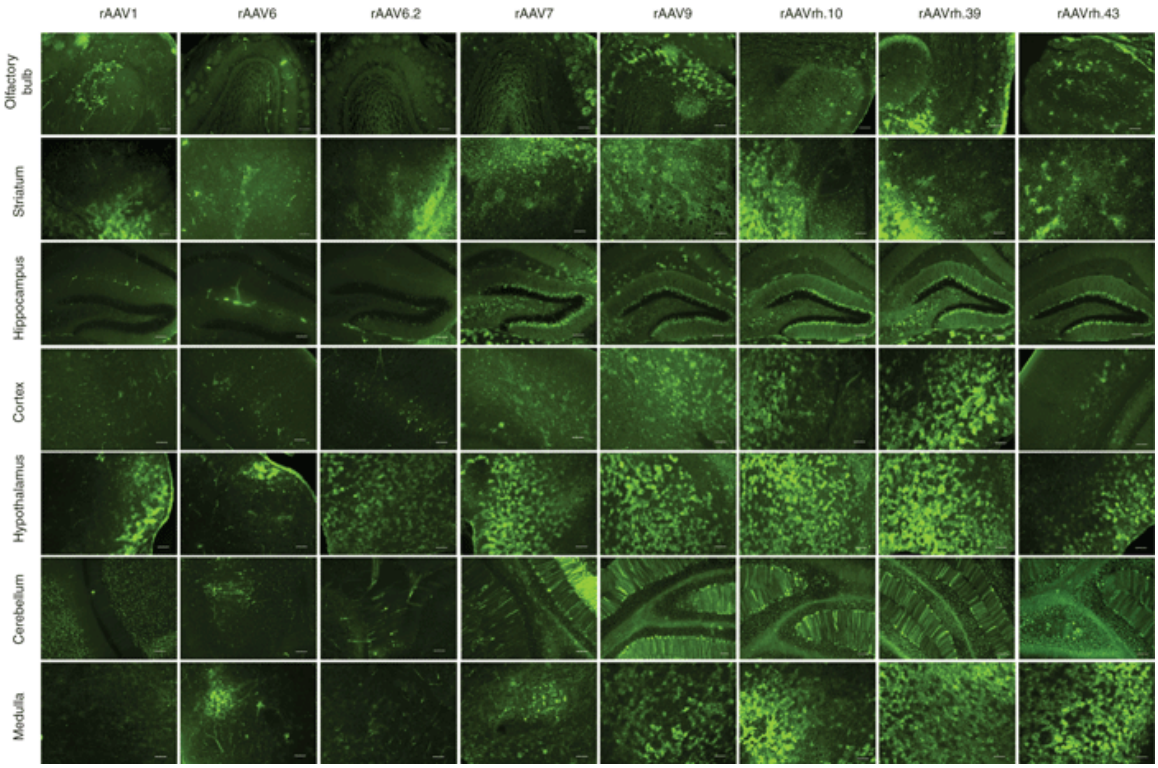

Hypothalamus. The most impressive EGFP signal was observed in the hypothalamus for all eight effective vectors. Intravenous administration of rAAVrh.10 resulted in EGFP expression in the entire hypothalamus, followed by rAAVrh.39, rAAV7, rAAV6.2, rAAVrh.43, rAAV9, rAAV1, and rAAV6 [Table 2.1 and Figures 2.1 & 2.2]. Interestingly most EGFP-positive cells in this structure have an astrocytic morphology which was confirmed by immunostaining. The strong and widespread astrocytic EGFP signal tended to obscure direct examination of morphological details of other transduced cells.

Cerebellum. EGFP-positive cells and fibers were easily detected in cerebellum for all rAAV vectors except for AAV2 and AAV5 [Table 2.1 and Figures 2.1 & 2.2]. A large number of EGFP-expressing cells were found in the Purkinje and granule cell layers for rAAV7, rAAV9, rAAVrh.10, rAAVrh.39, and rAAVrh.43 [Figure 2.2]. Interestingly, the transduction profile of rAAV1 vector was restricted to cells in the granule cell layer, while rAAV6 and rAAV6.2 were localized in cells in the Purkinje cell layer [Figure 2.2].

Medulla. As above, all rAAVs, except for rAAV2 and rAAV5, mediated moderate to robust EGFP expression in medulla with most green cells being present in the outer rim [Figure 2.2]. Transduction efficiencies of these rAAV in this region are ranked in the following order: rAAVrh.39 = rAAVrh.43 > rAAV.rh10 > rAAV1 > rAAV9 > rAAV7 > rAAV6.2 > rAAV6 [Table 2.1 and Figures 2.1a]. Most EGFP-transduced cells had an astrocytic morphology.

Spinal cord. rAAVrh.10, rAAV9, rAAVrh.39, and rAAVrh.43 gave rise to robust EGFP expression in cervical gray and white matter, while rAAV1, rAAV6.2, and rAAV7

showed moderate EGFP expression [Table 2.1 and Figures 2.1 & 2.3]. The EGFP signal was observed only in white matter for rAAV1. The transduction ability of all rAAVs decreased from cervical to lumbar spinal cord, although EGFP-positive cells were still visible in the latter region. Large populations of EGFP-positive cells with astrocytic morphology were observed throughout the spinal cord [Figure 2.3]. Additionally, rAAVrh.10, rAAV9, rAAVrh.39, rAAVrh.43, and rAAV7 also transduced cells with motor neuron morphology in the ventral regions of the spinal cord [Figure 2.3]. Ascending dorsal column fibers and dorsal root ganglia displayed remarkable transduction with strong EGFP expression in dorsal root ganglia neurons [Figures 2.4a & b]. The identities of rAAV transduced cell types in the spinal cord were characterized by co-immunofluorescence staining with antibodies against EGFP and cell-specific markers.

Seven rAAV vectors can achieve efficient global transduction of the adult mouse CNS where AAVrh.8 is the best

To determine the transduction efficiency of each serotype after intravenous injection in adult mice, we detected and quantified the enhanced green fluorescent protein (EGFP) signal from the coronal sections of brains and transversal sections of cervical, thoracic, and lumbar spinal cords [Figures 2.5, 2.6 & 2.7]. Based on the density of the transduced cells, we grouped 12 rAAVs into four groups [Figures 2.5, 2.6; Table 2.2]. Group 1 consisted of rAAVrh.8, rAAVrh.10, and rAAV9. This group ranked consistently as the top three in the transduction levels in both brain and spinal cord; the only exception being the spinal cord neurons, where the top seven vectors showed similar levels of

Figure 2.3 EGFP expression in mouse spinal cord after neonatal intravenous injection of rAAVs. 4×10^{11} genome copies of rAAVs were injected into neonatal postnatal day 1 (P1) pups, and distribution of EGFP expression in the spinal cord was analyzed at 21 days post-injection. Forty micrometer thick cryosections from cervical, thoracic and lumbar regions were stained with an anti-EGFP antibody for immunofluorescence. Representative sections are shown for each rAAV. Bars = 100μm. EGFP, enhanced green fluorescent protein; rAAV, recombinant adeno-associated virus.

Figure 2.3 EGFP expression in mouse spinal cord after neonatal intravenous injection of rAAVs.

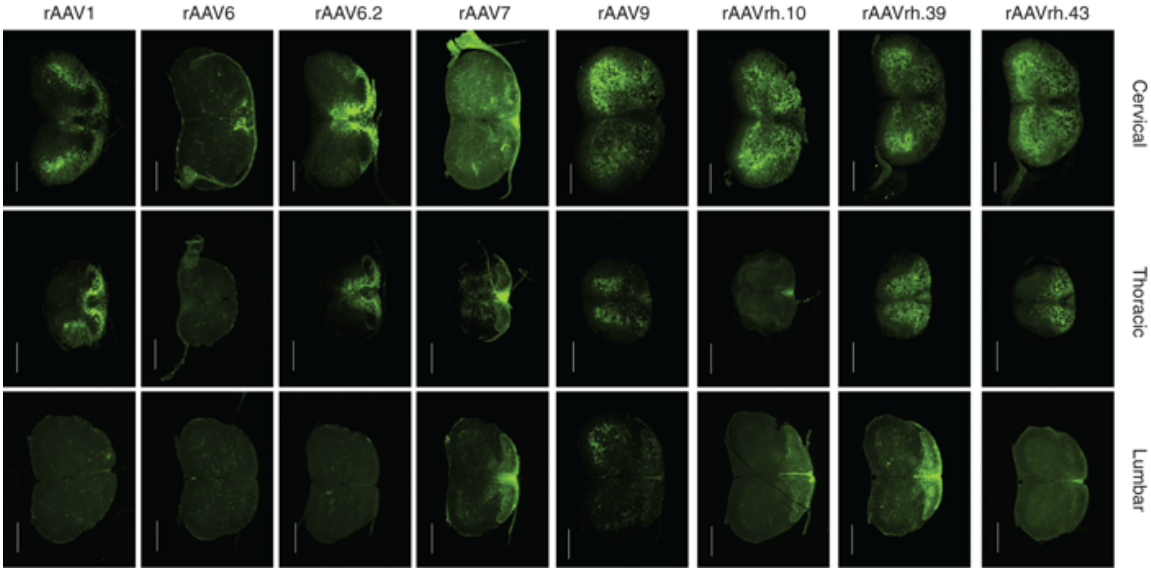

Figure 2.4 Transduction of dorsal root ganglia after neonatal intravascular infusion of rAAVs Neonatal P1 pups received 4×10^{11} GCs of rAAVs and EGFP expression in dorsal root ganglia analyzed at 21 days post-injection. (a) EGFP expression in dorsal root ganglia neurons was analyzed by double immunofluorescence staining for EGFP (green) and a neuronal-specific marker (NeuN, red) for systemically delivered rAAVs 7, 9, rh.10 and rh39. (b) Transduction of neonatal mouse dorsal root ganglia by systemically delivered rAAVs 1, 6, 6.2 and rh43 was stained only using anti-EGFP antibody. Scale bars represent 75μm.

Figure 2.4 Transduction of dorsal root ganglia after neonatal intravascular infusion of rAAVs.

a.

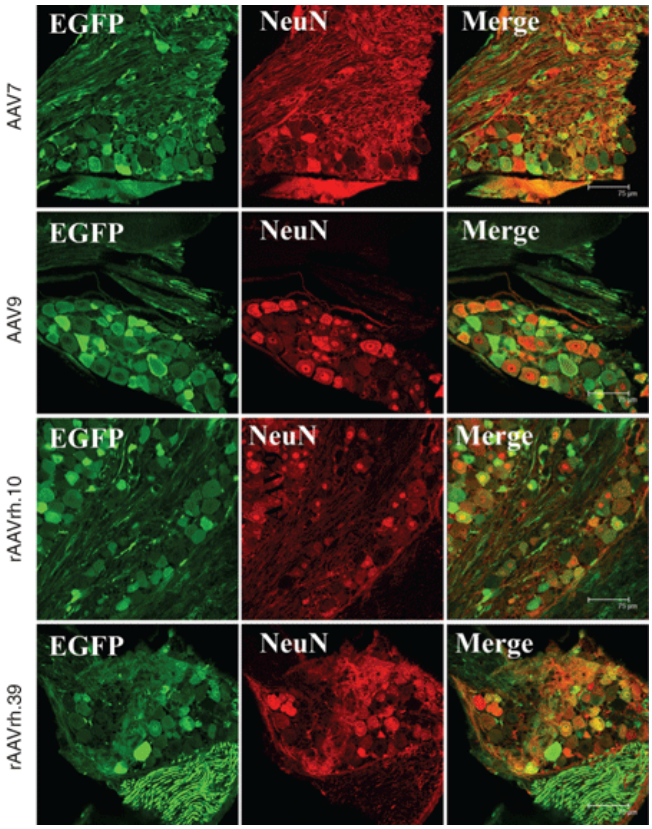

b.

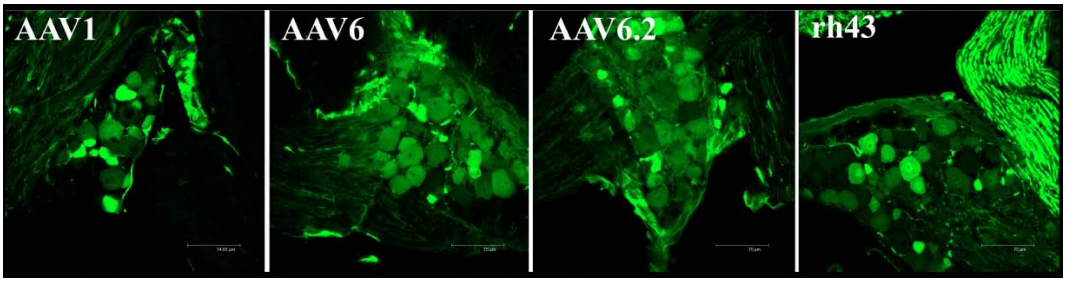

Figure 2.5 General transduction characteristics of 12 rAAVs in the adult mouse brain. rAAVEGFPs were injected into the tail vein of 10-week old mice at 4×10^{12} genome copies (GCs) per mouse (n = 3). Forty micrometer frozen sections of central nervous system (CNS) tissues were obtained 21 days postinjection and stained with antibody against EGFP. Staining was visualized with an avidin–biotin complex/3,3′-diaminobenzidine substrate system. Shown are composite images of bregma -2.00 mm brain sections of rAAV-injected mice organized into four groups based on EGFP semiquantitative score and extend of distribution. Bar = 1,000 μm. EGFP, enhanced green fluorescent protein.

Figure 2.5 General transduction characteristics of 12 rAAVs in the adult mouse brain.

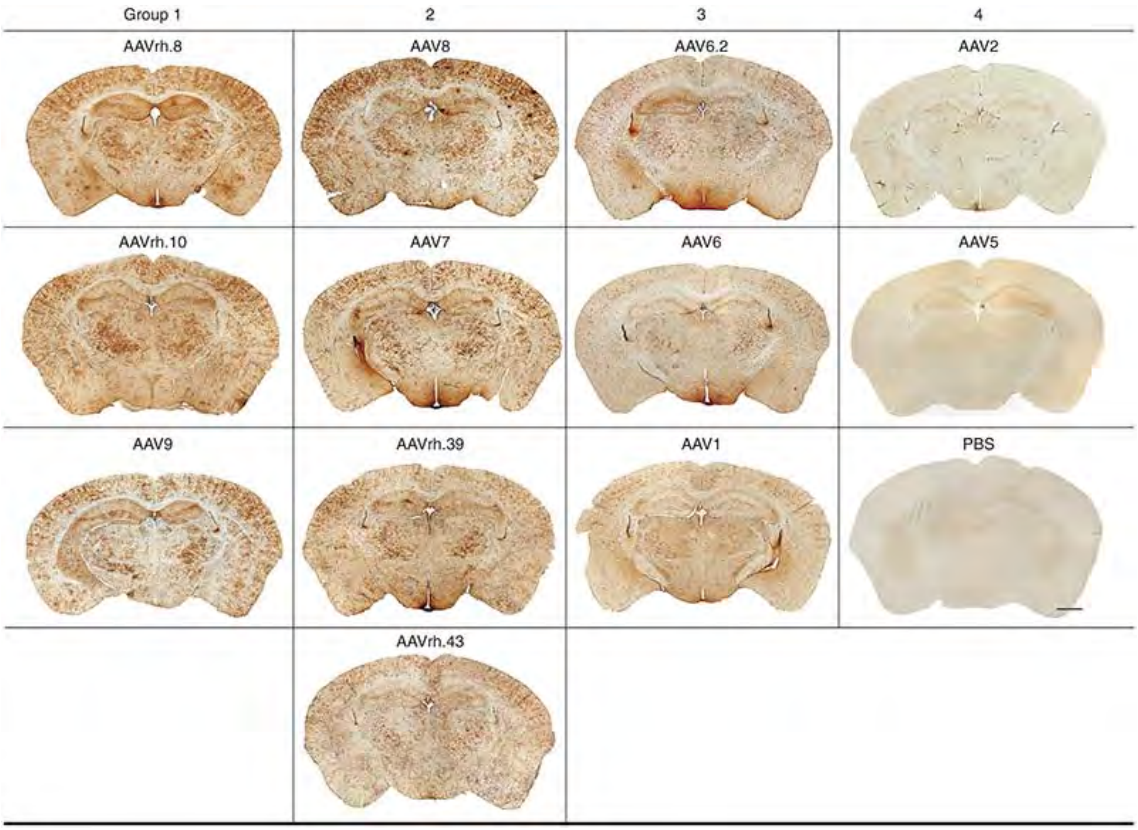

Figure 2.6 General transduction characteristics of 12 rAAVs in the adult mouse spinal cord. rAAVEGFPs were injected into the tail vein of 10-week old mice at 4×10^{12} genome copies (GCs) per mouse (for further description, see Figure 1, n = 3). Shown are composite images of cervical spinal cord, thoracic spinal cord, and lumbar spinal cord sections of rAAV-injected mice organized into four groups based on EGFP semiquantitative score and extent of distribution. Bar = 250μm.

Figure 2.6 General transduction characteristics of 12 rAAVs in the adult mouse spinal cord.

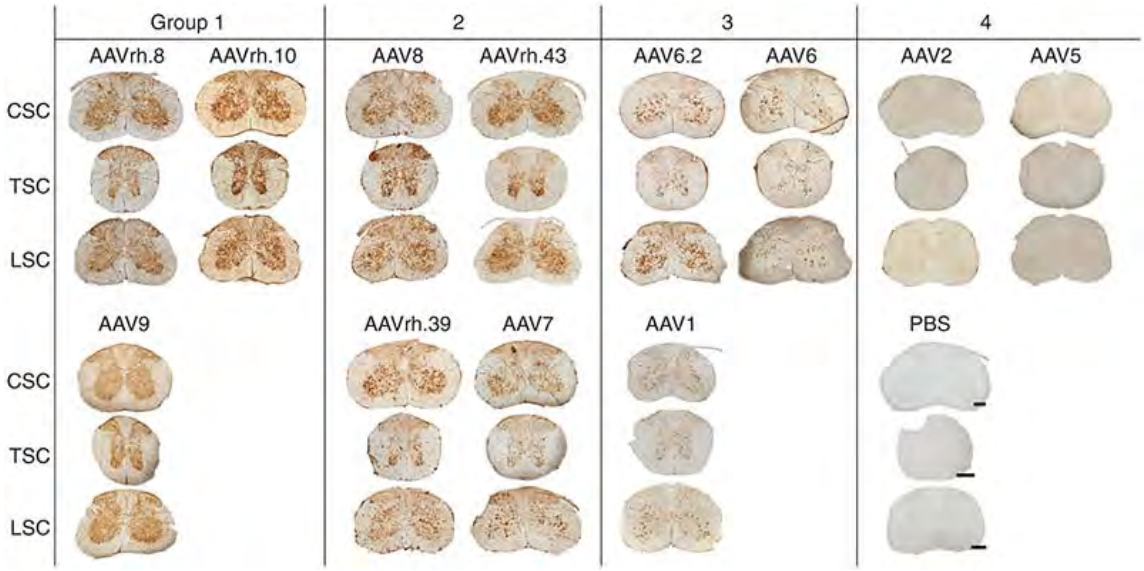

Figure 2.7 Quantification of transduced cell types in the central nervous system (CNS) of adult mice. EGFP-positive CNS cell types are microscopically scored, and the means of (e,h) rAAV transduced astrocytes, (d,g) neurons, and (f,i) oligodendrocytes in the (b,d–f) brains and (c,g–i) spinal cords are shown (n = 3). **P < 0.0033, ***P < 0.001, ****P < 0.0001. ns, not significant.

Figure 2.7 Quantification of transduced cell types in the central nervous system (CNS) of adult mice.

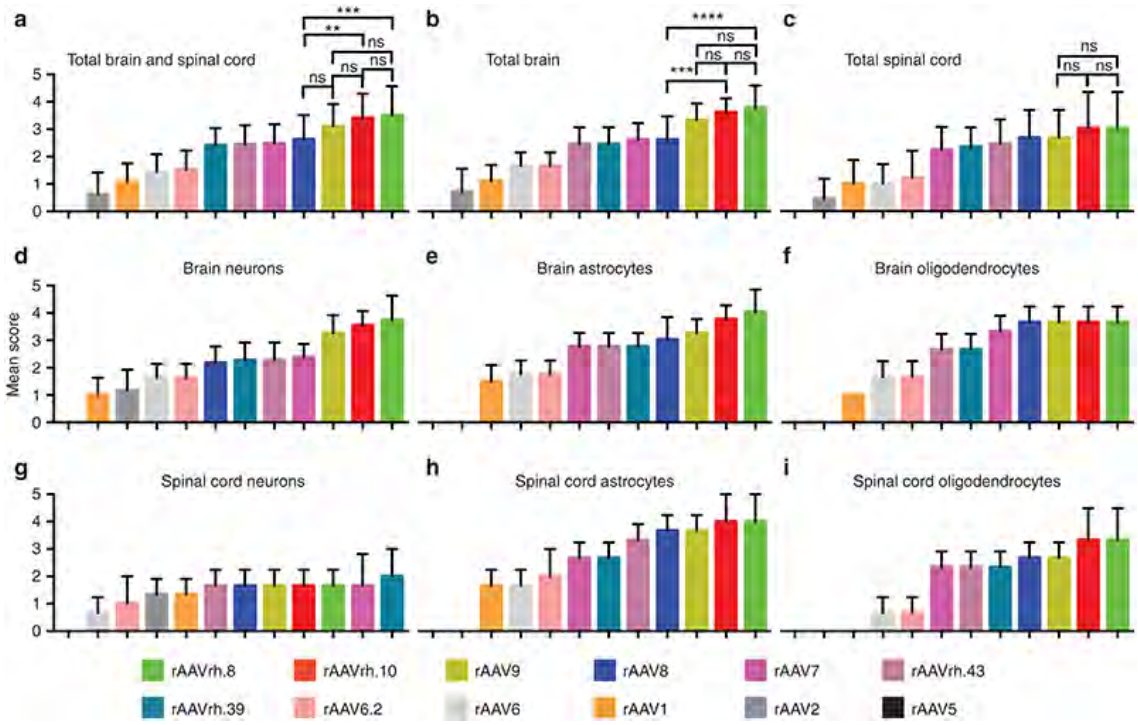

transduction [Figures 2.7g & 2.8]. Group 2 had four vectors, rAAV7, rAAV8, rAARrh.39, and rAAVrh.43 and ranked lower than the group 1; however their overall transduction levels were still excellent. In some cases (e.g., total spinal cord and spinal cord neurons), the differences between this group and group 1 were small and insignificant [Figures 2.5, 2.6 & 2.7c&g; Table 2.2]. All group 1 and group 2 vectors transduced spinal cord motor neurons robustly [Figure 2.8]. Group 3 consisted of three vectors, rAAV1, rAAV6, and rAAV6.2. The transduction levels by this group were lower than groups 1 and 2. In most instances, rAAV6.2 ranked the highest and the AAV1 the lowest within this group [Figures 2.5, 2.6, 2.7 & 2.8]. Group 4 consists of two vectors, rAAV2 and rAAV5.This group had the lowest transduction levels [Figures 2.5, 2.6 & 2.7]. Based on these assessments, we focused our detailed analysis on the group 1 vectors and some representatives of group 2 and group 3 vectors. The group 1 vectors transduced cells in wide areas of the CNS, including cortex, striatum, hippocampus, thalamus, hypothalamus, amygdala, corpus callosum [Figures 2.5, 2.9, 2.10 & 2.11], the choroid plexus [Figure 2.12], and all three spinal cord regions (i.e., cervical, thoracic, and lumbar) [Figures 2.6 & 2.8]. Overall, rAAVrh.8 appeared to transduce most robustly relative to other vectors. rAAVrh.8 consistently ranked first in different regions and in different cell types [Figure 2.7] by a semiquantitative scoring system (see Materials and Methods). The only exceptions were the spinal neurons, where the top seven serotypes had the same transduction efficiency [Figure 2.7g].

Table 2.2 Groups of rAAVs based on transduction efficiency.

			Scores in various regions of mouse CNS																
Serotype	Cell Type	Blood Vessel	OB	CC (O)	Amygdala (N)	CP (N)	Hippocampus(N)	Cortex	Thalamus	Hypothalamus (N)	SN (N)	MB (N)	Cerebellum	Medulla	Cervical	Thoracic	Lumbar	Brain	SC
AAV.rh8	A/O/N	VS	+++A, ++++N	++++	++++	+++++	++++	++++A, ++++N	+++++A, ++++N	+++	+++	+++	++++B, ++++G, ++++P	++++A, ++N	+++++A, ++++O, ++N	+++A, ++O, +N	++++A, ++++O, ++N	20+A, ++++O, 45+N	12+A, 10+O, 5+N
AAV.rh10	A/O/N	VS	+++A, ++++N	+++	++++	++++	++++	++++A, ++++N	++++A, ++++N	+++	+++	+++	+++B, +++G, ++++P	++++A, ++N	+++++A, ++++O, ++N	+++A, ++O, +N	++++A, ++++O, ++N	18+A, +++O, 43+N	12+A, 10+O, 5+N
AAV9	A/O/N	VS	+++A, ++++N	+++	+++	++++	++++	+++A, ++++N	++++A, +++N	+++	++	+++	+++B, +++G, ++++P	+++A, +++N	++++A, +++O, ++N	+++A, ++O, +N	++++A, +++O, ++N	16+A, +++O, 39+N	11+A, 8+O, 5+N
AAV8	A/O/N	VS	++A, +++N	+++	++	+++	++	++++A, ++N	+++A, ++N	++	++	+++	++++B, +++G, ++P	+++A, +N	++++A, +++O, ++N	+++A, ++O, +N	++++A, +++O, ++N	16+A, +++O, 27+N	11+A, 8+O, 5+N
AAV7	A/O/N	VS	++A, +++N	+++	++	+++	++	+++A, ++N	+++A, ++N	++	++	++	++++B, ++G, ++P	+++A, +++N	+++A, ++O, +N	++A, ++O, +N	+++A, ++O, +++N	15+A, +++O, 29+N	8+A, 6+O, 5+N
AAV.rh43	A/O/N	VS	+++A, +++N	++	++	+++	++	++A, +++N	+++A, +N	++	+++	++	+++B, ++G, ++P	+++A, ++N	+++A, ++O, +N	+++A, ++O, ++N	+++A, +++O, ++N	14+A, ++O, 27+N	9+A, 7+O, 5+N
AAV.rh39	A/O/N	VS	++A, +++N	+++	++	+++	+++	+++A, ++N	+++A, ++N	++	++	++	+++B, ++G, +++P	+++A, +++N	+++A, ++O, ++N	++A, ++O, +N	+++A, +++O, ++N	14+A, +++O, 29+N	8+A, 7+O, 5+N
AAV6.2	A/O/N	VS	+A, ++N	+++	+	++	++	++A, +N	++A, +N	++	++	+	+++B, ++G, ++P	++A, ++N	++A, +O, ++N	+A	+++A, +O, +N	10+A, ++O, 20+N	6+A, ++O, +++N
AAV6	A/O/N	VS	+A, ++N	++	++	++	++	++A, +N	++A, +N	+	++	+	+++B, ++G, ++P	++A, ++N	++A, +O, +N	+A	++A, +O, +N	10+A, ++O, 20+N	5+A, ++O, ++N
AAV1	A/O/N	VS	+A/N	+	-	+	+	++A, +N	+A	+	++	+	+B, +G, +P	++A, ++N	++A, +N	++A, +N	++A, +N	7+A, +O, 12+N	6+A, +++N
AAV2	N only	W	+N	-	+	+	++	+N	+N	+++	+	-	+G, +P	+N	+N	+N	+N	14+N	+++N
AAV5	-	VW	-	-	-	-	-	-	-	-	-	-	-	-	-	-	-	-	-

Scoring: (−) no transduction, (+) very few positive cells, (++) some positive cells, (+++) many positive cells, (++++) large areas of positive cells, (+++++) saturated with positive cells
OB=Olfactory Bulb, CC= Corpus Callosum, CP=Caudal-Putamen, SNR= Substantia Nigra, MB= Mid-brain

Cell type, A=Astrocyte, N=Neuron, O=Oligodendrocyte
Cerebellar, G=Granulocyte, P= Purkinje Cells, B=Bergmann glia
Blood Vessel, VW=Very Weak, W=Weak, S=Strong, VS=Very Strong

Figure 2.8 Motor neuron transduction patterns of different rAAVEGFPs in the lumbar spinal cords of adult mice.

rAAVvectors were injected into the tail vein of 10-week-old mice at 4×10^{12} genome copies per mouse. Staining for EGFP was carried out as described in Figure 1 legend. Shown are the compilation of high-magnification images of central nervous system (CNS) cell transduction and their corresponding locations in a low-magnification view Bars, 20μm.

Figure 2.8 Motor neuron transduction patterns of different rAAVEGFPs in the lumbar spinal cords of adult mice.

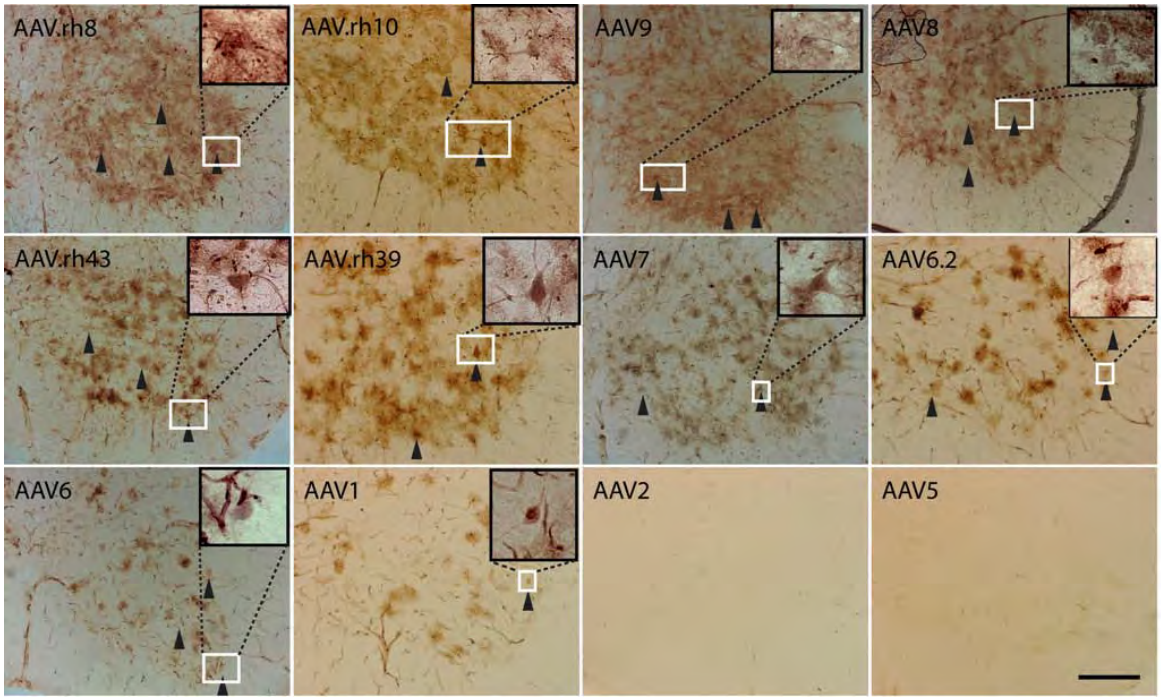

Figure 2.9 Transduction profiles of various neuronal populations by rAAVrh.8. rAAVrh.8 vectors were injected into the tail vein of 10-week-old mice at 4×10^{12} genome copies per mouse. Staining for EGFP was carried out as described in Figure 1 legend. Shown are the compilation of high-magnification images of central nervous system (CNS) cell transduction and their corresponding locations in a low-magnification view at bregma -2.00 mm (a–i) as well as some other clinical relevant brain regions (i.e., olfactory bulb (OB), substantia nigra (SN), and lateral septal nucleus (LSN) and cerebellum) that were not present in the lower magnification view of the selected brain section. CC, corpus callosum; CA2, CA2 region of hippocampus; DG, dentate gyrus; PC, piriform cortex. Scale bars in a, c, h = 10μm; in d, f, i = 15μm, and b, e, g = 20μm.

Figure 2.9 Transduction profiles of various neuronal populations by rAAVrh.8.

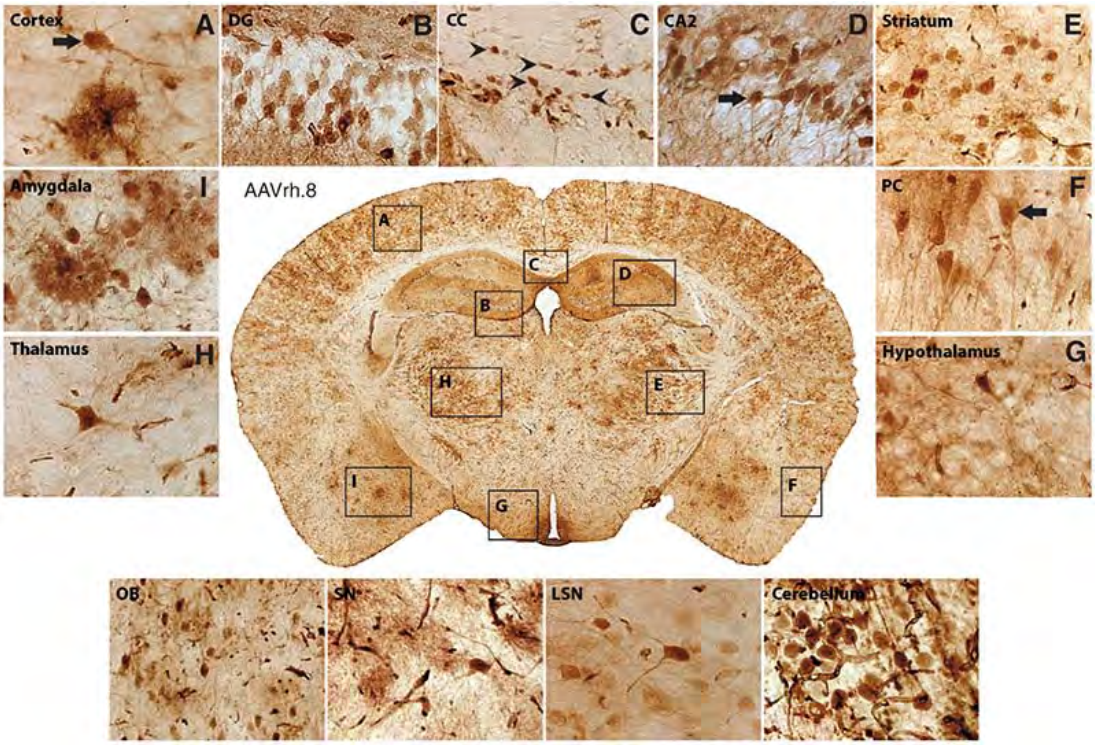

Figure 2.10 Regional transduction patterns of rAAVs in the adult mouse brains. rAAV vectors were injected into the tail vein of 10-week-old mice at 4×10^{12} genome copies per mouse. Staining for EGFP was carried out as described in Figure 1 legend. Shown is the compilation of low-magnification images of central nervous system (CNS) regions. Bars = 20μm.

Figure 2.10 Regional transduction patterns of rAAVs in the adult mouse brains.

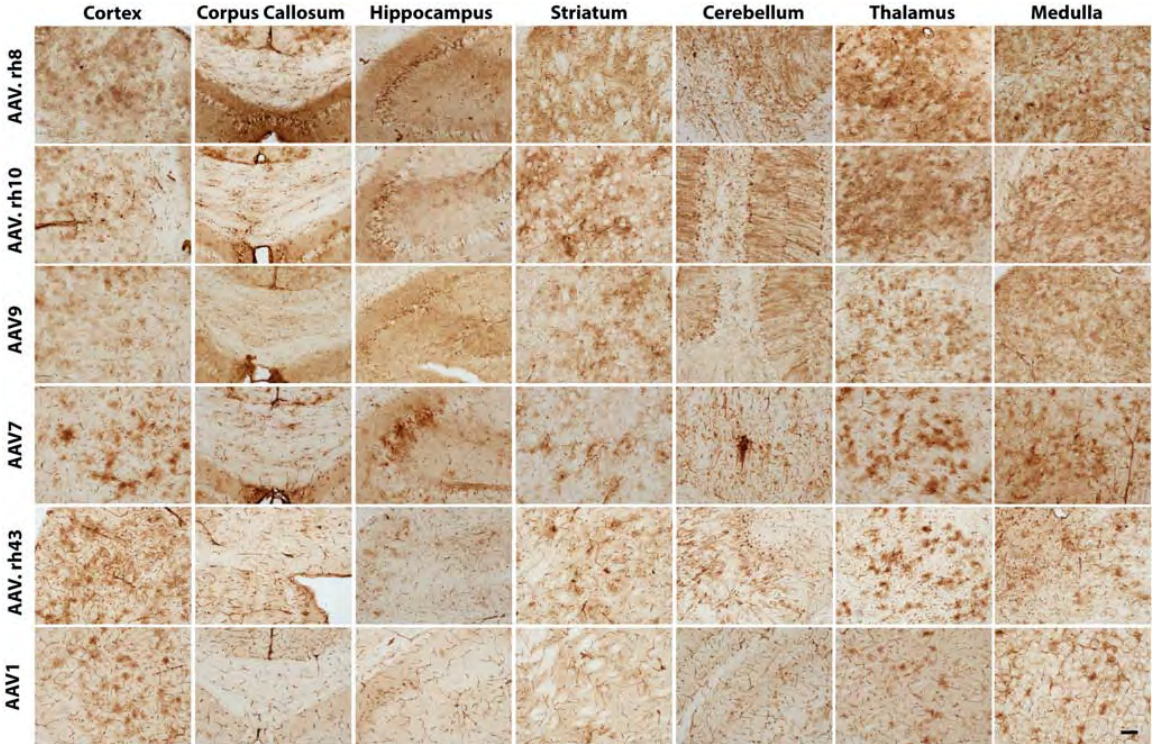

Figure 2.11 Transduction profiles of various neuronal populations by rAAVrh.10 and 9. rAAVvectors were injected into the tail vein of 10-week-old mice at 4×10^{12} genome copies per mouse. Staining for EGFP was carried out as described in Figure 1 legend. Shown is the compilation of high-magnification images of central nervous system (CNS) regions. Bars = 20μm.

Figure 2.11 Transduction profiles of various neuronal populations by rAAVrh.10 and 9.

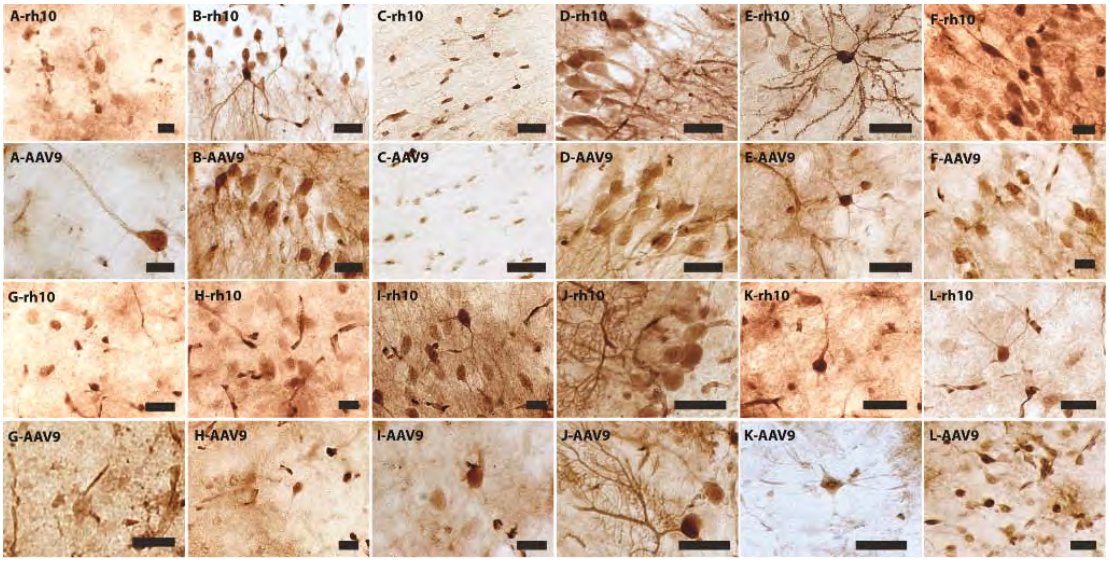

Figure 2.12 Choroid plexus transduction pattern of different I.V. delivered rAAV serotypes in mouse. rAAV vectors were injected into the tail vein of 10-week-old mice at 4×10^{12} genome copies per mouse. Staining for EGFP was carried out as described in Figure 1 legend. Shown is the compilation of low-magnification images of the choroid plexus above the third ventricle. Bars = 20μm.

Figure 2.12 Choroid plexus transduction pattern of different I.V. delivered rAAV serotypes in mouse.

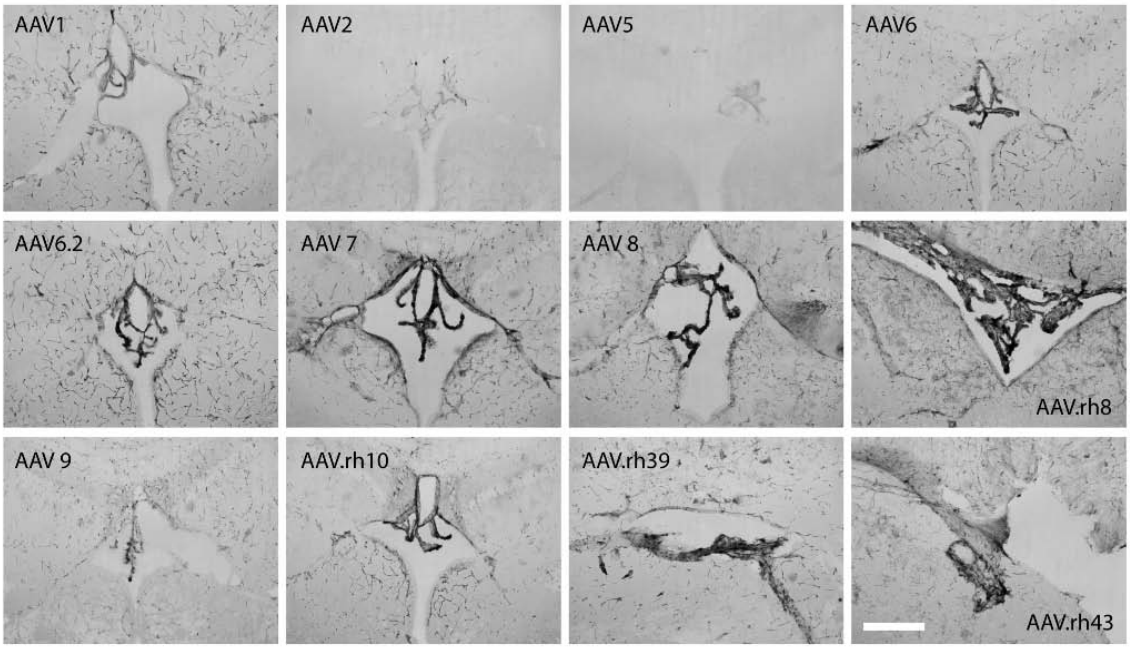

Intravenous rAAV administration leads to transduction of different cell types in the CNS

<u>*Neonatal injections*</u>: To confirm the identity of transduced cells in different regions of the CNS, we performed double immunofluorescent staining with antibodies against EGFP and NeuN (generic neuronal marker), glial fibrillary acid protein (GFAP; astrocyte marker), calbindin-D28K (Purkinje cell marker), choline acetyl transferase (ChAT; motor neuron marker), and tyrosine hydroxylase (TH; marker of dopaminergic neurons) [Figure 2.13]. The immunostaining results showed that a large number of NeuN positive cells expressed EGFP throughout the mouse brain, which indicated widespread neuronal transduction. The regions with high density of transduced neurons included striatum, hippocampus, cortex, and hypothalamus. rAAVrh.10, rAAV9, rAAV7, and rAAVrh.39 vectors are very efficient in mediating neuronal transduction, followed by rAAV6.2, rAAV1, and rAAV6 [Figures 2.2 & 2.13]. The most abundant transduced cells throughout the CNS were the GFAP-positive astrocytes with small cell bodies and highly ramified processes [Figure 2.13]. The calbindin-D28K immunostaining confirmed the identity of a large number of transduced cells in the cerebellum as Purkinje cells, with robust EGFP expression in both cell body and their tree-like processes [Figure 2.13]. The rAAVs proficient in transducing Purkinje cells include: rAAVrh.10, rAAV9, rAAVrh.39, rAAV7, rAAV6.2, and rAAVrh.43. rAAV1 and rAAV6 only transduced a small portion of Purkinje cells with low EGFP intensity [Figure 2.2]. Transduction of motor neurons was confirmed by the presence of large EGFP+/ChAT+ cells in the ventral spinal cord for several rAAV vectors [Figure 2.13]. rAAVrh.10, rAAV9, rAAV7, rAAVrh.39

showed comparable high efficiency transduction of motor neurons [Figure 2.3]. TH+ dopaminergic neurons in the substantia nigra were also transduced [Figure 2.13].

Adult injections: The group 1, 2, and 3 vectors transduce multiple cell types and various neuronal populations in the CNS. To identify the cell types that the vectors transduce, we first carried out morphological analysis on the CNS tissue sections stained for GFP. By high-magnification microscopy, we observed extensive transduction of neurons, astrocytes, and oligodendrocytes in various areas of the CNS [Figures 2.7, 2.8, 2.9, 2.10 & 2.11]. For example, the group 1 vectors transduced granular cells in dentate gyrus [Figure 2.9b, 2.10 & 2.11b], pyramidal neurons in CA2 [Figure 2.9d, 2.10 & 2.11d], medial spiny neurons and astrocytes in striatum [Figure 2.9e, 2.10 & 2.11e], Purkinje neurons in cerebellum [Figure 2.9, 2.10 &2.11j], neurons and astrocytes in thalamus [Figure 2.9h, 2.10 & 2.11h], hypothalamus [Figure 2.9g & 2.11g], amygdala [Figure 2.9i & 2.11i], layer 3–6 of the cortex [Figure 2.9a, f, 2.10 & 2.11a, f], substantia nigra [Figure 2.9 & 2.11k] and lateral septal nucleus (LSN) [Figure 2.9h & 2.11l]. Additionally, they also transduced oligodendrocytes in corpus callosum [Figure 2.9c, 2.10 & 2.11c]. A similar cellular transduction pattern was also observed for group 2 and 3 vectors, albeit that the density of transduced cells was lower than group 1 vectors [Figures 2.5, 2.6 & 2.10].

To verify the transduced cell types, we performed double fluorescence staining on the rAAVrh.8-treated CNS tissues. Using markers for specific cell types, including NeuN for neurons, glial fibrillary acidic protein for astrocytes, adenomatous polyposis coli for

oligodendrocytes, Iba1 for microglia, and CD31 for blood vessels, we verified that EGFP was expressed in neurons, astrocytes, oligodendrocytes, and blood vessels but not in microglia [Figure 2.14].We also verified EGFP expression in several specific neuronal subpopulations, including Purkinje cells (calbindin), motor neurons (ChAT), medial spiny neurons (Darpp-32), and dopaminergic neurons (tyrosine hydroxylase) [Figure 2.15].

Intravenous administration of AAV vectors in neonates mediated robust transduction in ventricles and brain blood vessels

Strong EGFP expression was observed in choroid plexus cells in lateral, 3rd and 4th ventricles of the animals infused with rAAVrh.39, rAAVrh.10, rAAVrh.43, rAAV7, and rAAV9 (ranked by transduction efficiency) [Table 2.1 & Figure 2.16]. Ependymal cells lining the ventricles were also transduced. An interesting observation was an apparent gradient with the highest number of eGFP transduced cells in periventricular regions and progressively lower numbers with increasing distance from the ventricles. This was more obvious around the 3rd and 4th ventricles than the lateral ventricles [Figure 2.16]. Extensive EGFP signal was also found associated with blood vessels throughout the brain and spinal cord. This was verified by dual immunofluorescence staining for EGFP and a blood vessel endothelium specific marker, CD34. [Figure 2.17a & b]. Unlike the distinct rAAV transduction profiles in different regions of the brain parenchyma, the EGFP transduction of blood vessels throughout the CNS seemed to be quite uniform for any given vector.

Intravenous injection of AAV vectors did not cause microgliosis in neonates

Brain sections were stained for microgial cells using Iba1. Iba-1-positive cells in the brain of rAAVrh.10-infused mice were comparable to PBS-injected mice [Figure 2.18]. This result suggested that intravascularly delivered rAAVs do not cause sustained inflammation in the CNS of mice 3 weeks after the injection of P1 neonates. However, it remains to be determined if facial vein injection of rAAVs caused any acute microgliosis in the CNS at the neonatal stage since the present analysis was performed 3 weeks later.

rAAVrh.8 injections result in reduced peripheral tissue dissemination in adult mice

In addition to strong and widespread transduction in the CNS, low peripheral tropism is an important property of an ideal viral vector for systemically delivered CNS-targeted gene therapy. To characterize biodistribution profiles of intravenous delivered rAAV in various tissues of the injected mice, qPCR quantification of rAAV genomes was carried out for the group 1 vectors in brain, spinal cord, lung, kidney, pancreas, skeletal muscle, heart, and liver tissues [Figure 2.19a]. Persistent rAAVrh.8 genomes were similar in amounts to those of rAAV9 and rAAVrh.10 in the brain but significantly lower in the liver. To assess the degree of transduction in the brain relative to peripheral tissues, we calculated ratios between the genome copies in the brain and periphery. There was no significant difference between the vectors in the group 1 probably due to a high degree of variation among the injected animals [Figure 2.19b]. Nevertheless, we observed a trend toward relatively high CNS transduction over the periphery for rAAVrh.8 compared with rAAVrh.10 and rAAV9.

Figure 2.13 Analysis of transduced cell phenotype in mouse CNS after neonatal intravascular delivery of rAAVs.

Forty micrometer thick sections of brain and spinal cord from AAV-injected mice were stained for immunofluorescence using antibodies against EGFP and cell-type specific markers for neurons [neuronal-specific marker (NeuN)], astrocytes [glial fibrillary acid protein (GFAP)], cerebellar Purkinje cells (calbindin-D-28k), spinal cord motor neurons [choline acetyl transferase (ChAT)], and dopaminergic neurons in the sustantia nigra [Tyrosine hydroxylase (TH)]. All rAAVs were examined, but for each cell type, only one representative picture is shown. Scale bars sizes are indicated in each picture. AAV, adeno-associated virus; CNS, central nervous system.

Figure 2.13 Analysis of transduced cell phenotype in mouse CNS after neonatal intravascular delivery of rAAVs.

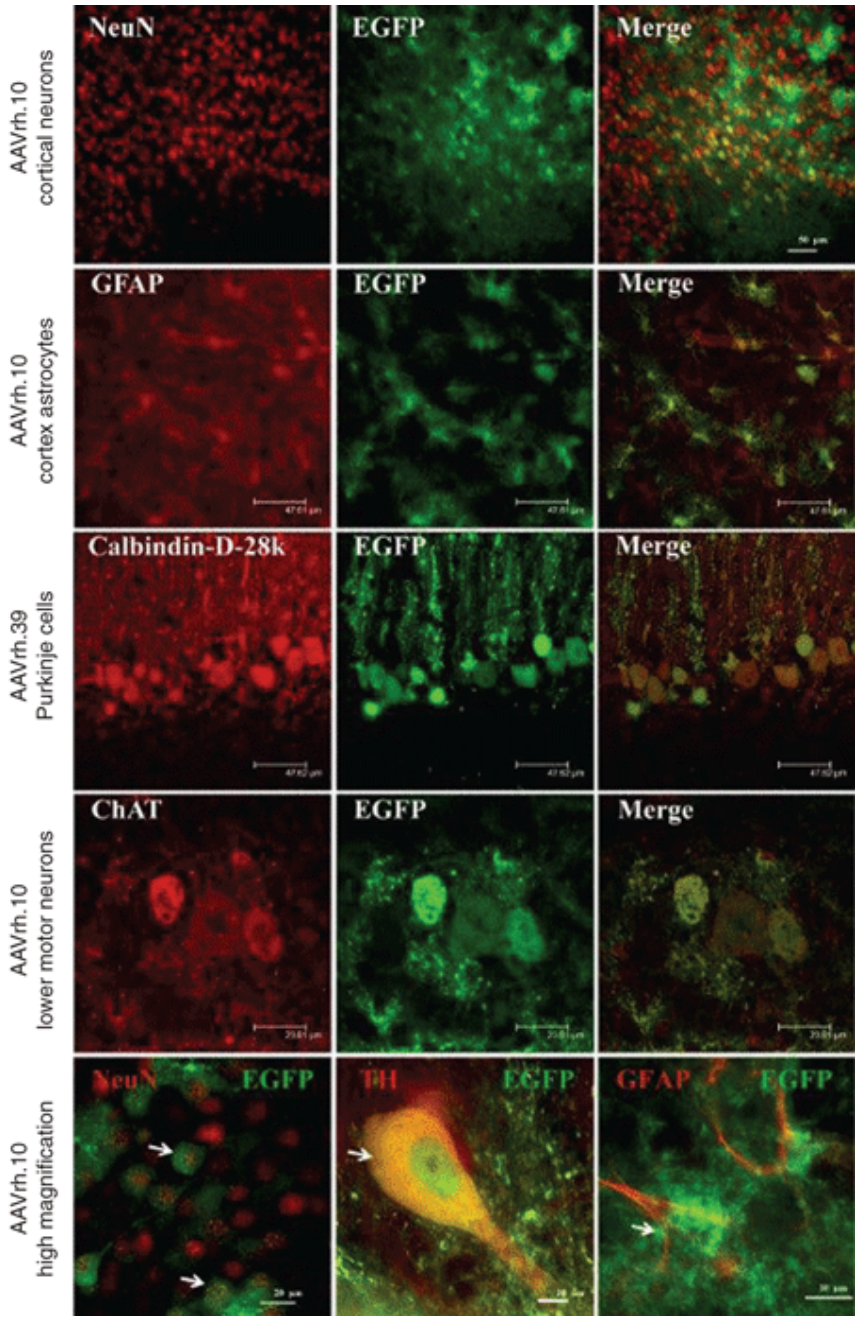

Figure 2.14 Identification of cell types transduced in the CNS of adult mice injected with rAAVrh.8EGFP. Sections were stained with antibodies against EGFP, NeuN (neurons), GFAP (astrocytes), APC (oligodendrocytes), Iba1 (microglia), CD31 (blood vessels). Objective ×60. Bar = 20 µm. APC, adenomatous polyposis coli; GFAP, glial fibrillary acidic protein.

Figure 2.14 Identification of cell types transduced in the CNS of adult mice injected with rAAVrh.8EGFP.

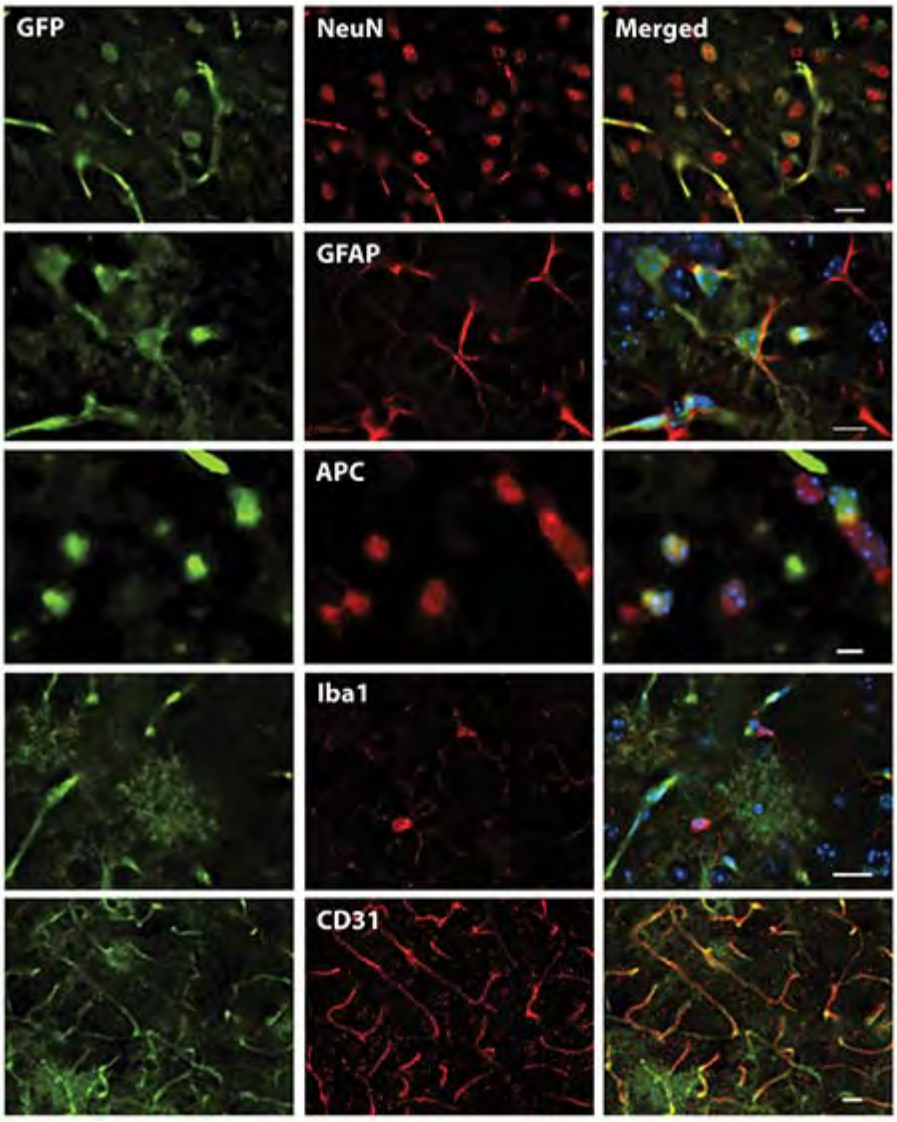

Figure 2.15 Identification of neuronal populations transduced in the CNS of adult mice injected with rAAVrh.8EGFP Sections were stained with antibodies against EGFP, calbindin (Purkinge cells); ChAT (Motor neurons); Darpp32 (medial spiny neurons) and TH (dopaminergic neurons Objective ×60. Bar = 20 µm. ChAT, Choline acetyl trasnferase; TH, Tyrosine hydroxylase.

Figure 2.15 Identification of neuronal populations transduced in the CNS of adult mice injected with rAAVrh.8EGFP.

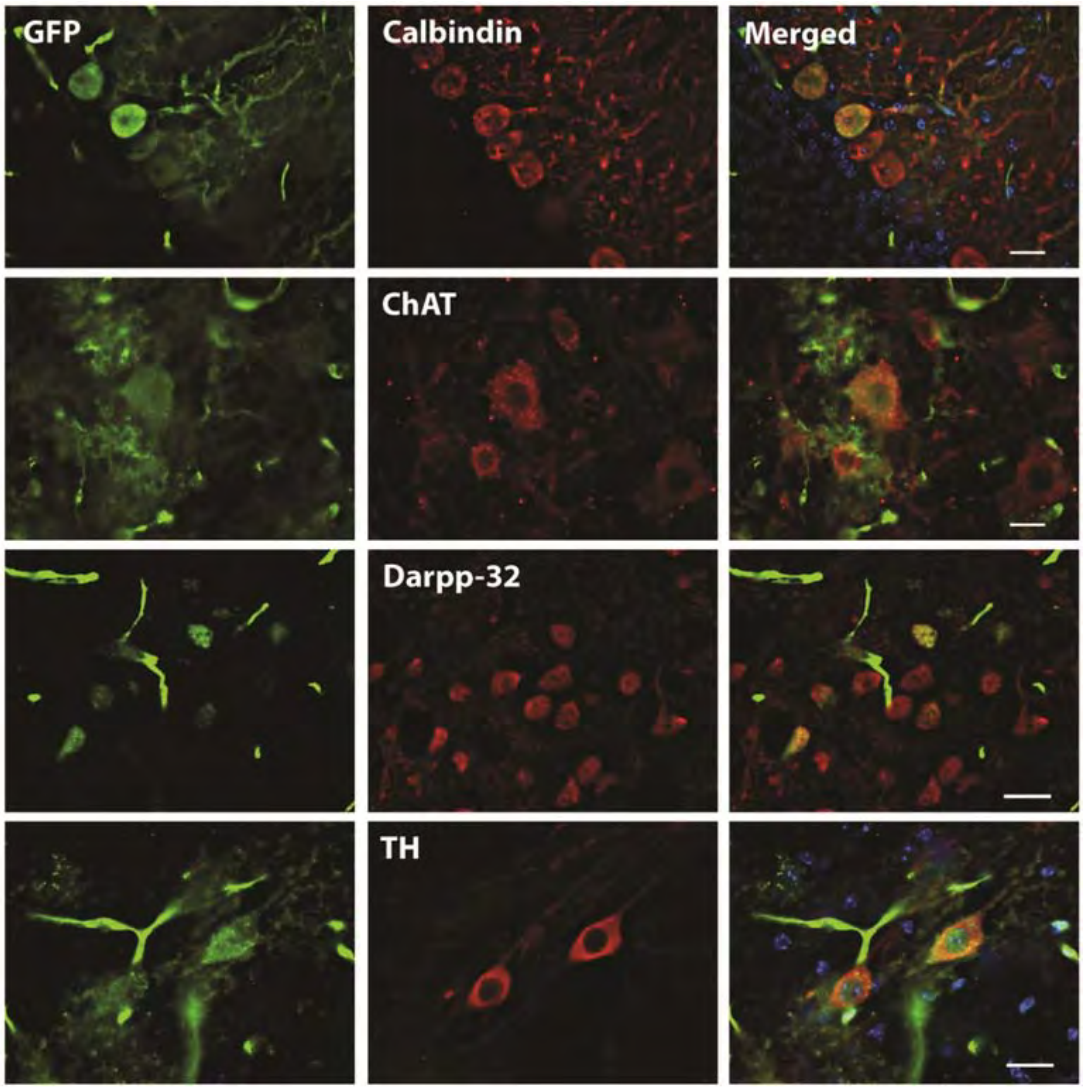

Discussion

Though it is well documented that intravascular-delivered rAAVs are excellent vectors for CNS gene therapy in neonatal animals (Foust et al., 2009; Rahim et al., 2011), there is no comprehensive characterization of such vectors. We characterized the CNS transduction profile of 10 different rAAV vectors delivered by intravascular infusion in neonatal mice and found eight out of ten rAAVs can cross the BBB and mediate gene transfer to the neonatal mouse CNS with varying degrees of efficiency [Figures 2.1, 2.2 & 2.3 and Table 2.1]. After systemic administration, rAAVrh.10, rAAVrh.39, rAAVrh.43, and rAAV9 are the most effective rAAVs with similar transduction capabilities and cellular tropism, as assessed by overall EGFP expression in the CNS. Specifically, a number of regions in the mouse CNS, including striatum, hippocampus, cortex, hypothalamus, cerebellum, medulla, and cervical spinal cord, all revealed substantial EGFP expression. In addition, rAAV6.2 and rAAV7 were also very effective, but the efficiencies of EGFP transduction in the targeted regions were consistently lower than those obtained with the four top vectors. Still further down the spectrum were rAAV1 and rAAV6, which did achieve some CNS transduction, but their efficiency was quite low. Finally, rAAV2 and rAAV5 revealed little or no CNS gene delivery after systemic administration [Table 2.1]. It is worth noting that native EGFP expression was clearly detectable in brain and spinal cord sections for most of the rAAVs without immunostaining, which further demonstrates the robustness and extensiveness of CNS transduction in our study [Figure 2.20].

In addition to the global delivery properties of several rAAVs described above, some rAAVs showed unique transduction profiles in the CNS. For instance, rAAV1 primarily transduced granule cells in the cerebellum, while rAAV6 and rAAV6.2 mostly transduced Purkinje cells, and yet others transduced both [Figure 2.2]. This suggests that once across the BBB, the rAAVs display different tropisms, which can be attributed to the capsid given that the vector genome used in all vectors was the same.

The situation however would be different in adult mice where intravenous injected rAAVs would generate limited CNS transduction due to the advanced BBB development (Fu et al., 2003; Manfredsson et al., 2009). We demonstrate that several rAAVs are capable of crossing the BBB efficiently following intravenous injection in adult animals using a semiquantitative scoring system (Cearley et al., 2008). We do, however, recognize that this system has disadvantages in assessing absolute differences between serotypes and more extensive quantitative analyses are needed. Another caveat of this study is the number of animals per group (n = 3). Although, three to four animals per group are widely used to evaluate the transduction efficiency of rAAV (Cearley and Wolfe, 2006; Fu et al., 2003; Gray et al., 2011; Zincarelli et al., 2008), animal-to-animal variations even with inbred animals may influence the final results. To minimize this possibility, we exclusively injected male mice. Despite the limitations of the method, the semiquantitative characterization provides useful reference points for the future use of these AAV serotypes for intravenous delivery.

Figure 2.16 Efficient transduction of brain ventricular structures after intravascular delivery of rAAVs in neonatal mice. The choroid plexus appears to be transduced at high efficiency for multiple rAAV. Bars = 100 μm.

Figure 2.16 Efficient transduction of brain ventricular structures after intravascular delivery of rAAVs in neonatal mice.

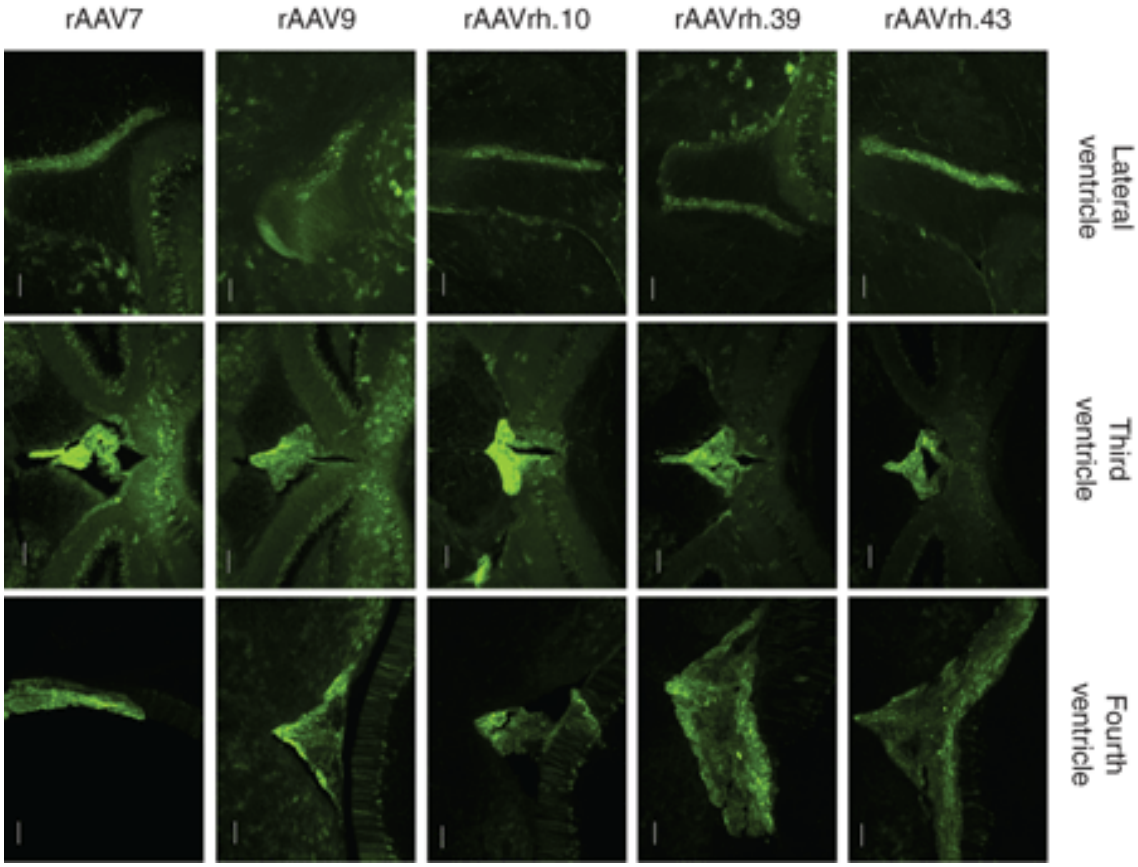

Figure 2.17 Transduction of the brain capillary vessels by intravascularly delivered rAAVs. Sections were stained with antibodies against EGFP to show staining of blood vessels. Lower panel shows representative brain section showing specificity of staining by using antibodies against both eGFP and CD34 (blood vessels). Objective ×60. Bar = 20 μm.

Figure 2.17 Transduction of the brain capillary vessels by intravascularly delivered rAAVs.

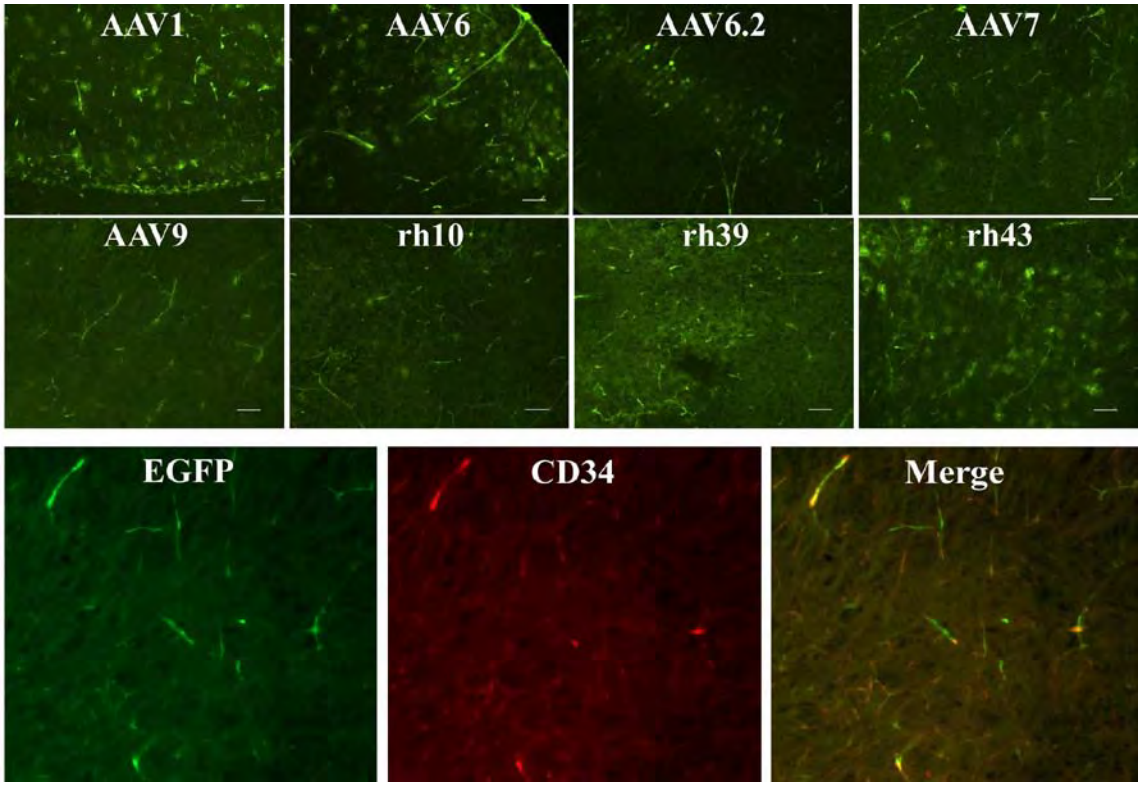

Figure 2.18 Evaluation of microgliosis in mice brain after systemic delivery of rAAVs to P1 neonates. Forty micrometer brain sections were stained with antibodies against Iba1 for microgliosis (blood vessels). Objective ×60. Bar = 20 μm.

Figure 2.18 Evaluation of microgliosis in mice brain after systemic delivery of rAAVs to P1 neonates.

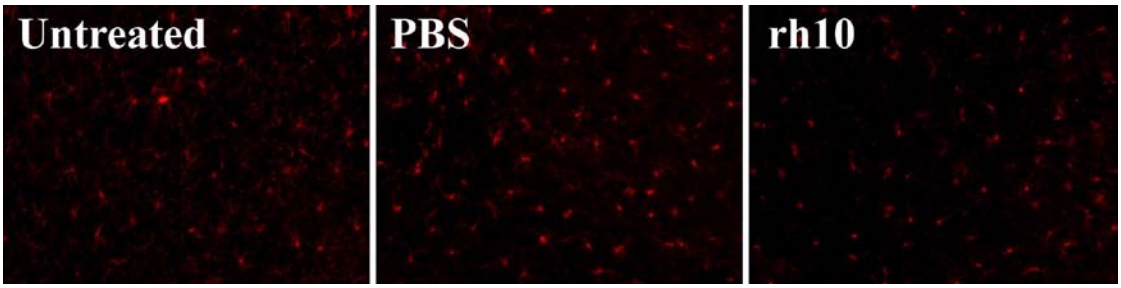

Figure 2.19 Biodistribution Profiles in mice. (a) Biodistribution profiles of rAAVEGFPs in the adult mice after intravenous injections. Persistent rAAV-EGFP vector genomes in eight different tissues of rAAV-treated mice were quantified by quantitative polymerase chain reaction using primers/probe set targeting poly A region of the vector genome (n = 3). (b). Ratios of vector genomes detected in the brains to those in the liver, heart, lung, and pancreas tissues respectively (n = 3). ****$P < 0.0001$. ns, not significant.

Figure 2.19 Biodistribution Profiles in mice.

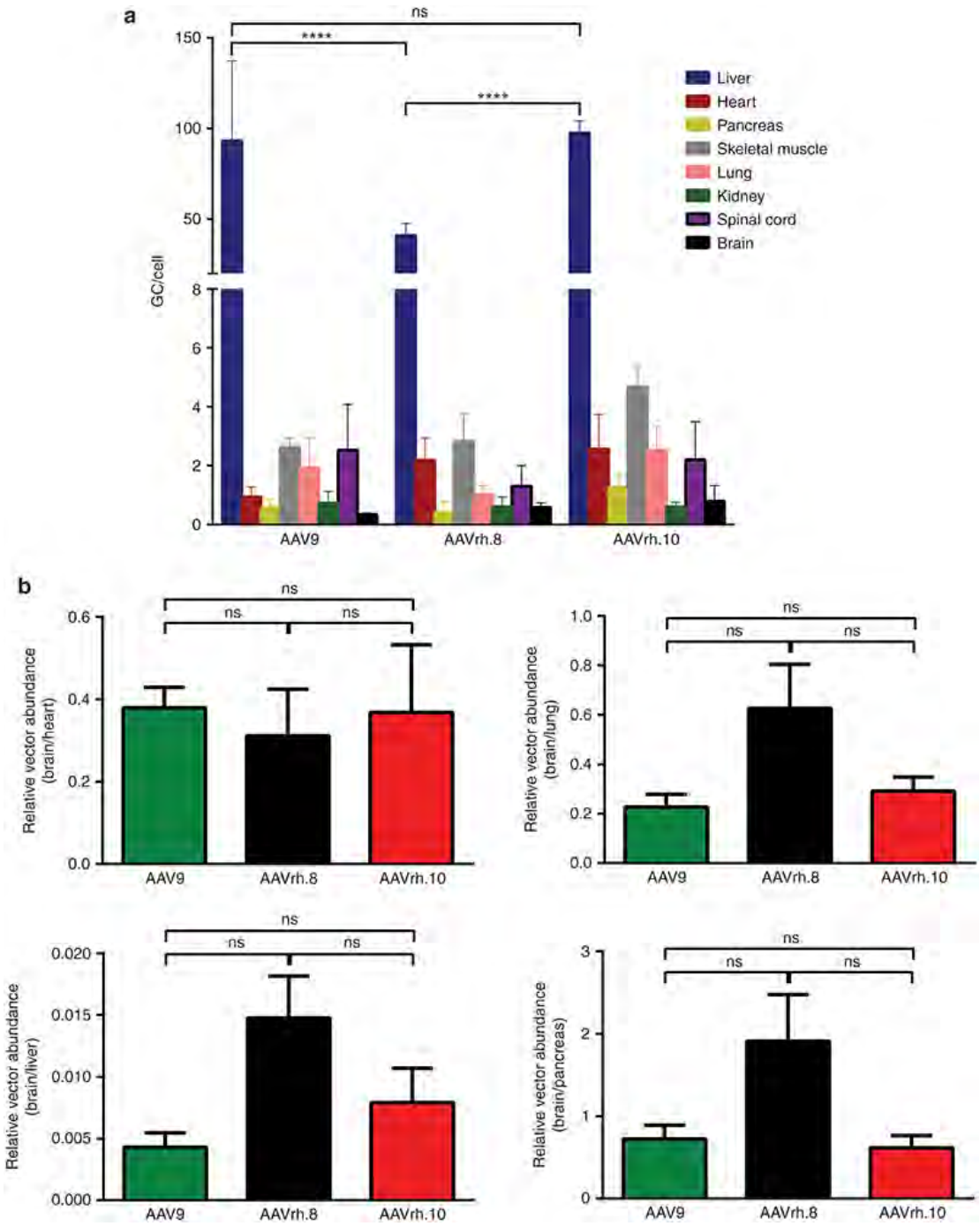

Figure 2.20 Native EGFP expression in mice CNS after systemic delivery of rAAVs to P1 neonates. Neonatal P1 pups received 4×10^{11} GCs of rAAVs and EGFP expression analyzed at 21 days post-injection. Forty micron thick cryosections were mounted on slides and EGFP expression observed without immunostaining. The exposure times for each image are indicated**.**

Figure 2.20 Native EGFP expression in mice CNS after systemic delivery of rAAVs to P1 neonates.

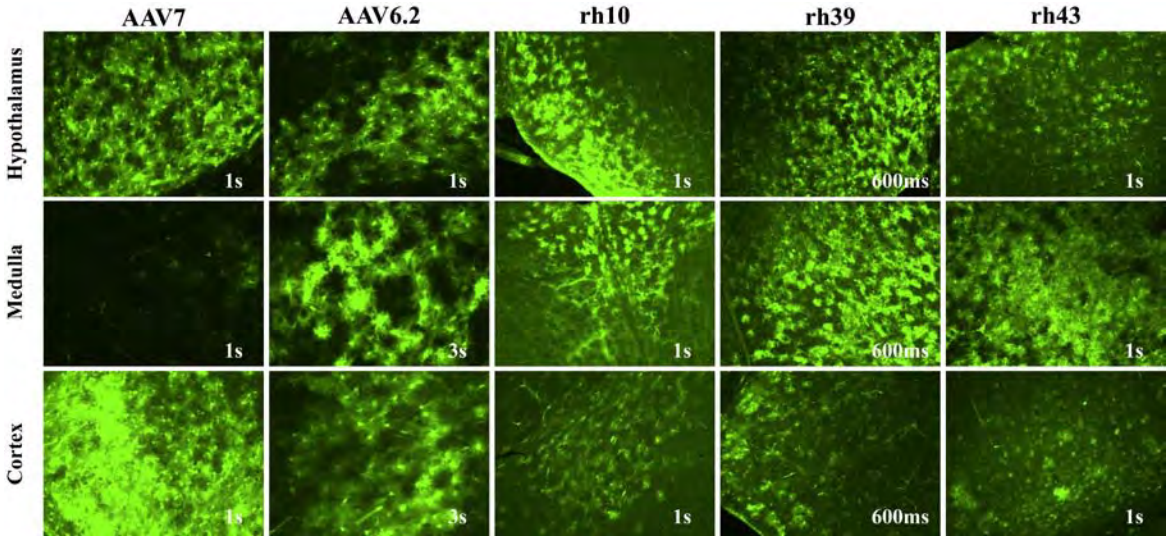

Of all the rAAV serotypes tested in adult animals, the most robust in crossing the BBB are the group 1 vectors consisted of rAAV8, rh.10, and 9 [Figures 2.5, 2.6, 2.7 & Table 2.2]. Although less robust than the group 1 vectors, the group 2 vectors, consisted of rAAV8, 7, rh.43, and rh.39, also show strong capability of transducing cells in broad CNS areas following intravenous injection. These results suggest that the group 1 and group 2 vectors achieve similar results and expand the repertoire to be used as alternative vectors to deliver therapeutic genes for treating CNS diseases via intravenous injection.

Among the top vectors, one that particularly stands out is the rAAVrh.8. With its global and robust transduction of the CNS cells, rAAVrh.8 consistently ranked first in broad CNS areas and in different cell populations [Figure 2.7]. A particularly attractive feature for rAAVrh.8 is its naturally lower peripheral tissue dissemination than other vectors, particularly in the liver [Figure 2.19], which enhances the safety profile of systemic gene delivery to the CNS. These qualities suggest that rAAVrh.8 is a top candidate vector for the treatment of the CNS diseases that afflict broad areas of the CNS.

The robust transduction of the CNS cells following intravenous injection is a surprising but useful character of some rAAV vectors. How these rAAVs cross the BBB remains elusive (Daya and Berns, 2008; Di Pasquale et al., 2003; Manfredsson et al., 2009). The fact that different AAV serotypes can efficiently transduce brain capillary endothelial cells, neurons, and astrocytes in neonatal animals strongly suggest that these vectors are able to extravasate from the circulation and reach the CNS parenchyma, possibly by crossing the BBB (Wolburg and Paulus, 2010). Our results in adult animals

suggest two possible routes for the rAAVs to enter and transduce the CNS. First, the rAAVs may cross the BBB by exploiting the fenestrated capillary vessels of circumventricular organs (Duvernoy and Risold, 2007). This is supported by the fact that we consistently observed strong EGFP expression in or near circumventricular organs such as the choroid plexus, ventricles [Figures 2.12 & 2.16] specially the third ventricle [Figure 2.10] and ependymal cells (e.g., see ventricle below corpus callosum in the rAAVrh.43 and rAAVrh.10 panels in Figure 2.10]. The second possibility is direct transcytosis of rAAVs via the innermost layer of blood vessels (Di Pasquale et al., 2003). In the neonatal study too, choroid plexuses and their surrounding parenchymal tissue were efficiently transduced. In addition, there was an apparent gradient of EGFP intensity from periventricular (higher) to deep parenchymal (lower) tissue. These observations suggest an alternate route for AAV entry into the neonatal murine CNS through the choroid plexus (Wolburg and Paulus, 2010), followed by widespread distribution via CSF and/or interstitial fluid flow to transduce neuronal and glial cells. Perivascular astrocytes have been shown to regulate the tightness and exchange of molecules across the BBB (Abbott et al., 2006; Janzer and Raff, 1987). Therefore, the presence of intensely stained blood vessels and their surrounding astrocytes suggest that rAAVs use this second route of entry into the CNS [Figures 2.14 & 2.17]. Further studies will be needed to understand the transduction mechanism of rAAVs.

In summary, our study has revealed that many rAAVs are capable of crossing the BBB and transducing the CNS cells in both neonates as well as in adults. Of these, the group 1 vectors, including rAAVrh.8, rAAVrh.10, and rAAV9 have demonstrated the

strongest capacity for transducing CNS cells after the systemic intravenous injection. Importantly, rAAVrh.8 appears superior to its group 1 peers in its global CNS transduction and decreased peripheral tissue targeting, and thus, is currently the best option for delivering CNS gene therapy via intravenous injection in adult animals.

CHAPTER III: A SINGLE INTRAVENOUS rAAV INJECTION AS LATE AS P20 ACHIEVES EFFICACIOUS AND SUSTAINED CNS GENE THERAPY IN CANAVAN MICE

The following chapter contains the manuscript**:**

Ahmed SS, Li H, Cao C, Sikoglu EM, Denninger AR, Su Q, Eaton S, Liso Navarro AA, Xie J, Szucs S, Zhang H, Moore C, Kirschner DA, Seyfried TN, Flotte TR, Matalon R, Gao G.(2013) A single intravenous rAAV injection as late as P20 achieves efficacious and sustained CNS Gene therapy in Canavan mice. Molecular Therapy Dec; 21(12):2136-47 [PMID: 23817205].

The study was devised and results were interpreted by me under the supervision of Dr Gao. All experiments except for the ones listed below have been performed by me. Figure 3.2c was prepared by Dr Huapeng Li. Figures 3.2 f,g and were prepared by Dr Elif Sikoglu, Ana Navarro and Dr Constance Moore while data for Figures 3.3c, d was provided by them; figures were analyzed and assembled by me. Figure 3,2 h was provided by Sylvia Szucs. Figure 3.6 c, d , Fig 3.7, Tables 3.1 and 3.2 were contributed by Dr Thomas Seyfried and Samuel Eaton. Figure 3.8 was contributed by Andrew Denninger and Dr Daniel Kirschner. Viral vectors were made by Qin Su. CD mice were provided by Dr Reuben Matalon. Electron Microscopy was done by the EM Core at UMass Medical School. The manuscript was prepared by me and Dr Gao.

CHAPTER III: A Single Intravenous rAAV Injection as Late as P20 Achieves Efficacious and Sustained CNS Gene Therapy in Canavan Mice

Introduction

Canavan disease (CD) is a rare lethal pediatric leukodystrophy characterized by extensive demyelination, edema, and progressive spongy degeneration of the central nervous system (CNS) (Van Bogaert L, 1949). Currently, there is no effective treatment. Clinical symptoms include blindness, severe psychomotor retardation and early death (Beaudet, 2001; Matalon and Michals-Matalon, 2000; Traeger and Rapin, 1998). CD is caused by autosomal recessive mutations in aspartoacylase (AspA) (EC 3.5.1.15) (Kaul et al., 1993; Matalon et al., 1988); an enzyme that deacetylates N-acetyl aspartic acid (NAA) to produce aspartic acid and acetate (Baslow and Resnik, 1997; Birnbaum et al., 1952). Since the NAA accumulates mainly in the urine, NAA aciduria provides a unique biomarker for CD (Matalon et al., 1988).

The first AspA knockout mouse strain was engineered by an insertional interruption in exon 4 of the AspA gene. These mice, also known as CD mice, have a short lifespan (<4 weeks), hydrocephaly, NAA aciduria, extensive white matter vacuolation and motor dysfunction providing a bona-fide model to study the severest forms of CD (Matalon et al., 2000). In addition, there is a naturally occurring CD model, called tremor rat with a large deletion spanning four genes including AspA as well as two other more recently created mouse models, all of which have less severe phenotypes and near normal lifespans (Kitada et al., 2000; Mersmann et al., 2011; Traka et al., 2008).

Gene replacement therapy is a promising clinical intervention for inborn errors like CD. Novel recombinant adeno associated viruses (rAAVs) derived from primates represent a promising gene delivery platform because of their wide range of tissue tropism, low immunogenicity, highly efficient and sustained gene transduction, and clinically proven track record in safety (Gao et al., 2002; Mingozzi and High, 2007). In an earlier gene therapy attempt for CD, 23 patients were treated with multiple-site intracranial injections of the first-generation rAAV2 (Janson et al., 2002). A follow-up study on 13 of these patients revealed the safety of rAAV-mediated therapeutic gene transfer to the CNS over a decade. The treatment resulted in slight reductions of NAA levels in some brain regions; but importantly, it indicated the necessity of early intervention in CD patients. This study also suggests that a global CNS gene transfer is necessary for alleviating widespread neuropathology in CD patients (Leone et al., 2012).

Thus, one potentially viable strategy for CD gene therapy to target the CNS globally is through intravenous (IV) gene delivery using novel rAAVs that can cross the blood-brain barrier (Foust et al., 2009). Based on the initial report on rAAV9, our expanded vector characterization study in neonatal mice as well as preliminary results from a separate comprehensive study to screen rAAVs for IV gene delivery to adult CNS (Yang et al., 2014; Zhang et al., 2011), we selected rAAV9, rAAVrh.8, and rAAVrh.10 for our proof-of-concept gene therapy study. We also designed a therapeutic cassette containing microRNA-binding sites (miRNA-BS) to detarget rAAV expression from peripheral tissues to minimize potentially untoward consequences of IV delivery (Xie et al., 2010).

An interesting alternative is to use endogenous microRNAs (miRNAs) to suppress transgene expression outside the CNS. miRNAs are small, noncoding RNAs that regulate gene expression by post-transcriptional silencing. miRNAs silence genes by two mechanisms. When partially complementary to mRNA sequences, they typically reduce target mRNA stability and protein expression by two- to fourfold or less, probably to tune mRNA expression (Bartel, 2009). In contrast, when miRNAs are nearly perfectly complementary to their mRNA targets, they cleave the mRNA, triggering its wholesale destruction (Brennecke et al., 2005).

miRNA-binding sites were first used in lentiviral vectors to suppress transgene expression in hematopoietic cells, thereby attenuating transgene immunogenicity (Brown et al., 2006). The strategy was subsequently used to regulate naked DNA-mediated gene transfer, detarget oncolytic viral therapeutics from noncancer tissues to reduce host toxicity, and develop attenuated virus-based vaccines to reduce toxicity in recipients (Brown and Naldini, 2009). Since the systemic delivery of rAAVs may lead to possible off-target peripheral tissue expression, we explored the use of miRNAs to detarget rAAV9 expression both separately and concurrently in the liver, heart, and skeletal muscle, the three tissues most efficiently targeted by intravenously delivered rAAV9 (Pacak et al., 2006; Xie et al., 2010; Zincarelli et al., 2008). One consideration is that intravascularly administered rAAV for CNS-targeted transduction requires suppressing high levels of rAAV expression in multiple peripheral tissues even when transgene transcripts are successfully expressed in the brain (Xie et al., 2010). Hence in addition to such endogenous miRNA-regulated restriction of transgene expression, an expanded

repertoire of rAAV vectors with strong tropism for the CNS and reduced affinity for peripheral tissues would also be important. This would limit potential peripheral toxicity, allow for greater therapeutic control and flexibility as well as bypass possible pre-existing immunity to rAAV9 in patient populations (Calcedo et al., 2009; Mingozzi and High, 2007).

Here, we documented progressive neuropathology and retinopathy in CD mice during early postnatal development. For gene therapy, we tested rAAV9, carrying the human AspA cDNA with and without miRNA regulation in CD mice by IV injections at postnatal day 0 (P0), which restored AspA activity, normalized NAA metabolism, alleviated neuropathy and retinopathy, and improved motor functions. We expanded P0 injection study in CD mice to include rAAVrh.8 and rAAVrh.10, which improved their growth and extended survival up to 2 years (for rAAV9 and rAAVrh.8 groups thus far). Early lethality of CD mice (<4 weeks) was also completely rescued with rAAV9 administration at P6, P13, and even P20, a few days before their death. We also demonstrate that AspA helps to maintain integrity of myelin sheaths and affects the content and distribution of myelin-enriched brain lipids. Most importantly, our study demonstrates, for the first time, an efficacious and sustained IV gene therapeutic for treating terminal stage CD mice as well as successful preclinical in vivo application of miRNA-regulated peripheral tissue detargeting in CNS-directed rAAV gene therapy.

Materials and Methods

Viral production: All rAAV vectors were produced by transient transfection of 293 cells and CsCl gradient sedimentation as previously described (Sun et al., 2010) Vector preparations were titered by quantitative PCR, purity of vectors was assessed by 4–12 % SDS-acrylamide gel electrophoresis and silver staining (Invitrogen, Carlsbad, CA) and morphological integrity of virions was assessed by Transmission electron microscopy of negative stained recombinant AAV virions at Electron Microscopy Core, UMass Medical School, Worcester.

Animal procedures: All animal procedures were approved by the Institutional Animal Care and Use Committee (IACUC) of UMass Medical School. $AspA^{+/-}$ Sv129/Ev mice littermates were bred using programmatic timing and newborn pups were dosed on P0. Vectors were injected in the facial vein of P0 pups at doses of $4X10^{11}$ GC/mouse. P6, P13 and P20 pups were injected in the retro-orbital sinus with $8X10^{11}$, $1.2X10^{12}$ and $4X10^{12}$ GC/mouse respectively. After the injection pups were cleaned, rubbed with bedding, and then returned to their cage. The dam was reintroduced after brief nose numbing using ethanol pads.

Immunohistochemistry: Animals were anesthetized, transcardially perfused with 4% paraformaldehyde (v/v) in PBS. Whole carcasses were postfixed in fixative for 1 day. Organs were extracted, rinsed in PBS, and sagitally sectioned. One half was cryoprotected in 30 % sucrose (w/v) in PBS at 4°C, embedded in OCT compound (Sakura Finetek, Torrance, CA) and frozen in a dry ice/ethanol bath. 40 μm floating

sections of the entire brain were cut in a Cryostat (Thermo Microm HM 550) for immunostaining. The other half was processed for Hematoxylin and Eosin staining for morphological studies.

Floating sections were stained in 12-well plates. Sections were washed once in PBS for 5 mins, and incubated in blocking solution containing 0.05 % Tween-20 (v/v) (Fisher, Pittsburgh, PA), and 10 % goat serum (v/v) (Invitrogen) for 1 hour at room temperature. Sections were incubated with primary antibodies at 4°C overnight, washed twice in 0.05 % Tween-20 in PBS (PBST) for 15 mins each followed by incubation in appropriate secondary antibodies at room temperature for 1 hour. Sections were washed twice in PBST for 10 mins each before mounting on glass slides. Vectashield with 4,6 -diamidino- 2-phenylindole (Vector Laboratories, Burlingame, CA) was used to mount all slides. Omission of either the primary or the secondary antibody in single-label experiments resulted in no labeling.

The ABC stain was performed according to standard kit instructions (Elite ABC kit, Vectastain, Burlingame, California). DAB was used as the substrate for the peroxidase enzyme reaction (Vectastain).

The primary antibodies used were as follows: mouse aspartoacylase (Abmart, New Jersey), rabbit aspartoacylase (provided by Dr Aryan Namboodiri); mouse NeuN (MAB-377, clone A60; Millipore); rabbit NeuN (ABN-78, Millipore) and appropriate secondary antibodies from Invitrogen.

Imaging and Image Analysis: Stained sections were examined using DM 5500B Upright microscope (Leica Microsystems, Wetzlar, Germany), and images were captured with

Leica DFC365 FX high-sensitivity monochrome digital camera. Regions of interest were identified according to the mouse brain atlas. Z stack of images were taken with a 63X objective and 1.6X additional magnification for each channel and overlaid to obtain a multicolor image at 100.8X. Deconvolution was performed using Leica Application Suite Advanced Fluorescence software.

Electroretinography (ERG): Mice were dark-adapted overnight and anesthetized with 100 mg/kg ketamine and 20 mg/kg xylazine in saline before testing. Both pupils were topically dilated with phenylephrine hydrochloride and 1 % tropicamide, and mice were placed on a heated platform. Rod-dominated responses were elicited in the dark with 10 μs flashes of white light (1.37 × 105 cd m−2) presented at intervals of 1 min in a Ganzfeld dome. ERGs were monitored simultaneously from both eyes with a silver wire loop electrode in contact with each cornea wetted with celluvisc containing Carboxy Methyl Cellulose Sodium 1 %.

Western blot: Mice were sacrificed and their tissues were extracted and homogenized as described (Xie et al., 2010) . Protein in equal quantities was loaded into a 12% Tris–HCl gel well (Bio-Rad Laboratories, CA) and transferred to a nitrocellulose membrane (Bio-Rad). The membrane was incubated in blocking buffer for 1hr followed by AspA polyclonal antibody overnight. After three washes in 0.1 % PBST, it was incubated with secondary antibodies conjugated to LI-COR IRDye for 1 hour at room temperature. After two washes with 0.1 % PBST signal was detected using the Odyssey Imager (LI-COR).

Genome copy number: rAAV genomes were quantified in 1μg of genomic DNA extracted from mouse tissues using the QIAamp DNA mini kit for quantitative detection

of vector genome copies by Taqman® probes (Applied Biosystems) with a single-copy endogenous GAPDH gene) as the diploid cell number reference. The Taqman® real-time PCR kit was run with primer sets which amplified regions of the nRBG poly A (Probe, 6FAM-ATG AAG CCC CTT GAG CAT CTG ACT TCT-TAMRA; Fwd, GCC AAA AAT TAT GGG GAC AT; Rev, ATT CCA ACA CAC TAT TGC AAT G). The sensitivity of the assay was 10 copies/µg gDNA.

AspA activity assay: Mice were sacrificed 3 months after injection, and brain homogenates were used for the enzyme assay (Matalon et al., 2000) . Briefly, the brain was homogenized and incubated with 50mM Tris–HCl (pH 8.0), 0.5% (w/v) NP-40, 50 mM NaCl, 1 mM $CaCl_2$, 2.8 mM NAA in a total volume of 600 µl. After incubation at 37°C for 3h, the assay mixture was centrifuged and the supernatant was incubated with malic dehydrogenase, glutamic oxalacetic transaminase, and NADH for 10 min at 37°C. The amount of L-aspartate released was estimated by decrease in absorbance due to the conversion of NADH to NAD using a spectrophotometer (Shimadzu, MD) at 340 nm. One milliunit of aspartoacylase activity is equivalent to 1 nmol of aspartate released in 1 min. Values were calculated using ANOVA. $P < 0.05$ was considered significant.

^{1}H Magnetic Resonance Imaging and Spectroscopy study: Mice were anesthetized with 2% isofluorane and constantly monitored for vital signs. All experiments were carried out on a Bruker 4.7T/40 cm horizontal magnet (Oxford, UK) equipped with 250 mT/m magnetic field gradient and interfaced with a ParaVision 4.0 console. A ^{1}H radiofrequency (RF) coil configuration (Insight NeuroImaging Systems, MA) with inner diameter (ID) of 4 cm was used for the experiments.

T2-weighted anatomical images were acquired using a fast spin-echo sequence (RARE) (TR=3000 msec, TE=48 msec, matrix size=256×256, FOV=2.5 cm×2.5 cm, slice number=16, slice thickness=1 mm). 1H MRS Data was acquired using single voxel (Pont Resolved Spectroscopy Sequence (PRESS) (TR=2500 msec, TE=20 msec, Naverage=1024, voxel size=3 mm×3 mmX3 mm).

Proton spectra were fit using LCModel (Version 6.2-2B) which analyzed *in vivo* proton spectrum as a linear combination of model *in vitro* spectra from individual metabolite solutions (Provencher, 2001) and generated data as absolute fits (in institutional units) and standard deviations (SD%). Standard deviation was used as a measure of the reliability of the fit. The spectral inclusion criteria were SD less than 20% for NAA, Cr and Ins.

Behavioral studies: Negative geotaxis test was performed on P7-P17 pups where they were placed on a 45° inclined plane; head facing downwards and their latency to turn with the head pointing upwards was recorded.

For the beam balance test, animals were placed in the middle of a horizontal wooden balance beam (1.5 cm × 100 cm) with pads underneath to protect mice that might fall off the beam. Latency to fall was recorded, with a 3min time limit for each trial.

Neuromuscular function of the mice was assessed by testing grip strength on an inverted screen. Mice were placed in the center of a screen (30 cm^2 square-wire mesh, 25 mm^2 holes) until they gripped the mesh. The screen was then inverted above a cushioned surface for a 2sec period with the mouse's head declining. Latency to fall from the screen was recorded, with a 2min time limit for each trial.

Mice were subject to a rotarod test to evaluate motor coordination and balance. Each animal was placed on the rotarod after which speed was adjusted to 3 rpm. The latency to fall off the rotarod within this time period was recorded for fixed speed. Animals were also tested for their latency to fall off at accelerated speeds going from 4 to 40 rpm in 5mins.

Animals were tested for each experiment 3 times with an inter-trial interval of approximately 30 min for each animal and mean of 3 trials was used to plot the graphs.

Transmission Electron Microscopy: Mice were anesthetized and perfused with a solution of 2.5 % glutaraldehyde in 0.05 M Sodium Phosphate buffer, pH 7.2. The brain was extracted and incubated in 2.5 % glutaraldehyde in 0.05 M Cacodylate buffer overnight at 4°C. It was sectioned into 1 mm thick sections, rinsed twice in the same buffer and post-fixed with 1 % osmium tetroxide for 1h at room temperature. Sections were washed in DH_2O (heavy water) for 20 mins at 4°C and then dehydrated in graded ethanol series of 20% increments, before two changes in 100 % ethanol. Sections were infiltrated with two changes of 100% Propylene Oxide and then with a 50%/50% propylene oxide / SPI-Pon 812 resin mixture overnight. After three changes of fresh 100 % SPI-Pon 812 resin, sections were polymerized at 68°C in plastic capsules. Regions of interest were cut out and thick-sectioned for toluidine blue. Chosen regions were reoriented and approximately 70nm thin sections were placed on copper support grids and contrasted with Lead citrate and Uranyl acetate. Sections were examined using the FEI Tecani 12 BT with 80Kv accelerating voltage, and images were captured using a Gatan TEM CCD camera.

Total Lipid Isolation: Total brain lipids were evaluated from the frozen cerebrum, cerebellum, and medulla of P25 and P60 WT, CD/PBS, and CD/rAAV9 mice. Tissues were homogenized in water and lyophilized for 24 hr. After desiccation, the dried tissue was weighed, rehydrated in water (0.05 ml), and lipids were extracted overnight in $CHCl_3$:CH_3OH (1:1; v/v) according to standard procedures (Baek et al., 2009; Hauser et al., 2004). Lipids were further separated into a neutral (F1) and acidic/ganglioside (F2) fraction via ion exchange chromatography over a Sephadex column (Baek et al., 2009; Macala et al., 1983). Neutral lipids and cholesterol were eluted with a $CHCl_3$:CH_3OH:dH_2O (30:60:8; v/v/v) solution, while acidic phospholipids and gangliosides were eluted with a $CHCl_3$:CH_3OH:0.8M CH_3COONa (30:60:8; v/v/v) solution. Gangliosides were separated from acidic phospholipids by Folch partitioning, base treated, and desalted as previously described (Folch et al., 1957). Neutral lipids were dried by rotary evaporation and resuspended in 10 ml $CHCl_3$:CH_3OH (2:1; v/v).

Sialic acid quantification: Total ganglioside content was quantified before and after desalting using the resorcinol assay (Hauser et al., 2004; Svennerholm, 1957). Three aliquots of each ganglioside sample were dried under vacuum. Resorcinol reagent: water (1:1 v/v) solution (resorcinol reagent – HCl:0.2M resorcinol: DH_2O: 0.1 M CuSO4, 40:5:5:0.125 v/v/v/v) was added to each sample, followed by submersion in a boiling water bath for 15 min. After cooling on ice, the reaction was stopped with butyl acetate: N-butanol (85:15; v/v) (Seyfried et al., 1978). Each sample was vortexed and centrifuged at 700x g for 2 min. The absorbance of the upper aqueous layer was recorded at 580 nm

using a Shimadzu UV-1601 Spectrophotometer (Shimadzu, Torrance, CA). Sialic Acid values were fit to a standard curve using N-acetylneuraminic acid as a standard.

Thin-Layer Chromatography: All lipids were analyzed by high-performance thin-layer chromatography (HPTLC) as previously described (Kasperzyk et al., 2004; Macala et al., 1983). Neutral and acidic lipids were spotted using a Camag Linomat II auto-TLC spotter (Camag Scientific Inc., Wilmington, NC, USA.). The amount of neutral lipid spotted corresponded to 70µg dry weight. The plate was developed in solvent system I to 4.5 cm which contained Chloroform:Methanol: acetic acid: formic acid:H_2O (70:30:12:4:2 by vol.) and solvent system II to the top which contain hexane: isopropyl ether: acetic acid (65:35:2 by vol.). The amount of acidic lipid spotted corresponded to 200 µg of dry weight and was developed in solvent system I to 6.0 cm and in solvent II to the top. Bands for both neutral lipids and acidic lipids were visualized by charring with 3 % cupric acetate in 8% phosphoric acid solution in an oven at 160°C for 7 min. Gangliosides were spotted based on 1.5 µg of sialic acid and were developed in chloroform:methanol:0.02% calcium chloride (C:M:.02%$CaCl_2$). Individual lipid bands were scanned using Camag TLC Scanner 4 and the concentration of cerebrosides and sulfatides were calculated from a standard curve (Baek et al., 2009). The total brain ganglioside distribution was normalized to 100 % and the percentage distribution values were used to calculate sialic acid concentration of GM1.

X-ray Diffraction Analysis: X-ray diffraction was performed as described (Avila et al., 2005). Briefly, optic nerves and spinal cords were dissected from mice sacrificed using isoflurane. Optic nerves and sagitally bisected segments of cervical spinal cord were

maintained in physiological saline (154mM NaCl, 5mM phosphate, pH 7.4) and loaded into thin-walled, quartz capillary tubes which were then filled with saline and sealed with wax and enamel. X-ray diffraction experiments were carried out using nickel-filtered, single-mirror focused CuKα radiation from a fine-line source on a 3.0 kW Rigaku X-ray generator operated at 40 kV by 10 mA. Exposure times were 30 min. Diffraction patterns were collected using a linear, position-sensitive detector (Molecular Metrology, Inc., Northampton, MA) and analyzed using PeakFit (Jandel Scientific, San Rafael, CA). Myelin period was calculated from the positions of the intensity maxima in the diffraction patterns. The relative amount of myelin in each sample was calculated by measuring the total integrated intensity of all maxima over background, excluding small-angle scatter around the beam stop and wide-angle scatter.

Statistical Analyses: Statistical calculations included Log rank Mantel Cox test for the survival table and one way ANOVA followed by Tukey's Multiple Comparison test for all other experiments. *$P < 0.05$; **$P < 0.01$; ***$P < 0.001$, NS not significant.

Results

AspA deficiency causes progressive neuropathy and retinopathy in early postnatal mice

Histologic examination of the brains from wild-type (WT) and CD mice (n = 4 each) at P0, P6, P13, P20, and P25 showed appearance of vacuoles in the CNS of CD but not WT mice at P13, which gradually increased in size and number with age. Neurodegeneration was considered severe by P25 [Figure 3.1a] with afflicted mice dying shortly afterwards. Quantification of intact tissue areas showed progressive pathology in the striatum, thalamus and brainstem [Figure 3.1b], suggesting that AspA helps to maintain CNS integrity.

After full eye opening at P16, WT and CD mice (n = 4) were evaluated for retinal response to light flickers by scotopic electroretinography (ERG) at P16, P20, P23, and P27. The ERG trace is produced by the electrophysiological action of the retinal cells and typically consists of a- and b-waves that indicate photoreceptor and glial cell activities respectively. Sequential ERGs revealed progressive reductions in retinal responses of CD mice [Figure 3.1c] indicating the importance of AspA for maintaining visual acuity.

IV injections of rAAV9hAspA and rAAV9hAspAmiRNA-BS reconstitute AspA in the CNS

CD mice injected with rAAV9hAspA (CD/rAAV9) at P0 were killed at 3 months to evaluate brain AspA levels by western blot. AspA levels in the gene-corrected (GC)

Figure 3.1 Progressive neuropathology and retinopathy in postnatal CD mice. (a) Representative images of hematoxyline and eosin (H&E) stained brain sections (n = 4). Bars: 4.8 mm. (b) Semiquantitative analyses of neuropathology normalized to WT animals using Image J. Ob, olfactory bulb; Cx, cortex; Hp, hippocampus; St, striatum; Th, thalamus; Ce, cerebellum; BS, brain stem. (c) Scotopic ERGs of overnight dark-adapted WT and CD mice (n = 4 each) to test the response of rods recorded as waveforms (μV) to flickers of light in increasing intensity called steps. CD, Canavan disease; ERG, electroretinography; WT, wild-type.

Figure 3.1 Progressive neuropathology and retinopathy in postnatal CD mice.

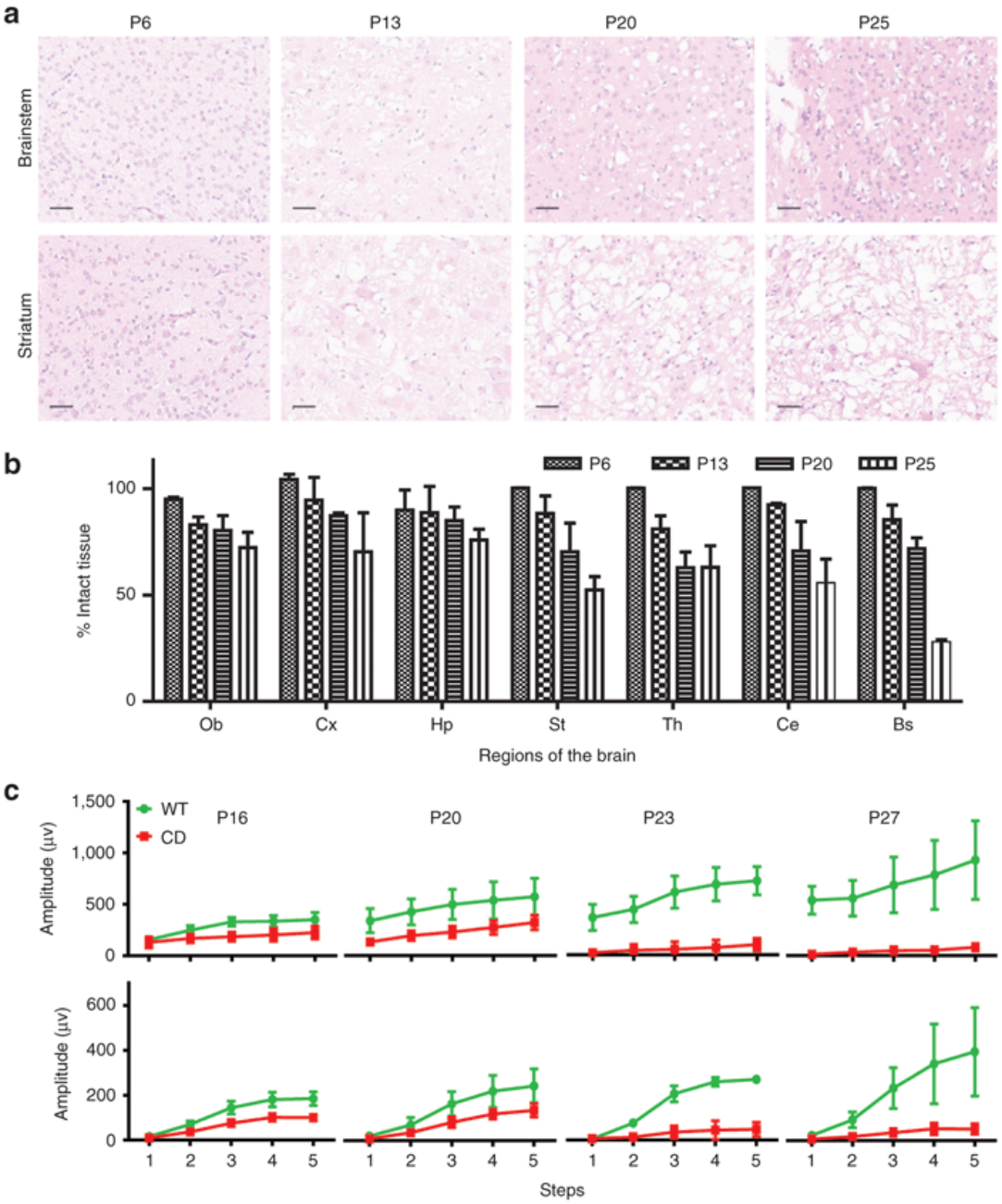

Figure 3.2 Enzymatic and metabolic correction of AspA deficiency by systemically delivered rAAV-mediated gene therapy in CD mice. (a) Western blot of brain homogenates from WT (P90), Het (P90), and CD mice treated with PBS (P27) or rAAVhAspA (P90). Loading control: GAPDH. (b) Aspartoacylase activity in brain homogenates of the study groups. (c) Persistent vector genomes (by quantitative PCR) and aspartoacylase expression (by western blot) in P90 CD/rAAV9hAspA and CD/rAAV9hAspAmiRBS. (d) Representative images of avidin-biotin-complex (ABC) stained brain sections. (e) Immunofluorescence images of brain sections from P90 WT and CD/rAAV9 for AspA (green) and neuronal marker, NeuN (red) and colocalization (yellow). Bars: 10 μm. (f) Representative MRS spectra of brain NAA levels in WT and CD/PBS mice at P26 (n = 3 each) showing NAA peaks at 2.018 ppm. (g) Quantification of in vivo brain metabolite levels from the proton spectra as ratio to total creatine. Ins: inositol, tCho: total choline, tNAA: total NAA, tCr: total creatine, Glx: glutamate + glutamine. (h) Mass spectrometry of urine from P27 WT, Het and CD/PBS or CD/rAAV9 mice. WT, wild-type; Het, heterozygote; CD/PBS, CD/rAAV9, CD mice treated with PBS or rAAV9 respectively. CD, Canavan disease; MRS, magnetic resonance spectroscopy; NAA, N-acetyl aspartic acid; NS, not significant; PBS, phosphate-buffered saline; rAAV, recombinant adeno-associated virus.

Figure 3.2 Enzymatic and metabolic correction of AspA deficiency by systemically delivered rAAV-mediated gene therapy in CD mice.

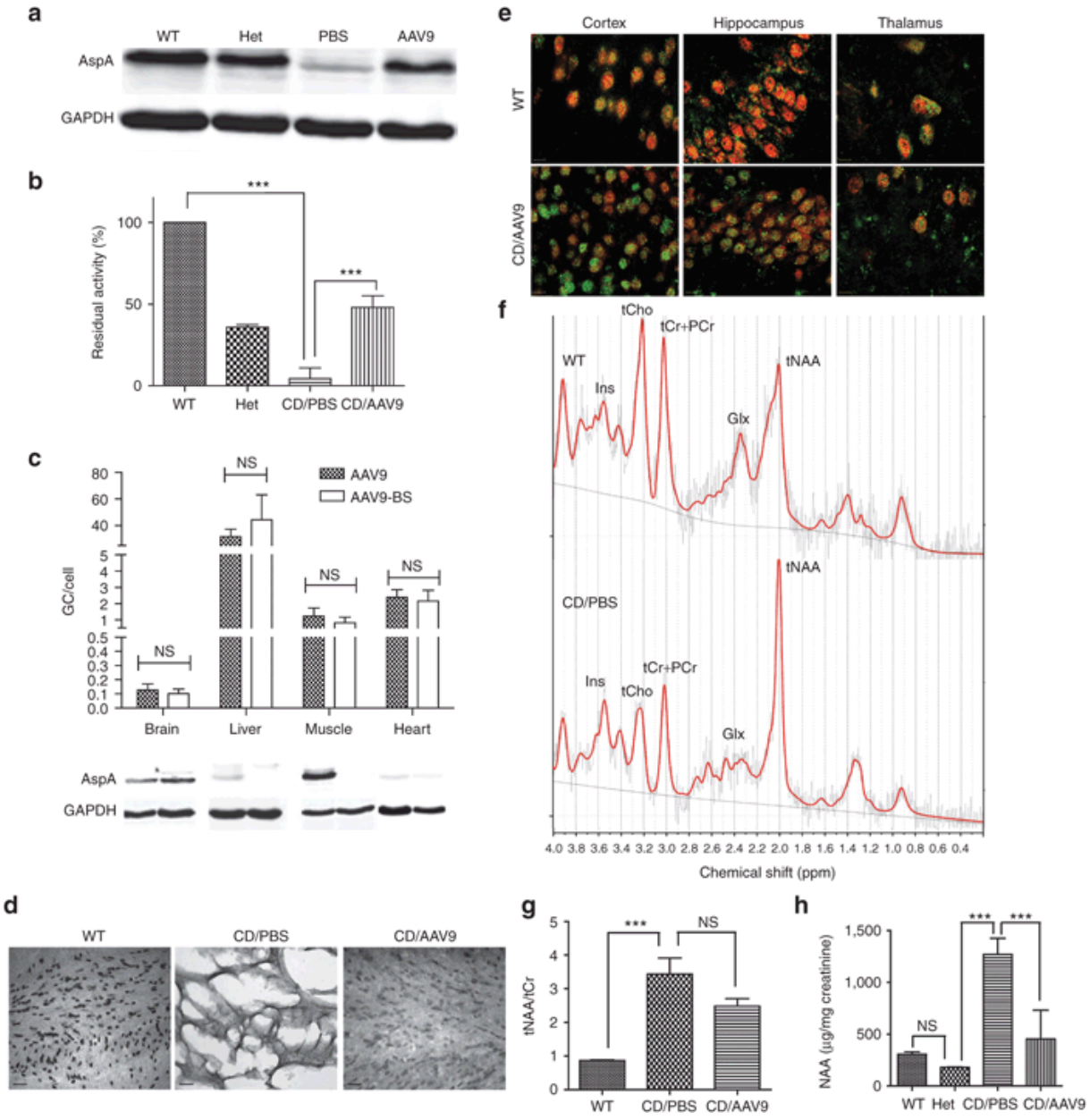

mice were similar to age- matched phenotypically normal heterozygous (Het) mice [Figure 3.2a]. Protein levels depicted in the blot were typical of the trend observed, although there was significant variability in the level of protein expression among the different vector-treated animals.

AspA enzyme activity (normalized to WT mice) in brain homogenates of GC mice were similar to Het mice ($P > 0.05$) [Figure 3.2b]. To reduce transduction in peripheral tissues such as liver, heart, and skeletal muscle by systemically delivered rAAV9 hAspA, a miRNA-regulated vector genome was designed for CNS-restricted gene transfer (Xie et al., 2012). Equal doses of rAAV9hAspA and rAAV9hAspA-(miR-1BS)3-(miR-122BS)3 (i.e., rAAV9hAspAmiRBS) with three copies each of the miRNA-BS specific to miR-1 and miR-122 (enriched in heart, skeletal muscle, and liver, respectively) were infused into CD mice at P0. Both vectors targeted brain, liver, heart, and muscle tissues equally; but the miRNA-regulated vector abolished AspA expression only in peripheral tissues not the brain [Figure 3.2c], establishing specificity of miRNA-regulated therapeutic expression from rAAV.

Immunohistochemistry illustrated similar numbers and distribution patterns but different staining intensities of AspA positive cells in the brains of WT and GC mice [Figure 3.2d]. Large vacuoles in CD mouse brain sections made detection of residual AspA difficult. Double immunofluorescence staining showed efficient neuronal AspA gene transfer by rAAV9 in the cortex, hippocampus, and thalamus in GC mice [Figure 3.2e].

Spectral peak integrals for total NAA (2.02 ppm) and total creatine (tCr, 3.05 ppm) (Grodd et al., 1990; Matalon and Michals-Matalon, 2000) were determined by acquiring ^{1}H 1^{H} proton magnetic resonance spectroscopy data from live animals (n = 3). Abnormally high endogenous NAA levels were detected in CD mice relative to WT mice as expected (Matalon et al., 2000; Pioro et al., 1998) [Figure 3.2f]. Integrated values of NAA/creatine ratios were significantly different between WT (0.886 ± 0.03), and CD (2.63 ± 0.16) ($P > 0.001$); such values were reduced in GC mice (2.18 ± 0.64) [Figure 3.2g]. N-acetylaspartic aciduria (excretion of NAA in the urine), a biomarker of CD (Matalon et al., 1988) was significantly reduced in GC mice ($P > 0.001$) compared with CD mice [Figure 3.2h].

AspA gene therapy in CD mice alleviates neuropathology, cerebral edema, and retinopathy

Hematoxylin and eosin stained coronal sections of brain and spinal cord from terminal stage (P27) CD and P90 GC mice were examined [Figure 3.3] and quantified [Figure 3.3b] for neuropathology. Our data suggest significant improvements in all regions of spinal cord and most regions of the brain.

T2-weighted magnetic resonance imaging was used to detect cerebral edema (Matalon et al., 1993) in WT (P60, n = 3), CD (P27, n = 3), and GC animals treated with rAAV9hAspA and rAAV9hAspA-miRBS (P60 and P365, n = 3). CD brains exhibited widespread high signal intensities, indicating water accumulation particularly in the thalamus (mainly midbrain) and brainstem [Figure 3.3c], which mirror conditions in

patients (Matalon, 1997); but T2-weighted hyperintensity in both groups of GC mice was generally reduced [Figure 3.3c]. More importantly, reduction of edema seemed to be sustained in P0-treated GC mice for 1 year [Figure 3.3c]; however, NAA levels in rAAV9hAspA-treated mice were lower than in AAV9hAspAmiRBS–injected mice [Figure 3.3d]. Thus, single rAAV injections were able to partially, but sustainably, relieve cerebral edema.

Retinal responses of GC mice were similar to those of age-matched WT mice even after 1 year, although amplitudes of both a- and b-waves were lower, suggesting partial but sustained correction of visual acuities [Figure 3.3e].

Figure 3.3 Intravenous (IV) gene therapy using rAAV9 mitigates neuropathology, reduces water accumulation in the brain and improves visual acuity. (a) Representative images from hematoxylin and eosin (H&E) stained paraffin sections (n = 4 for each group). (b) Quantification of neuropathology by ImageJ. Ob, olfactory bulb; Cx, cortex; Hp, hippocampus; St, striatum; Th, thalamus; Ce, cerebellum; BS, brain stem; CSP cervical spinal cord; TSP, thoracic spinal cord; LSP, lumbar spinal cord. (c) Representative T2-weighted magnetic resonance imaging images showing water accumulation (white) in P25, CD/PBS; P60, P365 GC; and WT animals. (d) Quantification of MRS data for metabolites in brains of mice injected with rAAV9 or rAAV9BS at P0 at age P90. (e) Scotopic ERG of WT, CD/PBS and CD/rAAV9 at P25 and P365, respectively, to test visual acuity. WT, wild-type; CD/PBS, CD/rAAV9, CD mice treated with PBS or rAAV9 respectively. CD, Canavan disease; ERG, electroretinography; MRS, magnetic resonance spectroscopy; NS, not significant; PBS, phosphate-buffered saline; rAAV, recombinant adeno-associated virus.

Figure 3.3 Intravenous (IV) gene therapy using rAAV9 mitigates neuropathology, reduces water accumulation in the brain and improves visual acuity

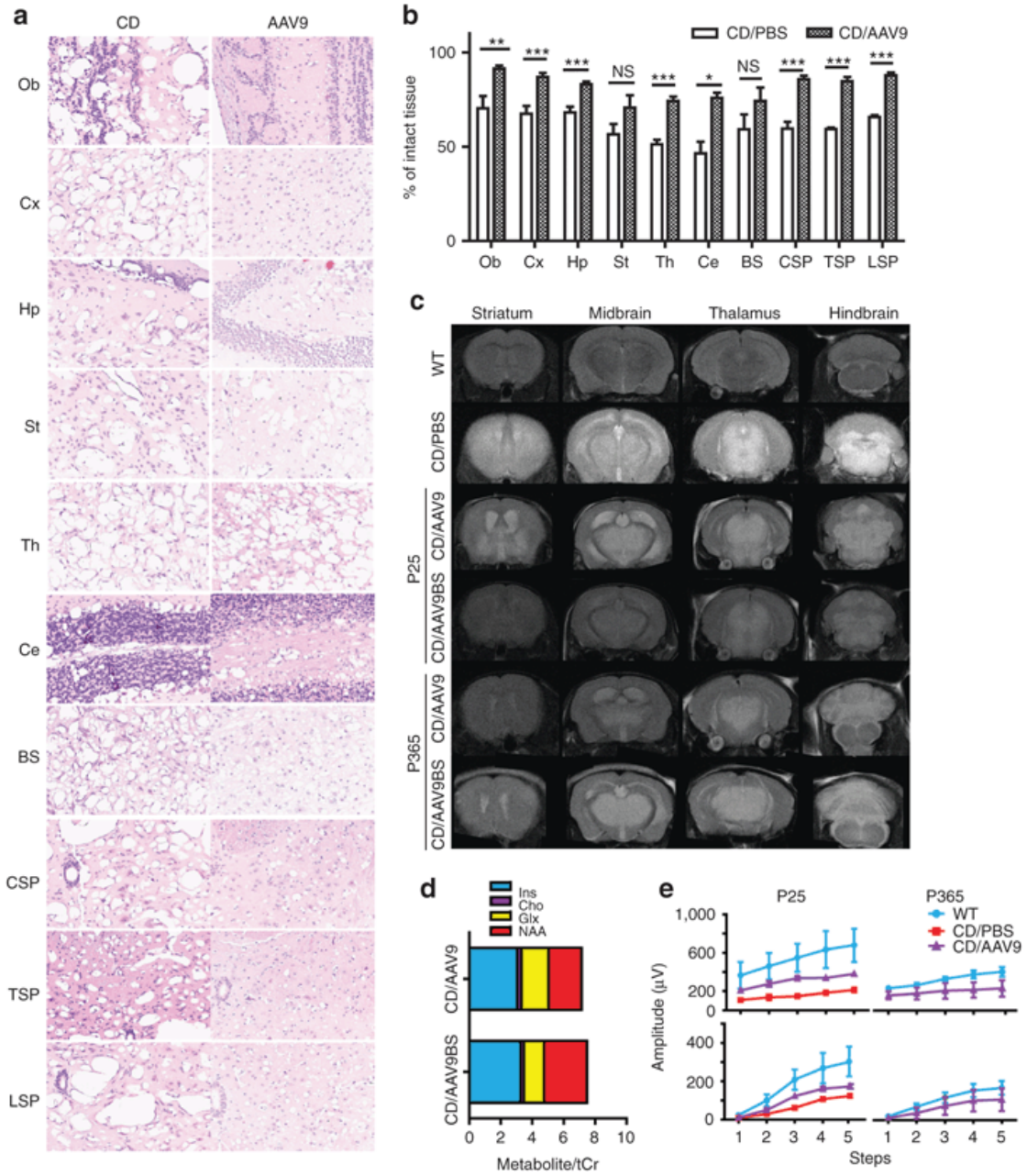

Systemic and CNS-restricted AspA gene therapy by different rAAVs is therapeutic for CD mice

In addition to rAAV9, two other rAAVs (i.e., rAAVrh.8 and rh.10) were selected for this proof-of-concept gene therapy study in CD mice. Therapeutic efficacies of these vectors (i.e., rAAV9hAspA, rAAV9hAspA-miRBS, rAAVrh.8hAspA or rAAVrh.10hAspA) were evaluated in CD mice by comparison of growth, survival and negative geotaxis (all four vectors) as well as other motor functions (rAAV9hAspA and rAAV9hAspA-miRBS only) All these vectors were delivered intravenously at P0.

Growth profiling showed that CD mice were phenotypically similar to WT littermates until P13 after which they steadily lost weight until their death [Figure 3.4a, inset]. Compared to rAAV9, GC mice treated with other vectors showed no significant differences in survival or growth [Figure 3.4a].

Since survival is an important criterion for therapeutic benefits, survival of >50 GC mice was examined using the Kaplan–Meier curve [Figure 3.4b]. There was a uniform rescue of lethality with extended survival as long as 2 years for rAAV9- and rAAVrh.8-injected animals. Long-term study of rAAVrh.10 was initiated about 1 year later; the animals have survived well for 11 months thus far. The negative geotaxis test for early postnatal spatial locomotive behavior showed that GC mice but not CD mice performed similar to their WT littermates [Figure 3.4c]. CD/rAAV9 mice were compared with CD/ phosphate-buffered saline (PBS) mice at P27 and WT at P27, P90, and P180 to further evaluate motor functions. GC mice significantly improved in balance ($P < 0.001$)

[Figure 3.4d], and grip ($P < 0.001$) [Figure 3.4e] over CD mice at P27. Data from later timepoints revealed that the treatment fully and sustainably restored grip strength but not balancing abilities in GC mice [Figure 3.4 d & e]. GC animals performed significantly better than CD mice on the rotarod at P27 [Figure 3.4 f & g] but were significantly behind WT mice at later timepoints [Figure 3.4 f & g]. The GC mice that received the miRNA-regulated vector performed similar to rAAV9hAspAtreated mice in the fixed speed rotarod test but not in balance ($P< 0.001$), inverted screen ($P < 0.05$) and accelerated rotarod ($P < 0.01$) tests at P90 (Figure 4h). We noticed variability in the performance of P1 treated mice on the inverted screen and balance beam in later generations of CD mice. This suggests that genetic modifiers in the Sv129 background strain may alter the penetrance of the gene knockout, as has been observed with other gene knockouts [Flotte, personal communication]. Overall, our data suggest that IV gene therapy can largely restore motor functions of CD mice.

Figure 3.4 Intravenous (IV) gene therapy using novel rAAVs improves growth profile, rescues early lethality and corrects motor function defects of CD mice. (a) Weight of animals at 2-week intervals plotted as a function of time. Early growth rate was assessed by weights at 2-day intervals for the first month (inset). (b) Kaplan–Meier survival curves for groups treated with different vectors at P0 ("closed circles" = WT, "closed squares" = CD/PBS, "closed triangles" = CD/rAAV9, "closed up-side down triangles" = CD/rAAV9mirBS, "closed diamonds" = CD/rAAVrh.8, and "closed hexagon" = CD/rAAVrh.10, respectively). (c) Negative geotaxis test at intervals of 1 day from P7 (day 8) to P17 (day 16). Motor functions of study groups were tested at P27, P90, and P180 based on their performance on the (d) balance beam, (e) inverted screen and rotarod moving at (f) fixed speed (3 rpm) and (g) accelerated speed (4–40 rpm in 5 minutes). The same tests were performed on (h) P90 CD/rAAV9 and CD/rAAV9mirBS. WT, wild-type; CD/PBS, CD/rAAV9, CD/rAAV9mirBS, CD/rAAVrh.8, and CD/rAAVrh.10: CD mice treated with PBS, rAAV9hAspA, rAAV9hAspA-mirBS, rAAVrh.8hAspA, and rAAVrh.10hAspA at P0, respectively. CD, Canavan disease; NS, not significant; PBS, phosphate-buffered saline; rAAV, recombinant adeno-associated virus.

Figure 3.4 Intravenous (IV) gene therapy using novel rAAVs improves growth profile, rescues early lethality and corrects motor function defects of CD mice.

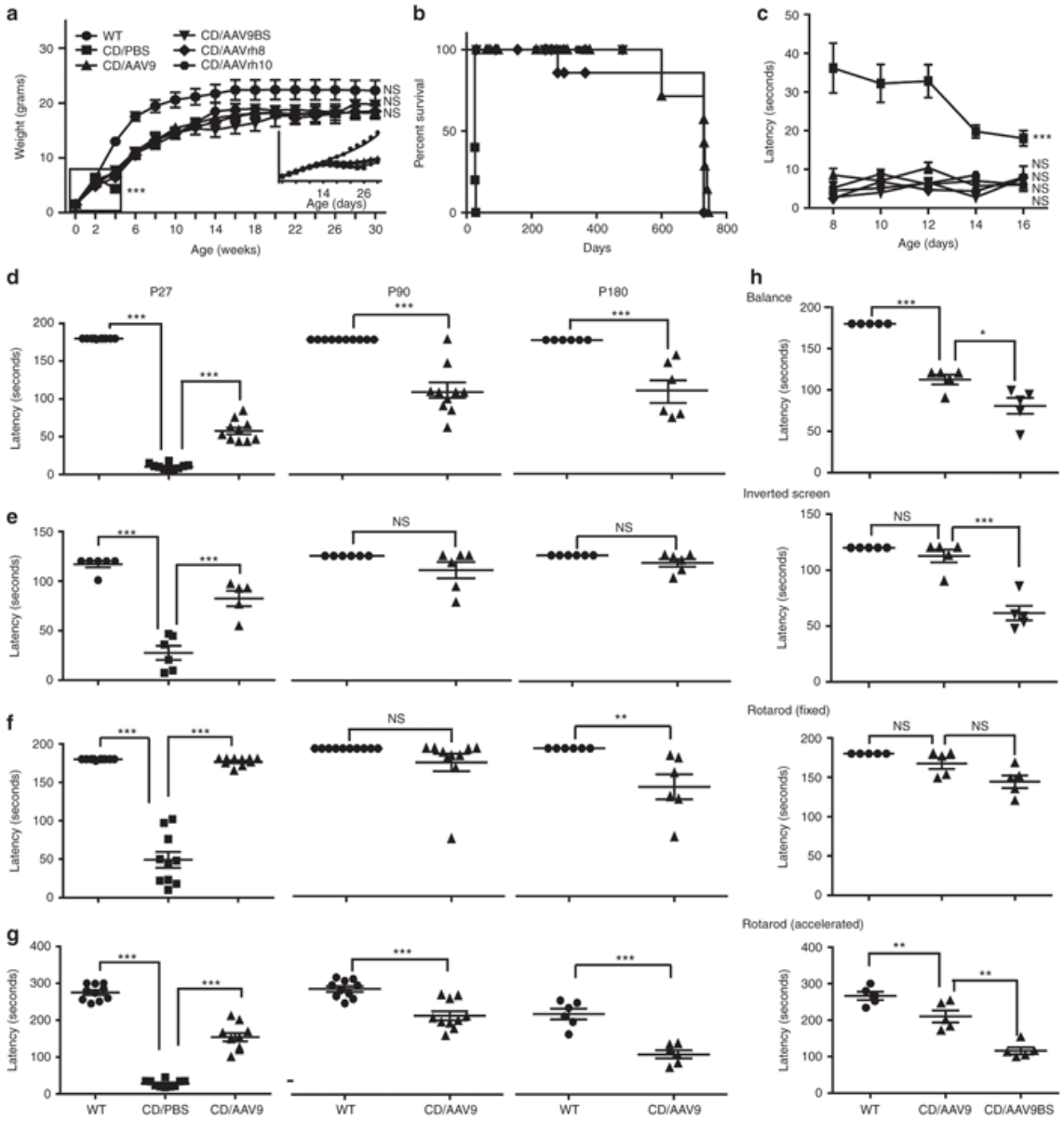

Figure 3.5 Intravenous (IV) gene therapy with rAAVs as late as P20 improves growth profile, rescues early lethality and corrects motor function defects of CD mice. (a) Kaplan–Meier survival curves for all groups treated with different vectors at P0. (b) Weight of animals at 2-week intervals plotted as a function of time. (c) Early growth rate assessed by weights at 2-day intervals for the first month. (d) Negative geotaxis test at intervals of 1 day from P7 (day 8) to P17 (day 16). Motor functions of study groups were tested at P90 based on their performance on the (e) balance beam, (f) inverted screen and rotarod moving at (g) fixed speed (3 rpm) and (h) accelerated speed (4–40 rpm in 5 minutes). WT, wild-type; CD/PBS, CD/P0, CD/P6, CD/P13, and CD/P20: CD mice treated with PBS and rAAV9hAspA at P0, P6, P13 and P20 respectively.

Figure 3.5 Intravenous (IV) gene therapy with rAAVs as late as P20 improves growth profile, rescues early lethality and corrects motor function defects of CD mice

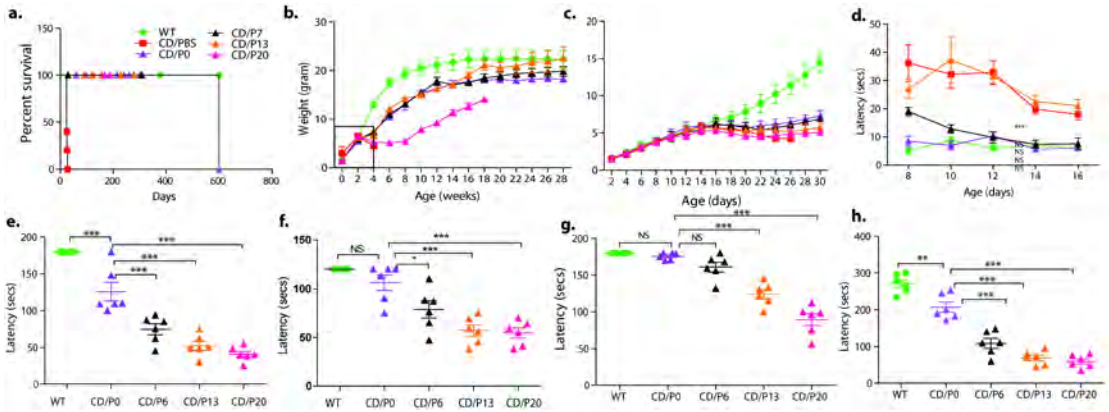

Figure 3.6 Intravenous (IV) gene therapy using rAAV9 improves myelin synthesis and partially corrects lipid profile of myelin in CD mice. (a) Electron microscopy of the motor cortex of P27 age-matched mice (n = 3 for each cohort). Bar: 2 μm. Inset: higher magnification. Black arrows: unmyelinated axons; white arrows: myelin sheath. (b) G ratios of myelinated axons calculated from toluidine blue stained sections of the cortex using ImageJ. (c) High-performance thin-layer chromatography of gangliosides in cerebrum, cerebellum, and medulla of different mouse groups (n = 3 for each group). Lower panel: quantification of the plate. (d) Quantification of the high-performance thin-layer chromatography plate.

Figure 3.6 Intravenous (IV) gene therapy using rAAV9 improves myelin synthesis and partially corrects lipid profile of myelin in CD mice.

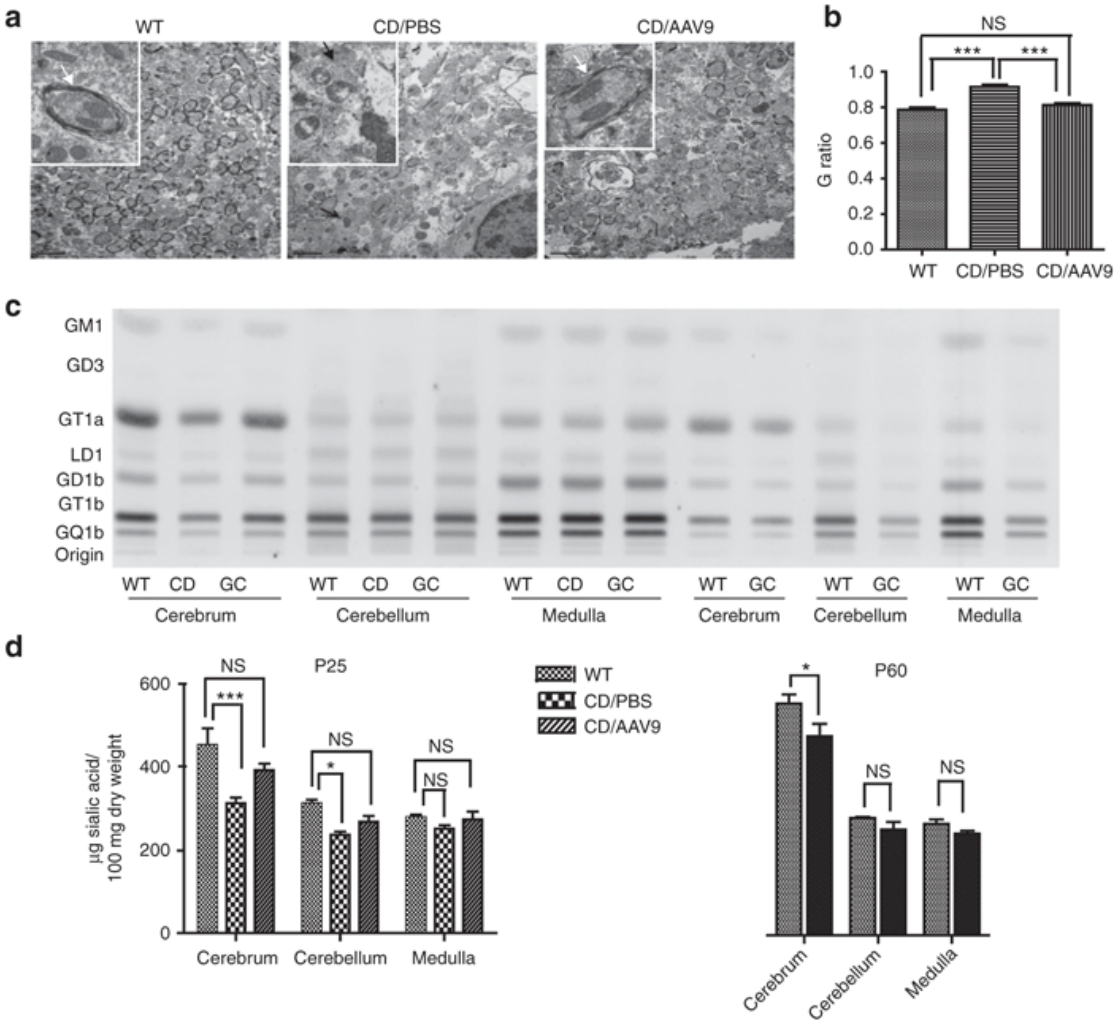

rAAV-mediated intravascular AspA gene delivery to the CNS as late as P20 is therapeutic

To define a therapeutic window, CD mice were systemically injected with only rAAV9hAspA at P0, P6, P13, and P20 (n = 6 each). IV injections at all the timepoints resulted in 100% rescue of early lethality, extended survival [Figure 3.5a] and improved growth profiles [Figure 3.5 b & c]. There was significant variability in the performance of the facial injection, as judged by direct observation of blanching of the vein during injection. A number of the animals in which poor blanching was observed died within 28 days, in a manner similar to the non-injected animals. While the number of suboptimal injections decreased over time, certain animals experienced early mortality (less than 28 days) even with what appeared to be robust blanching of the vein. Because of this variability in the injection procedure, all vector-treated animals dying prior to 28 days were excluded. Tests for negative geotaxis [Figure 3.5d], balance [Figure 3.5e], grip strength [Figure 5f], and abilities to stay on the rotarod [Figure 3.5g & h] at P90 clearly showed that early intervention was more beneficial to the diseased animals, although injections as late as P20 were sufficient to completely rescue early lethality and partially restore growth and mobility [Figure 3.5].

Hypomyelination and abnormal brain lipid profiles are improved by IV gene therapy

Electron microscopy on the brain cortices of P25 mice (n = 3 each) showed demyelination around neurons in CD/PBS mice (Adachi et al., 1972; Beaudet, 2001). In contrast, the myelin sheaths in GC mice were similar to those of WT in most of analyzed

regions [Figure 3.6a]. A highly reliable structural index of optimal myelination is the ratio of inner axonal diameter to the outer diameter of the myelin sheath known as the g-ratio (Chomiak and Hu, 2009). A higher ratio indicates less myelin and altered conduction capabilities. A semiquantitative comparison of the g ratios between mouse groups further supports the crucial role of AspA in maintaining axonal integrity and myelination [Figure 3.6b].Neurochemistry in CD and GC mice was studied by quantitative high-performance thin-layer chromatography (HPTLC) on 21 brain lipids in the cerebrum, cerebellum and medulla collected from WT (P25 and P60), CD (P25 only), and GC (treated at P0, analyzed at P25 and P60) mice (n = 3 each). Compared with WT mice, at P25, the total concentration of gangliosides was lower in the cerebrum and cerebellum of CD mice whereas gene therapy largely corrected this defect [Figure 3.6 c & d]. Concentrations of neuronal-enriched gangliosides (GD1a, GT1b, and GQ1b) at P25 were significantly lower in CD mice than the WT mice but were largely corrected in the GC mice [Figure 3.6c, Table 3.1]. Although the concentrations of all major gangliosides were lower in the GC mice compared with WT mice, none of these reductions was significant except for GM1 in the cerebrum [Table 3.1]. CD mice had significantly lower cholesterol content in the cerebrum and medulla compared with WT mice. Though largely corrected in the GC mice at P25, significant reduction was still seen in the cerebrum and cerebellum of GC mice at P60 [Figure 3.6c, Table 3.1].

It is noteworthy that deficiencies in cerebrosides and sulfatides were not completely corrected in the GC mice at either age [Table 3.2]. Cerebrosides and sulfatides migrate as double bands on the HPTLC due to differences in their hydroxyl

fatty acid content [Figure 3.7 a & b] (Baek et al., 2009). The slower (lower, L) migrating band mostly contains short-chain hydroxylated fatty acids; whereas, the faster (upper, U) band mostly contains longer chain nonhydroxylated fatty acids(Baek et al., 2009). Our HPTLC data [Table 3.2] suggests that the increased L/U (lower/upper band) ratio in the CD and GC mice is due to a greater deficiency of the non-hydroxylated fatty acids.

Myelin structure in optic nerves and spinal cords from WT (n = 4), CD/PBS (n = 5), and CD/rAAV9 mice at P26 (n = 4) [Figure 3.8] was examined using X-ray diffraction to quantify structural parameters like myelin period and relative amount of myelin(Agrawal et al., 2009; Avila et al., 2005). Diffraction from both tissues yielded strong intensity maxima, indicating the presence of significant amounts of multilamellar myelin [Figure 3.8a & b]. Each group displayed similar relative amounts of myelin [Figure 3.8c & d]. Myelin period is defined as the distance between subsequent pairs of bilayers. Any aberration in periodicity indicates inadequate insulation and subsequent neurological impairment. Spinal cords from CD/rAAV9 mice displayed a significantly higher myelin period (160.3 ± 0.5 Å) ($P < 0.04$) compared with CD/PBS mice (159.1 ± 0.8 Å). Optic nerves, CD/rAAV9 samples had a significantly higher period (157.7 ± 0.7 Å) than WT (156.6 ± 0.7 Å) ($P < 0.006$) [Figure 3.8c & d]. Other differences in myelin period and amount were not statistically significant. The I2/I4 ratio is a measure of the relative intensity of the 2nd order X-ray reflection over the 4th order reflections. Comparison of the I2/I4 ratios revealed a statistically significant decrease in the CD/rAAV9 mice compared with WT [Figure 3.8e & f], indicating a small change in membrane structure.

Table 3.1 Regional brain ganglioside distribution in 25 day old normal (WT), Canavan disease (CD), and CD mice treated with AAV gene therapy (GC) and 60day old normal (WT) and CD mice corrected by gene therapy (GC).

25 Days

	Cerebrum			Cerebellum			Medulla		
	WT	CD	GC	WT	CD	GC	WT	CD	GC
GM3	trace	trace	trace	trace	trace	trace	trace	trace	trace
GM2	trace	trace	trace	trace	trace	trace	trace	trace	trace
GM1	35.3 ± 3.0	25.3 ± 1.3	29.7 ± 1.9	23.1 ± 2.3	18.8 ± 1.8	23.0 ± 2.4	26.1 ± 0.8	24.3 ± 1.5	26.4 ± 1.5
GD3	trace	trace	trace	6.9 ± 0.4	4.9 ± 0.4	6.7 ± 0.8	13.2 ± 0.6	10.3 ± 0.4	12.7 ± 2.4
GD1a	169 ± 14.0	113.7 ± 5.4*	150.7 ± 7.2†	58.6 ± 3.5	46.3 ± 2.4	53.5 ± 4.1	28.5 ± 0.8	25.8 ± 1.0	30.1 ± 2.6
LD1	22.0 ± 1.7	19.0 ± 0.6	22.7 ± 1.2	40.3 ± 4.0	30.8 ± 1.5	35.3 ± 1.7	15.3 ± 0.5	13.9 ± 0.5	16.2 ± 1.4
GD1b	53.3 ± 5.0	41.0 ± 1.7	49.0 ± 2.3	37.0 ± 1.0	31.1 ± 1.8*	35.3 ± 2.1	60.2 ± 2.0	55.3 ± 3.5	56.2 ± 2.4
GC1b	128.7 ± 13.5	82.3 ± 4.1*	105.3 ± 4.5†	99.6 ± 1.0	71.2 ± 1.9*	80.2 ± 2.6*	86.0 ± 2.1	75.6 ± 2.3*	82.8 ± 5.5
GQ1b	48.3 ± 4.8	34.3 ± 1.5*	38.3 ± 0.9	48.8 ± 2.2	35.3 ± 1.5*	36.0 ± 1.4	52.0 ± 1.0	47.9 ± 1.3*	51.2 ± 3.7

60 Days

	Cerebrum		Cerebellum		Medulla	
	WT	GC	WT	GC	WT	GC
GM3	trace.	trace	trace.	trace	trace.	trace
GM2	trace	trace	trace	trace	trace	trace
GM1	48.0 ± 2.3	39.3 ± 2.0*	21.4 ± 1.3	17.7 ± 1	36.4 ± 2.7	31.3 ± 0.7
GD3	trace	trace	trace	trace	trace	trace
GD1a	165.3 ± 4.7	145.7 ± 11.1	50.5 ± 1.5	44.2 ± 0.3	17.9 ± 1.0	22.8 ± 1.0
LD1	20.7 ± 6.3	13.3 ± 1.2	39.4 ± 0.7	37.2 ± 0.3	9.7 ± 0.6	12.3 ± 0.5
GD1b	75.0 ± 2.5	62.7 ± 8.7	35.4 ± 1.4	31.5 ± 3.6	55.8 ± 5.7	48.2 ± 1.1
GC1b	150.7 ± 5.6	132.3 ± 4.8	79.4 ± 1.2	71.2 ± 8.6	74.1 ± 0.7	66.9 ± 2.1
GQ1b	60.3 ± 3.8	54.0 ± 3	36.9 ± 1.6	35.9 ± 6	56.2 ± 2.8	46.6 ± 2.8

[a] Values represent concentration (μg sialic acid/100 mg dry weight) ± SE (n=3 independent samples). Determined from densitometric scanning of HPTLC plates

* Indicates that the value is significantly different from that of the WT mice at $p < 0.05$ as determined by the unpaired two-tailed t-test

† Indicates that the value is significantly different from that of the KO mice at $p < 0.05$ as determined by the unpaired two-tailed t-test

Figure 3.7 HPTLC of neutral and acidic lipids in cerebrum, cerebellum, and medulla of WT, CD/PBS, and CD/rAAV9. HPTLC of (a) neutral and (b) acidic lipids in cerebrum, cerebellum, and medulla of WT, CD/PBS, and CD/rAAV9 mice. The amount of neutral and acidic lipids spotted per lane was equivalent to approximately 70 μg and 200 μg brain dry weight respectively. The plate was developed to a height of 4.5 cm for neutral lipids and 6 cm for acidic lipids The bands were visualized by charring with 3% cupric acetate in 8% phosphoric acid solution. WT, wildtype; CD/PBS, GC; CD mice treated with rAAV respectively. Statistical tests include one way ANOVA followed by Tukey's Multiple Comparison Test. *$P < 0.05$; **$P < 0.01$; ***$P < 0.001$, NS not significant.

Figure 3.7 HPTLC of (a) neutral and (b) acidic lipids in cerebrum, cerebellum, and medulla of WT, CD/PBS, and CD/rAAV9 mice.

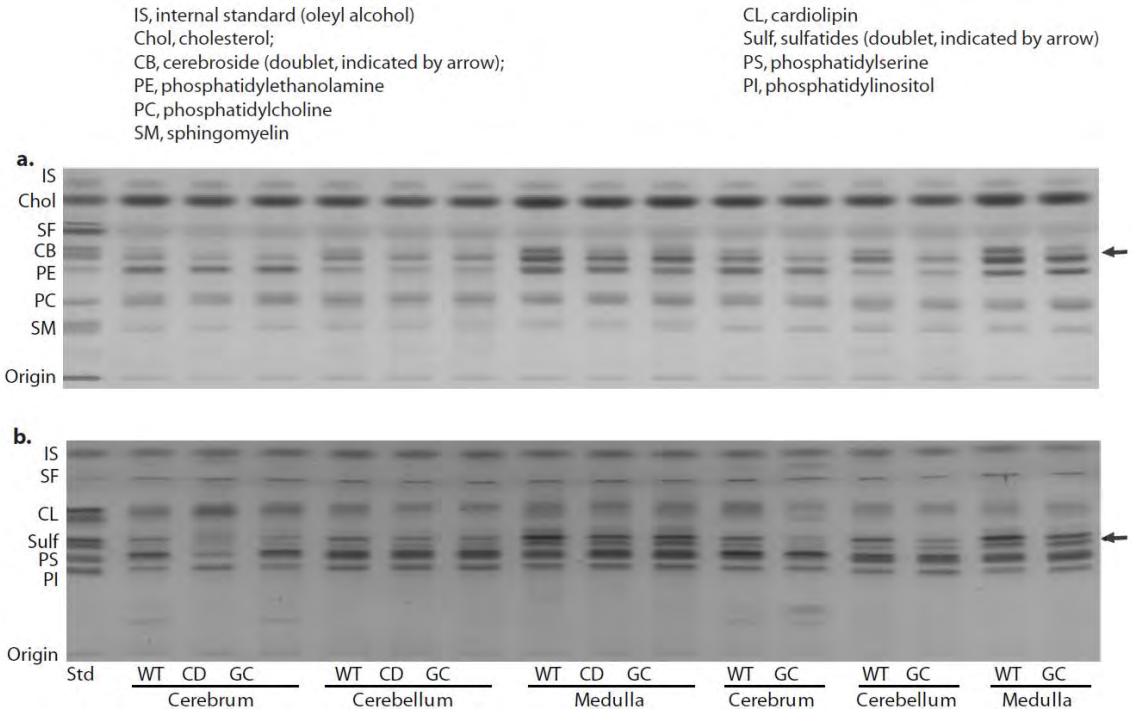

Table 3.2 Molecular species composition of cerebrosides and sulfatides in normal (WT), Canavan disease (CD) and CD mice treated with AAV gene therapy (GC). Brain from mice of different ages was isolated, homogenized and subject to High Performance Thin layer chromatography for isolation of molecular species of cerebrosides and sulfatides.

Table 3.2 Molecular species composition of cerebrosides and sulfatides in normal (WT), Canavan disease (CD) and CD mice treated with AAV gene therapy (GC).

			L/U ratio[a]	
Age	Brain region	Genotype	Cerebrosides	Sulfatides
25 days	Cerebrum	WT	2.23 ± 0.11	0.74 ± 0.07
		CD	4.95 ± 0.73*	1.06 ± 0.06*
		GC	7.87 ± 0.29**	1.12 ± 0.06*
	Cerebellum	WT	1.22 ± 0.03	0.38 ± 0.03
		CD	2.09 ± 0.24*	0.40 ± 0.08
		GC	1.98 ± 0.13*	0.37 ± 0.02
	Medulla	WT	1.38 ± 0.07	0.63 ± 0.02
		CD	1.53 ± 0.07	0.74 ± 0.02**
		GC	1.50 ± 0.08	0.81 ± 0.01**
60 days	Cerebrum	WT	2.07 ± 0.01	0.56 ± 0.07
		GC	4.47 ± 0.70*	0.85 ± 0.20
	Cerebellum	WT	1.47 ± 0.03	0.48 ± 0.03
		GC	2.47 ± 0.29	0.76 ± 0.10
	Medulla	WT	1.39 ± 0.07	0.49 ± 0.01
		GC	2.21 ± 0.21*	0.71 ± 0.04*

Abbreviations: AAV, adeno-associated virus; GC, gene-corrected mice; L/U ratio, lower (L)/upper (U) band ratio; WT, wild-type.

[a]Values represent ratio of the lower band (hydroxy fatty acids) to the upper band (non-hydroxy fatty acid) ± SE (n = 3 independent samples per group). Determined from densitometric scanning of high-performance thin-layer chromatography plates.

Significant difference from the WT mice at *$P < 0.05$, **$P < 0.01$ as determined by the unpaired two-tailed t-test.

Figure 3.8 X-ray diffraction patterns collected from optic nerves and spinal cords isolated from P26 mice. X-ray diffraction patterns collected from (a) optic nerves and (b) spinal cords isolated from P26 WT (n = 4), CD/PBS (n = 5), and CD/rAAV9 (n = 4) mice. The spectra, which represent averaged patterns from one spinal cord or two optic nerves from each animal in the group, have been offset along the y-axis for clarity. The Bragg orders for each reflection are indicated by numerals above their maxima. Scatter plots of M/(M+B) versus myelin period for (c) optic nerves and (d) spinal cords from WT, CD/PBS, and CD/rAAV9 mice. Error bars represent ±1 standard deviation centered on the average for each group. Comparison of the relative intensities of Bragg reflections measured from (e) optic nerves and (F) spinal cords among groups. Relative intensities are presented as the intensity of the 2nd order Bragg reflection divided by that of the 4th order reflection (I2/I4), normalized by myelin period. *P < 0.05; **P < 0.01 (Student's t-test).

Figure 3.8 X-ray diffraction patterns collected from optic nerves and spinal cords isolated from P26.

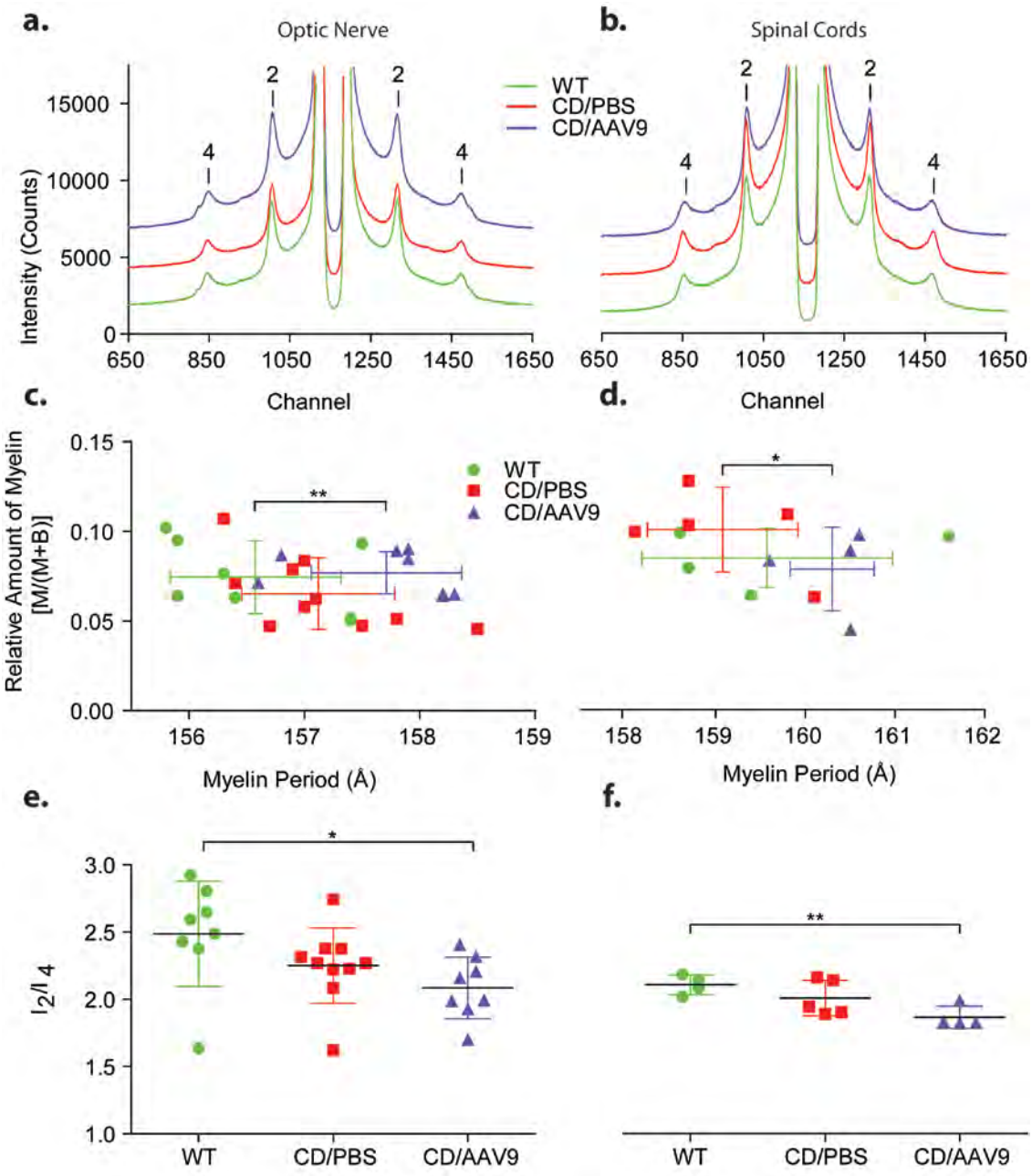

Discussion

Our study aims to develop efficacious therapeutics for CD using the AspA$^{-/-}$ KO mouse model and systemically delivered rAAVs for CNS-targeted AspA gene therapy as well as address off-target transgene expression in peripheral tissues. The AspA$^{-/-}$ mouse model in SV129/Ev background (Matalon et al., 2000) recapitulates the severest form of CD. Animals show progressive neuropathology and retinopathy, severe developmental delay, difficulties in mobility and whole body tremors around P19, which gradually worsens until their death around P27 [Figures 3.1 & 3.4a] making them a stringent preclinical model to study the molecular etiology of AspA deficiency and evaluate efficacious therapeutics, primarily based on the rescue of early lethality. Our study clearly demonstrated the feasibility of completely rescuing the early lethality, slowing down the disease progression, and extending the survival of CD mice [Figure 3.4b].

Our findings address several critical issues in systemically delivered CNS gene therapy. First, IV injections of rAAVrh.8 and rAAVrh.10 to CD mice at P0 are therapeutically equivalent to rAAV9, significantly improving their early motor function and growth, and effectively rescuing early lethality, which expands options in the existing rAAV repertoire to select serologically suitable vectors for patient populations. Our data also provide the first evidence of harnessing endogenous miRNA to regulate therapeutic expression of rAAV tissue specifically, which is shown to be safe, not disturbing homeostasis or function of endogenous miRNAs (Xie et al., 2010). In addition, the success of IV gene therapy as late as P20 in CD mice represent a clinically relevant

advance from the documented therapeutic benefit at P10 in a mouse model for spinal muscular atrophy (Foust et al., 2010). However, we did observe reduced mobility in the later treated animals [Figure 3.4d–g], which indicates that early intervention is therapeutically more beneficial, echoing the results of a recently concluded CD gene therapy study on patients (Leone et al., 2012).

Robust neuronal transduction in GC mice [Figure 3.2e] suggested that rAAV9 delivered AspA may improve myelin structures by hydrolyzing NAA at its source but may not help myelination by oligodendrocytes. Our detection of aspartoacylase-expressing neurons in the WT animals also differs from published data (Madhavarao et al., 2003; Madhavarao et al., 2004) but would explain the widespread activity detected in cerebral hemispheres [Figure 3.2d], although we cannot discount possible cross-reactivity of our AspA antibody with amidohydrolase I that has only 7% reactivity toward NAA (Goldstein, 1976; Mehta and Namboodiri, 1995).

Improved motor functions [Figures 3.4d–h & 3.5e–h] might result from reconstituted AspA and mitigated neuropathology in the pyramidal nuclei of the hindbrain and spinal cord of treated mice [Figure 3.3 a & b]. However, we did see partial hind limb paralyses with dragging of hind limbs and decline in mobility starting around 8 months post-injection [Video 3.4], although the animals still have intact righting reflexes, move around and eat with no obvious weight losses. One possible cause for the late-onset motor dysfunctions could be due to a gradual loss of rAAV-mediated AspA expression as a consequence of glial cell transduction and regeneration. Around 14 months, the animals

started showing infrequent and brief seizures. Readministration of serologically different rAAVs by a different route may help to sustain correction of myelin neurochemistry and motor function as CNS-directed rAAV gene.

Lipid abnormalities for myelin-enriched cerebrosides in CD mice were largely similar to those in the tremor rat model of CD (Saher et al., 2005; Wang et al., 2009). Since cholesterol is a major component of the myelin sheath, its reduction can be attributed to defects in myelin content (Saher et al., 2005). CNS-targeted AspA gene transfer by rAAVs appears to correct abnormalities in ganglioside and cholesterol levels but not the myelin-specific (cerebrosides) or myelin-enriched (sulfatides and GM1 ganglioside) lipids [Figure 3.6d & Table 3.2). The subtle differences in electron density distribution within the myelin sheath detected among all groups [Figure 3.8] are also consistent with altered lipid profiles. Further studies are warranted to compare the physiochemical properties and biophysical structures of myelin in the CD and GC mice. X-ray diffraction analysis, however, did not detect differences in relative amount of myelin between WT, CD, and GC mice. It is unclear whether this is a result of changes in axon diameter, lower total scatter from affected animals or region-specific differences in optic nerves and spinal cords. In addition, the dramatic loss of vision in CD mice [Figure 3.1c] might arise from demyelination of optic nerves, retinal degeneration, and pathological changes in cell types responsible for visual acuity, or all of the above.

When translated into human applications, the vector dose regimen used in our study is ~2×10^{14} vector genomes/kg. Even though similar doses have recently been

approved for systemic delivery of rAAV9 to pediatric patients of spinal muscular atrophy (2012); lower doses would reflect a more favorable risk-to-benefit ratio clinically and reduced vector manufacturing burden.

In conclusion, our study demonstrates the crucial role of AspA in myelination and early neurodevelopment as well as the feasibility of treating CD by CNS-targeted gene therapy using systemically delivered rAAVs. A more comprehensive comparison of three leading vectors (i.e., rAAV9, rAAVrh.8 and rAAVrh.10) in CD mice may be warranted to select a clinical candidate vector. Afterwards, a formal toxicology, safety and biodistribution study of the clinical candidate vector in nonhuman primates may constitute a critical path leading to human clinical applications for gene therapy of CD and other untreatable CNS diseases.

CHAPTER IV*:* CNS-RESTRICTED GENE DELIVERY USING RAAVS RESCUES LETHALITY BUT NOT MOBILITY DEFECTS SUGGESTING PERIPHERAL TISSUE INVOLVEMENT AND INFLAMMATION-MEDIATED PATHOLOGY IN CD MICE

The following chapter contains the manuscript:

Ahmed SS, Schattgen S, Sikoglu ME, Su Q, Hampton TG., Fitzgerald K, Matalon R, Gao G. CNS-restricted gene delivery using rAAVs rescues lethality but not mobility defects suggesting peripheral tissue involvement and inflammation-mediated pathology in CD mice (manuscript under preparation)

The study was devised and results were interpreted by me under the supervision of Dr Gao. All experiments except for the ones listed below have been performed by me and the manuscript was prepared by me and Dr Gao. Figure 4.6 c, d were contributed by Stefan Schattgen. Figure 4.1e was prepared by Dr Elif Sikoglu, Figure 4.5e upper panel was contributed by Dr Thomas Hampton. Dr Matalon kindly provided the mice. The manuscript was prepared by me and corrected by Dr Gao.

CHAPTER IV*:* CNS-restricted gene delivery using rAAVs rescues lethality but not mobility defects suggesting peripheral tissue involvement and inflammation-mediated pathology in CD mice

Introduction

Progressive spongy white matter degeneration and edema in the brain are hallmarks of a rare fatal pediatric leukodystrophy- Canavan disease (CD). Clinical symptoms include low muscle tone, blindness, severe motor retardation and premature death (Traeger and Rapin, 1998). The disease occurs due to autosomal recessive mutations in the enzyme aspartoacylase (AspA) (EC 3.5.1.15) that metabolizes N-acetyl aspartic acid (NAA) to yield acetate for myelination (Birnbaum et al., 1952 ; Kaul et al., 1993; Matalon et al., 1988; Mehta and Namboodiri, 1995). Aspartoacylase is known to regulate lipid synthesis in the brain and its substrate NAA is the second-most abundant metabolite in the brain. NAA is produced by neurons and used by oligodendrocytes to coordinate their differentiation, energy production, and lipid synthesis (Namboodiri et al., 2006). Absence of AspA leads to accumulation of NAA in the body and subsequent NAAduria that is a unique to CD (Matalon et al., 1988). NAA has been known to induce seizures and generate reactive oxygen species (Akimitsu et al., 2000; Pederzolli et al., 2009); however, it has not been studied if the NAA accumulated in the absence of AspA cause the activation of immune cells that result in the spongy degeneration of the brain.

Since CD is a monogenic neurodegenerative disease, use of recombinant adeno-associated viruses (rAAVs) promises to be an attractive therapeutic option. Additionally modulation of serotype and the route of delivery can enhance transduction specificity.

The first *bona-fide* animal model to study the disease was the aspartoacylase knockout mouse (CD mouse) (Matalon et al., 2000). In the Sv129/Ev background, these mice have a very short perinatal lifespan (<4 wks) and recapitulate clinical symptoms of the severest manifestation of CD (Ahmed et al., 2013; Matalon et al., 2000). Hence, they are a stringent preclinical model to evaluate therapeutics primarily based on the rescue of early lethality (Ahmed et al., 2013).

Our previous study used systemically delivered rAAVs for CNS-directed AspA gene therapy in the CD mouse model, a stringent preclinical model for the congenital form of the disease (Ahmed et al., 2013). The therapy completely rescued early lethality, slowed disease progression and extended survival of CD mice. rAAVrh.8 and rAAVrh.10 were found to be therapeutically equivalent to rAAV9, thus, expanding options in the existing rAAV repertoire for selection of serologically suitable vectors for patient populations. The vector dose used in the CD mice would translate to ~2×10^{14} vector genomes/kg in humans. Even though similar doses have recently been approved for systemic delivery of rAAV9 to pediatric patients of spinal muscular atrophy (2012); lower doses would reflect a more favorable clinical risk-to-benefit ratio and reduce vector manufacturing burden.

The intravenous delivery route allows for transduction of the whole body wherein only a small fraction gets in the brain justifying the large vector dosage. To make lower doses more effective, vectors should be delivered into the CNS. Intraparenchymal injections have been the most widely used delivery routes for the Central Nervous System (CNS) allowing the direct targeting of a defined cell population (Leone et al.,

2000). Though useful for region specific corrections, intraparenchymal injections are not suited for global CNS corrections since there is limited diffusion of the therapeutic from the injection site. To ensure global CNS delivery, use a lower dose of vector yet avoid unnecessary transduction of peripheral tissues, a promising avenue is the intracerebroventricular route of vector administration. The injections rely on the ability of rAAVs to cross the ependymal lining and enter the brain parenchyma from the cerebral ventricles within the first 24 hours of birth (Passini and Wolfe, 2001). Intraventricular injection of rAAVs at this age results in widespread transduction of neurons throughout the brain (Kim et al., 2014). Our previous studies and early reports on the abilities of rAAVs in mediating CNS transduction by intravascular delivery (Foust et al., 2009; Zhang et al., 2011) prompted us to compare the relative therapeutic abilities of these vectors in enhancing survival using intracerebroventricular delivery.

For gene therapy, we administered rAAV9, rAAVrh.8 and rAAVrh.10 carrying the human AspA gene intravascularly and intracerebroventricularly in CD mice at P0. Here, we demonstrate that a 50-fold lower dose than previously described for intravenous therapy (Ahmed et al., 2013) can still ameliorate disease symptoms; however, correction of the motor functions does not persist until the end of life. Additionally the previous study provided the first evidence of harnessing miRNA binding sites to regulate therapeutic expression of rAAV in a safe, tissue-specific manner without perturbing endogenous miRNA homeostasis or function (Ahmed et al., 2013; Xie et al., 2010). We also examined these animals and the ICV injected animals to study the role of AspA in peripheral tissues. We examined several morphological and functional aspects of

peripheral tissues of untreated mice and found that peripheral tissues do express AspA and its deficiency does cause pathology in these tissues. Our in-depth analyses of neuronal cell types help to understand their contribution to CD pathogenesis. Most importantly, our study demonstrates, for the first time, involvement of the immune system in response to accumulation of NAA and the importance of targeting peripheral tissues in CD.

Materials and Methods

Viral production: All rAAV vectors were produced by transient transfection of 293 cells and CsCl gradient sedimentation as previously described (Sun et al., 2010). Vector preparations were titered by quantitative PCR, purity of vectors was assessed by 4–12 % SDS-acrylamide gel electrophoresis and silver staining (Invitrogen, Carlsbad, CA) and morphological integrity of virions was assessed by Transmission electron microscopy of negative stained recombinant AAV virions at Electron Microscopy Core, UMass Medical School, Worcester.

Animal procedures: All animal procedures were approved by the Institutional Animal Care and Use Committee (IACUC) of UMass Medical School. $AspA^{+/-}$ Sv129/Ev mice littermates were bred using programmatic timing and newborn pups were dosed on P0. Vectors were injected in the facial vein of P0 pups at doses of $4X10^{11}$ GC/mouse and intracerebroventricularly at a dose of $2X10^{10}$ GC/mouse respectively. After the injection pups were cleaned, rubbed with bedding, and then returned to their cage. The dam was reintroduced after brief nose numbing using ethanol pads.

Immunohistochemistry: Animals were anesthetized, transcardially perfused with 4% paraformaldehyde (v/v) in PBS. Whole carcasses were postfixed in fixative for 1 day. Organs were extracted, rinsed in PBS, and sagitally sectioned. One half was cryoprotected in 30 % sucrose (w/v) in PBS at 4°C, embedded in OCT compound (Sakura Finetek, Torrance, CA) and frozen in a dry ice/ethanol bath. 40µm floating sections of the entire brain were cut in a Cryostat (Thermo Microm HM 550) for immunostaining. The other half was processed for Hematoxylin and Eosin staining for

morphological studies.

Floating sections were stained in 12-well plates. Sections were washed once in PBS for 5 mins, and incubated in blocking solution containing 0.05 % Tween-20 (v/v) (Fisher, Pittsburgh, PA), and 10 % goat serum (v/v) (Invitrogen) for 1 hour at room temperature. Sections were incubated with primary antibodies at 4°C overnight, washed twice in 0.05 % Tween-20 in PBS (PBST) for 15 mins each followed by incubation in appropriate secondary antibodies at room temperature for 1 hour. Sections were washed twice in PBST for 10 mins each before mounting on glass slides. Vectashield with 4,6-diamidino-2-phenylindole (Vector Laboratories, Burlingame, CA) was used to mount all slides. Omission of either the primary or the secondary antibody in single-label experiments resulted in no labeling. The primary antibodies used were as follows: mouse aspartoacylase (Abmart, New Jersey); mouse NeuN (MAB-377, clone A60; Millipore); rabbit NeuN (ABN-78, Millipore) and appropriate secondary antibodies from Invitrogen. For CD45 staining, the Dako dual link system was used. Briefly paraffin sections of the brain were deparaffinized and subject to heat-induced epitope retrieval (BD Retrievagen A). Slides were cooled and endogenous peroxidase was blocked using 3% (vol/vol) H_2O_2 for 15 min. They were incubated with primary antibody for 1hr at room temperature, washed and incubated with the secondary antibodies. The slides were then counterstained with haematoxylin, dehydrated and mounted.

Imaging and Image Analysis: Stained sections were examined using DM 5500B Upright microscope (Leica Microsystems, Wetzlar, Germany), and images were captured with Leica DFC365 FX high-sensitivity monochrome digital camera. Regions of interest were

identified according to the mouse brain atlas. Z stack of images were taken with a 63X objective and 1.6X additional magnification for each channel and overlaid to obtain a multicolor image at 100.8X. Deconvolution was performed using Leica Application Suite Advanced Fluorescence software.

Electrocardiography (ECG): ECGs were recorded non-invasively in conscious mice similar to a method described previously for mice (Chu et al., 2001). Briefly, mice were removed from their cages and positioned inside the ECGenie™ recording enclosure (Mouse Specifics, Inc., Boston, MA, USA). A pair of silver-chloride ECG electrodes were embedded in the floor of the enclosure and spaced to provide contact between the electrodes and animals' paws. Since even modest handling may induce alterations in heart rate, each mouse was permitted to acclimatize for ~10 min prior to collection of data. The signals were digitized at a sampling rate of 2000 samples/s. When mice were positioned such that a forepaw and hind paw were not uniquely in contact with one of the electrodes, the output from the amplifier was discarded. Only data from continuous recordings were used in the analyses. Each signal was analyzed using e-MOUSE™, which incorporates Fourier analyses and linear time-invariant digital filtering of frequencies below 3 Hz and above 100 Hz to minimize environmental signal disturbances. The software uses a peak detection algorithm to find the peak of the R-waves and to calculate heart rate. Subsequently, determination of first and second derivatives and algebraic "if-then" search the ECG signals for probable P-wave peaks and onset and termination of QRS complexes. The end of the T-wave of each signal was defined as the point where the signal returned to the isoelectric line (the mean voltage

between the preceding P-wave and QRS interval). The QT intervals were rate corrected (QTc) by application of an equation recommended for rodent electrocardiography (Mitchell et al., 1998). The software plots its interpretation of P, Q, R, S, and T for each beat so that spurious data resulting from unfiltered noise or motion artifacts may be rejected. e-MOUSE™ then calculates the mean of the ECG time intervals for each set of waveforms.

***Electroretinography (ERG)*:** Mice were dark-adapted overnight and anesthetized with 100 mg/kg ketamine and 20 mg/kg xylazine in saline before testing. Both pupils were topically dilated with phenylephrine hydrochloride and 1% tropicamide, and mice were placed on a heated platform. Rod-dominated responses were elicited in the dark with 10 μs flashes of white light (1.37×10^{5} cd m−2) presented at intervals of 1 min in a Ganzfeld dome. ERGs were monitored simultaneously from both eyes with a silver wire loop electrode in contact with each cornea wetted with celluvisc containing Carboxy Methyl Cellulose Sodium 1%.

Western blot: Mice were sacrificed and their tissues were extracted and homogenized. Protein in equal quantities was loaded into a 12% Tris–HCl gel well (Bio-Rad Laboratories, CA) and transferred to a nitrocellulose membrane (Bio-Rad). The membrane was incubated in blocking buffer for 1hr followed by AspA polyclonal antibody overnight. After three washes in 0.1 % PBST, it was incubated with secondary antibodies conjugated to LI-COR IRDye for 1 hour at room temperature. After two washes with 0.1 % PBST signal was detected using the Odyssey Imager (LI-COR).

Cell Titer Glo Assay: Brains were dissected from 1-month-old female mice, washed, and

homogenized in Krebs-Ringers bicarbonate buffer (125mM NaCl, 1.4mM KCl, 20mM HEPES [pH 7.4], 5mM $NaHCO_3$, 1.2mM $MgSO_4$, 1.2mM KH_2,PO_4, 1mM $CaCl_2$) containing 1% BSA. Protein concentrations were determined using the BCA assay (Pierce). 50µg of brain lysate was used to measure ATP concentration using the CellTiter-Glo Luminescent Cell Viability kit (Promega) in a 96-well format and assayed using manufacturer's instructions. To measure the recovery of ATP from brain lysates, known amounts of ATP were used to measure ATP bioluminescence using the CellTiter-Glo method as above. The recovery of ATP was calculated from these values.

Evans Blue injection: Vascular permeability was quantitatively evaluated by fluorescent detection of extravasated Evans blue dye. Briefly, 2% Evans blue dye in saline was injected intravenously as a BBB permeability tracer. Mice were deeply anesthetized with isofluorane and transcardially perfused until colorless perfusion fluid was obtained from the right atrium. Samples were weighted and homogenized in 10-fold volume of 50% trichloroacetic acid solution. The supernatant was obtained by centrifugation and diluted 4-fold with ethanol. Fluorescence intensity was determined by a microplate fluorescence reader (excitation 620 nm and emission 680 nm). Calculations were based on the external standards dissolved in the same solvent. The amount of extravasated Evans blue dye was quantified as micrograms per tissue.

Macrophage stimulation: Immortalized C57BL/6 macrophages were seeded in 6-well plates at 2 x 10^6 cells/well one day prior to stimulation. Cells were stimulated with 200 ng/mL LPS or 1, 10, and 100 uM NAA overnight. RNA was purified using an RNeasy kit (Qiagen)

qRT-PCR analysis: RNA was extracted using Trizol (Invitrogen), according to manufacturer's instructions. Total RNA (0.5–1μg) was reverse-transcribed (Reverse Transcriptase, Applied Biosystems). Quantitative PCR reactions were performed in triplicate with 0.3 μM gene-specific primer pairs using the GoTaq qPCR master mix (Promega) in a StepOne Plus Real-time PCR instrument (Applied Biosystems).

Flow cytometry and Splenocyte proliferation assay: Spleen and thymus were crushed with frosted glass slides, red blood cell lysis performed, and resulting suspension strained through 70 uM cell strainer (BD Biosciences) to make single cell suspensions. For splenocyte proliferation assays, cells were labeled with 5 uM CFSE for 15 minutes prior to plating in 96-well plate coated with 10 ug/mL anti-CD3e and soluble anti-CD28 added at 1 ug/mL. Cells were allowed to proliferate for 5 days before surface staining. Prior to staining, Fc receptors were blocked using supernatant from 2.4G2 hybridoma cells (anti-CD16/32). Cells were stained using anti-TCRb-PerCP-Cy5.5, anti-CD19-PerCP-Cy5.5, anti-B220-AlexaFluor 488, anti-CD11b-FITC, anti-CD11c-eFluor 450, anti-Ly6G-PE-Cy7, anti-Ly6C-APC, anti-NK1.1-APC, anti-CD3e-PerCP-Cy5.5, anti-FoxP3-eFluor450, (eBioscience), anti-CD45-V500, anti-CD8a-PE (BD Biosciences), anti-F4/80-PerCP-Cy5.5, and anti-CD25-APC (Tonbo Bioscience). Data acquisition was performed using a 4-laser LSRII (BD Biosciences). Analysis was performed using FlowJo analysis software (TreeStar).

Genome copy number: rAAV genomes were quantified in 10ng of genomic DNA extracted from mouse tissues using the QIAamp DNA mini kit for quantitative detection of vector genome copies by Taqman® probes (Applied Biosystems) with a single-copy

endogenous GAPDH gene) as the diploid cell number reference. The Taqman® real-time PCR kit was run with primer sets which amplified regions of the nRBG poly A (Probe, 6FAM-ATG AAG CCC CTT GAG CAT CTG ACT TCT-TAMRA; Fwd, GCC AAA AAT TAT GGG GAC AT; Rev, ATT CCA ACA CAC TAT TGC AAT G). The sensitivity of the assay was 10 copies/cell.

Assays for serum ALT and AST levels: Blood was collected from the ocular sinus of all of the animals in each group. ALT (serum glutamic pyruvic transaminase) or AST reagent (Teco Diagnostics, Anaheim, CA) was used, and the protocol was altered for use in 96-well flat-bottomed microplates. The plate was then read, and the aminotransferase concentrations were determined according to the manufacturer's instructions.

Neural cell culture: The culture of primary hippocampal and cortical neurons was performed as described (Huang and Richter, 2007) in neurobasal media (Invitrogen) containing B27 supplement (B27 media) and glutamine (1µg/ml). Oligodendrocytes and astrocytes were cultured as reported (Albuquerque et al., 2009; Chen et al., 2007)

AspA activity assay: Mice were sacrificed 3 months after injection, and brain homogenates were used for the enzyme assay. Briefly, the brain was homogenized and incubated with 50mM Tris–HCl (pH 8.0), 0.5% (w/v) NP-40, 50 mM NaCl, 1 mM CaCl2, 2.8 mM NAA in a total volume of 600 µl. After incubation at 37°C for 3-6h, the assay mixture was centrifuged and the supernatant was incubated with malic dehydrogenase, glutamic oxalacetic transaminase, and NADH for 10 min at 37°C. The amount of L-aspartate released was estimated by decrease in absorbance due to the conversion of NADH to NAD using a spectrophotometer (Beckman Coulter, DU 800) at

340 nm. One milliunit of aspartoacylase activity is equivalent to 1 nmol of aspartate released in 1 min. Values were calculated using ANOVA. The value $P < 0.05$ was considered significant.

^{1}H Magnetic Resonance Imaging and Spectroscopy: Mice were anesthetized with 2% isofluorane and constantly monitored for vital signs. All experiments were carried out on a Bruker 4.7T/40 cm horizontal magnet (Oxford, UK) equipped with 250 mT/m magnetic field gradient and interfaced with a ParaVision 4.0 console. A ^{1}H radiofrequency (RF) coil configuration (Insight NeuroImaging Systems, MA) with inner diameter (ID) of 4 cm was used for the experiments. T2-weighted anatomical images were acquired using a fast spin-echo sequence (RARE) (TR=3000 msec, TE=48 msec, matrix size=256×256, FOV=2.5 cm×2.5 cm, slice number=16, slice thickness=1 mm). 1H MRS Data was acquired using single voxel (Pont Resolved Spectroscopy Sequence (PRESS) (TR=2500 msec, TE=20 msec, Naverage=1024, voxel size=3 mm×3 mmX3 mm).

Proton spectra were fit using LCModel (Version 6.2-2B), which analyzed in vivo proton spectrum as a linear combination of model in vitro spectra from individual metabolite solutions (Provencher, 2001) and generated data as absolute fits (in institutional units) and standard deviations (SD%). Standard deviation was used as a measure of the reliability of the fit. The spectral inclusion criteria were SD less than 20% for NAA, Cr and Ins.

Behavioral studies: For the beam balance test, animals were placed in the middle of a horizontal wooden balance beam (1.5 cm × 100 cm) with pads underneath to protect mice that fall off the beam. Latency to fall was recorded, with a 3min time limit for each trial.

Neuromuscular function of the mice was assessed by testing grip strength on an inverted screen. Mice were placed in the center of a screen (30 cm^2 square-wire mesh, 25 mm^2 holes) until they gripped the mesh. The screen was then inverted above a cushioned surface for a 2sec period with the mouse's head declining. Latency to fall from the screen was recorded, with a 2min time limit for each trial.

Mice were subjected to a rotarod test to evaluate motor coordination and balance. Each animal was placed on the rotarod after which speed was adjusted to 3 rpm. The latency to fall off the rotarod within this time period was recorded for a fixed speed. Animals were also tested for their latency to fall off at accelerated speeds going from 4 to 40 rpm in 5mins.

Animals were tested for each experiment 3 times with an inter-trial interval of approximately 30 min for each animal and means of 3 trials were used to plot the graphs.

Transmission Electron Microscopy: Mice were anesthetized and perfused with a solution of 2.5 % glutaraldehyde in 0.05 M Sodium Phosphate buffer, pH 7.2. The brain was extracted and incubated in 2.5 % glutaraldehyde in 0.05 M Cacodylate buffer overnight at 4°C. It was sectioned into 1 mm thick sections, rinsed twice in the same buffer and post-fixed with 1 % osmium tetroxide for 1h at room temperature. Sections were washed in DH2O for 20mins at 4°C and then dehydrated in graded ethanol series of 20% increments, before two changes in 100 % ethanol. Sections were infiltrated with two changes of 100% propylene oxide and then with a 50%/50% propylene oxide / SPI-Pon 812 resin mixture overnight. After three changes of fresh 100 % SPI-Pon 812 resin, sections were polymerized at 68°C in plastic capsules. Regions of interest were cut out

and thick-sectioned for toluidine blue. Chosen regions were reoriented and approximately 70nm thin sections were placed on copper support grids and contrasted with lead citrate and uranyl acetate. Sections were examined using the FEI Tecani 12 BT with 80Kv accelerating voltage, and images were captured using a Gatan TEM CCD camera.

X-ray Diffraction Analysis: X-ray diffraction was performed as described (Agrawal et al., 2009). Briefly, sciatic nerves were dissected from mice sacrificed using isoflurane and were maintained in physiological saline (154mM NaCl, 5mM phosphate, pH 7.4) and loaded into thin-walled, quartz capillary tubes which were then filled with saline and sealed with wax and enamel. X-ray diffraction experiments were carried out using nickel-filtered, single-mirror focused CuKα radiation from a fine-line source on a 3.0 kW Rigaku X-ray generator operated at 40 kV by 10 mA. Exposure times were 30 min. Diffraction patterns were collected using a linear, position-sensitive detector (Molecular Metrology, Inc., Northampton, MA) and analyzed using PeakFit (Jandel Scientific, San Rafael, CA). Myelin period was calculated from the positions of the intensity maxima in the diffraction patterns. The relative amount of myelin in each sample was calculated by measuring the total integrated intensity of all maxima over background, excluding small-angle scatter around the beam stop and wide-angle scatter.

Statistical Analyses: Statistical calculations included Log rank Mantel Cox test for the survival table and one way ANOVA followed by Tukey's Multiple Comparison test for all other experiments. *$P < 0.05$; **$P < 0.01$; ***$P < 0.001$, NS not significant.

Results

Restoration of AspA by gene therapy systemically vs. in the CNS alone [IV vs. ICV]

CD mice mirror the attributes of human patients showing early perinatal lethality (>28days) and severe neurodegeneration, hence benefits of a therapeutic intervention would be best measured by monitoring longevity of treated animals. Long term survival was monitored using the Kaplan-Meier curve for treated mice (n=10 per group) injected intravenously [Figure 4.1a, upper panel] as well as intracerebroventricularly [Figure 4.1a, lower panel] with all three serotypes. We focused on rAAV9 to compare differences between the routes of delivery. Weight gain was monitored daily for the first month [Figure 4.1b, upper panel] and subsequently every two weeks [Figure 4.1b, lower panel] to compare differences between the routes of delivery using rAAV9 until the animals (n=10) caught up with their wildtype (WT) littermates. There was a uniform rescue of lethality and extended survival as long as 2 years with all the treated animals and there was no significant difference in weight gain between routes of administration.

As reported earlier, Hematoxylin & Eosin (H&E) staining of brain sections showed vacuoles that indicated severe neurodegeneration in untreated CD mice (Ahmed et al., 2013) (n=4) at postnatal day 25, P25. These were significantly reduced in mice treated both intravenously as well as intracerebroventricularly with rAAV9 [Figure 4.1c]. To evaluate changes in vision since CD patients eventually lose their sight, scotopic electroretinography (ERG) studies were performed on all groups of mice (n=4) at P90 to evaluate retinal response to light flickers as described earlier (Ahmed et al., 2013). Electrophysiological measurements of retinal cells produce the ERG trace consisting of

a-waves that indicate photoreceptor activity and b-waves that indicate glial cell activity b-waves [Figure 4.1d]. Both intravenous and intracerebroventricular delivery methods correct vision to the same extent (depicted by rAAV9). Cerebral edema is an important pathological effect in CD patients and hence MRI was performed to evaluate the status of the brain. Intracerebroventricular injections relieved edema to a greater extent than intravenous injections delivery methods [Figure 4.1c]. Motor functions were evaluated for both the IV and ICV injected animals and even though the latter performed much better on all the 4 motor tests, they were not able to sustain the correction over time [Figure 4.1f]. Since it seemed that restricting the therapeutic vector to the CNS did not allow complete alleviation of the pathology, we tested the animals injected with a previously described miRNA-regulated vector genome designed for CNS-restricted gene transfer, called rAAV9hAspA(miR-1BS)3-(miR-122BS)3 (i.e. rAAV9hAspA-miRBS) which carries 3 copies each of the miRNA binding sites specific to miR-1 and miR-122 (i.e. miRNAs enriched in heart and skeletal muscle, and liver respectively but not in the CNS)(Ahmed et al., 2013). These animals too showed a reduction in motor function abilities with the passage of time suggesting an involvement of peripheral tissues in CD pathology [Figure 4.2].

Aspartoacylase is present in peripheral tissues and its deficiency leads to morphological and functional abnormalities in multiple peripheral tissues including the Peripheral Nervous System

In order to investigate the importance of AspA in peripheral tissues we used fresh tissues from WT mice (n=4) powdered in liquid nitrogen to determine the presence of

AspA by qPCR [Figure 4.3a, upper panel] and western blot [Figure 4.3a, lower panel]. AspA was indeed expressed in varying amounts in different peripheral organs. We then examined the morphology of the various peripheral organs starting with their gross weight normalized to their body weight [Figure 4.3b, upper panel].

We examined the complete differential count of blood (n=5) [Figure 4.3c] to discover that diseased mice have lymphocytopenia and a biochemistry profile of their serum (n=5) revealed a propensity of these mice for low blood glucose and defective pancreatic function evident by amylase levels [Figure 4.3d]. We then examined the effect of AspA deficiency on the Central and Peripheral nervous systems by closely examining the morphology of the optic, sciatic and vagus nerves by Electron Microscopy studies [Figure 4.4a] and myelination status of sciatic nerve by X-Ray Diffraction [Figure 4.4b]. We found abnormalities in the myelin structure for all nerves in CD mice validated by the myelin period and I2/I3 ratio determined by X-Ray Diffraction studies [Figure 4.4b & c] similar to the reported behavior of the optic nerve. The I2/I3 ratio is a measure of the relative intensity of 2nd order X-ray reflection over the 3rd order reflections indicating a small change in membrane structure This suggests that AspA deficiency does affect the peripheral nervous system to a certain extent however the effect may be mild.

Figure 4.1 Systemically and intracerebroventricularly delivered rAAV-mediated gene therapy rescues lethality and metabolic defects but not motor functions in CD mice. (**a**) Kaplan Meier Survival curves for all groups treated with rAAV9, rAAVrh.8 and rAAVrh.10 at P0 (n=10) treated intravenously (upper panel) and intracerebroventricularly (lower panel) (**b**) Early growth rate was assessed by taking weights at 2 day intervals for the first month (upper panel) and then at 2 week intervals (lower panel) plotted as a function of time. rAAV treated animals were shown as a representative of the serotypes. (**c**) Hematoxylin & Eosin staining of brain sections showing neuropathology. (**d**) Scotopic ERGs of overnight dark-adapted WT and CD mice (n=4 each) to test the response of rods recorded as waveforms (μV) to flickers of light in increasing intensity called steps Upper panel, b wave; lower panel, a wave. (**e**) Representative T2 weighted MRI images showing water accumulation (white) in P25 CD/PBS and P60 GC and WT animals. (**f**) Motor functions of study groups were tested at P30 and P90 based on their performance on the balance beam, inverted screen and rotarod moving at fixed (3 rpm) and accelerated speed (4-40 rpm in 5mins).

Figure 4.1 Systemically and intracerebroventricularly delivered rAAV-mediated gene therapy rescues lethality and corrects phenotype and metabolic defects but not motor function in CD mice.

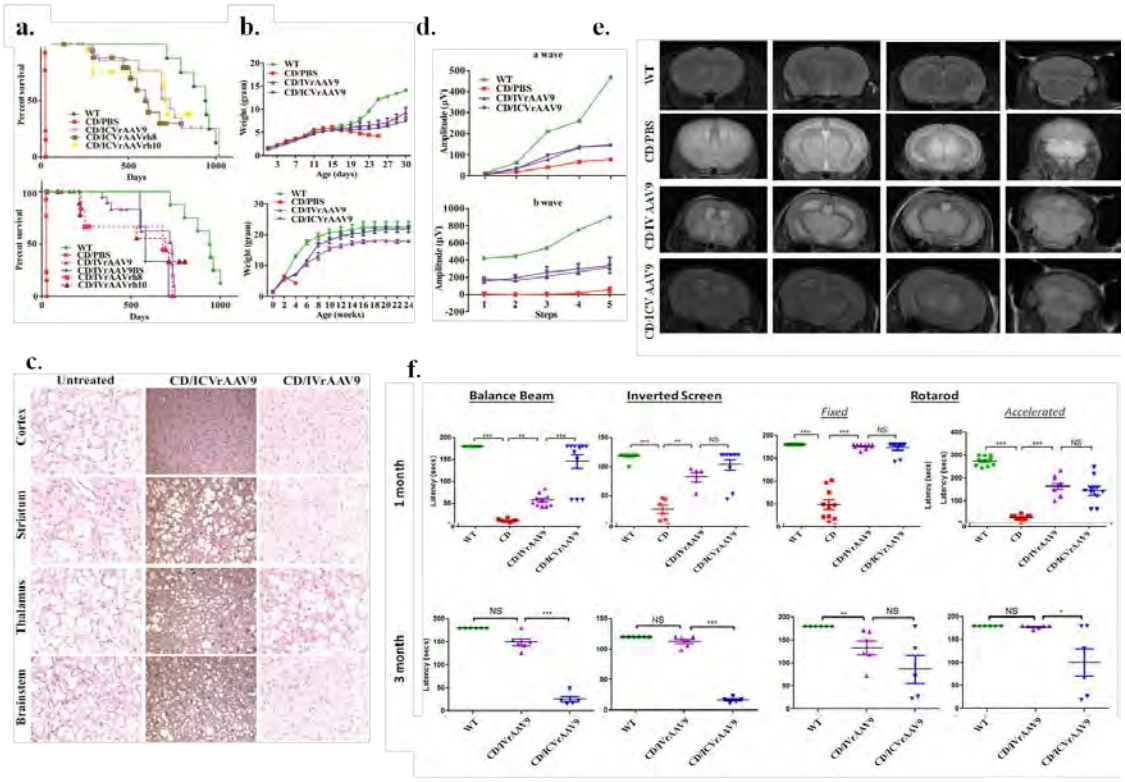

Figure 4.2 rAAV gene therapy using miRNA-mediated CNS restriction does not cause long-term correction of motor function in CD mice. Motor functions of study groups (n=6) were tested at P90 based on their performance on the balance beam, inverted screen and rotarod moving at fixed (3 rpm) and accelerated speed (4-40 rpm in 5mins).WT, wildtype; CD/PBS, CD/rAAV, CD mice treated with PBS or rAAV respectively.

Figure 4.2 rAAV gene therapy using miRNA-mediated CNS restriction does not cause long-term correction of motor function in CD mice.

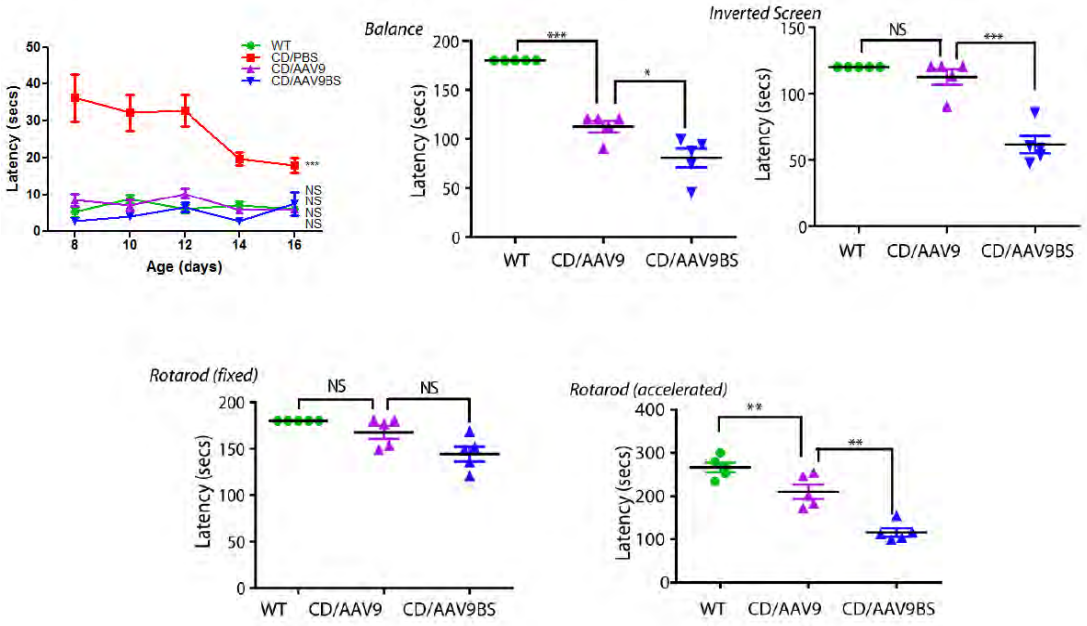

Figure 4.3: Importance of Aspartoacylase in peripheral tissues and general malaise in CD mice in addition to CNS pathology. (a) qPCR of Aspartoacylase mRNA and representative Western blot for aspartoacylase from fresh tissue homogenates of WT animals at P30 (n=4) showing extensive aspartoacylase expression in peripheral tissues. (b) Ratio of the weight of peripheral organs normalized to body weight of the animals (n=4) from which the tissues were collected; lower panel pictures of gross morphology of organs (c) Complete differential count of blood for CD and WT mice (n=4). (d) Serum of CD and WT mice (n=4) was tested for various biochemical markers.

WBC, White blood corpuscles; HCT, Hematocrit; MCV, Mean Corpuscular Volume; RBC, red blood corpuscles; HGB, Hemoglobin; MCH, Mean Corpuscular Hemoglobin; MCHC, Mean Corpuscular Hemoglobin Concentration; MPV, Mean Platelet Volume; PLT, Platelet; ALT, Alanine Aminotransferase; BUN, Blood Urea Nitrogen; Ca, Calcium; PO4, Phosphate; Na, Sodium; K, Potassium.

Figure 4.3 Importance of Aspartoacylase in peripheral tissues and general malaise in CD mice in addition to CNS pathology.

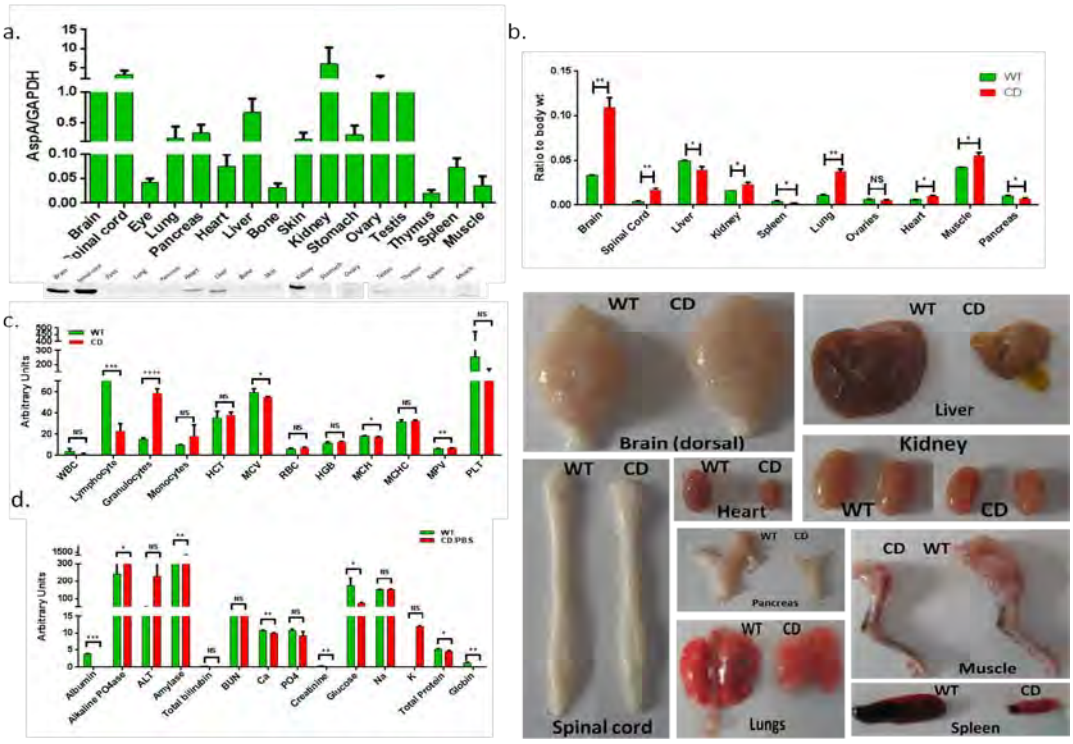

Figure 4.4 Examination of the Central and Peripheral Nerves. Nerves were isolated from perfused mice and sectioned. (a) Optic, Sciatic and Vagus nerves were processed for electron microscopy. Scale bars 200nm . Fresh sciatic nerve was isolated and used for X ray diffraction analysis (b) Myelin period and (c) Ratio of I2/I3 was estimated.

Figure 4.4 Examination of the Central and Peripheral Nerves.

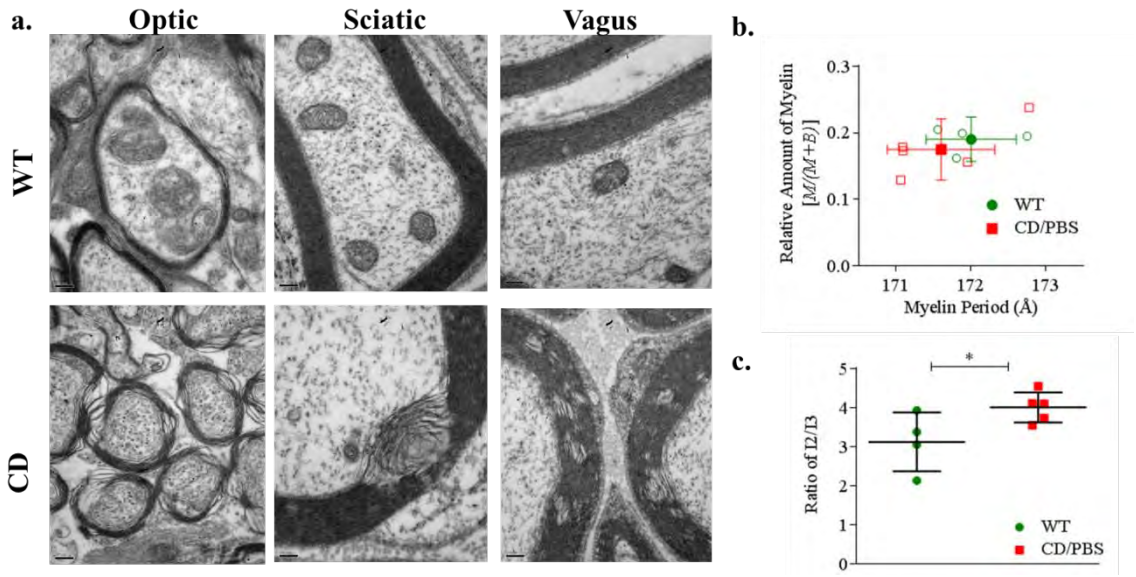

Figure 4.5 Peripheral organs like kidney, muscle and heart reveal abnormalities in morphology and functions contributing to additional pathology in CD mice. (a) Representative images from H&E stained paraffin sections of the kidney and medulla for WT and CD animals (n=4) (b) Electron microscopy of the renal cortex and medulla of P21 age matched mice (n=3 for each cohort) (lower panel). (c) Representative H&E stained sections of P26 mice where CD animals show more nucleation in muscle fibres of the tibialis anterior (TA) muscle (n=3). (d) Neuromuscular junction staining of the TA muscle showing several collapsed NMJs in CD mice compared to WT animals (n=3). Inset shows higher magnification picture of an individual NMJ. (e) Electrocardiography (ECG) trace of WT and CD mice at P21 revealing bradycardia (upper panel) and quantitation of the heart wall thickness using Image J using H&E section (3 sections at different levels each for n=3 animals per cohort).

Figure 4.5 Peripheral organs reveal abnormalities in morphology and functions contributing to additional pathology in CD mice.

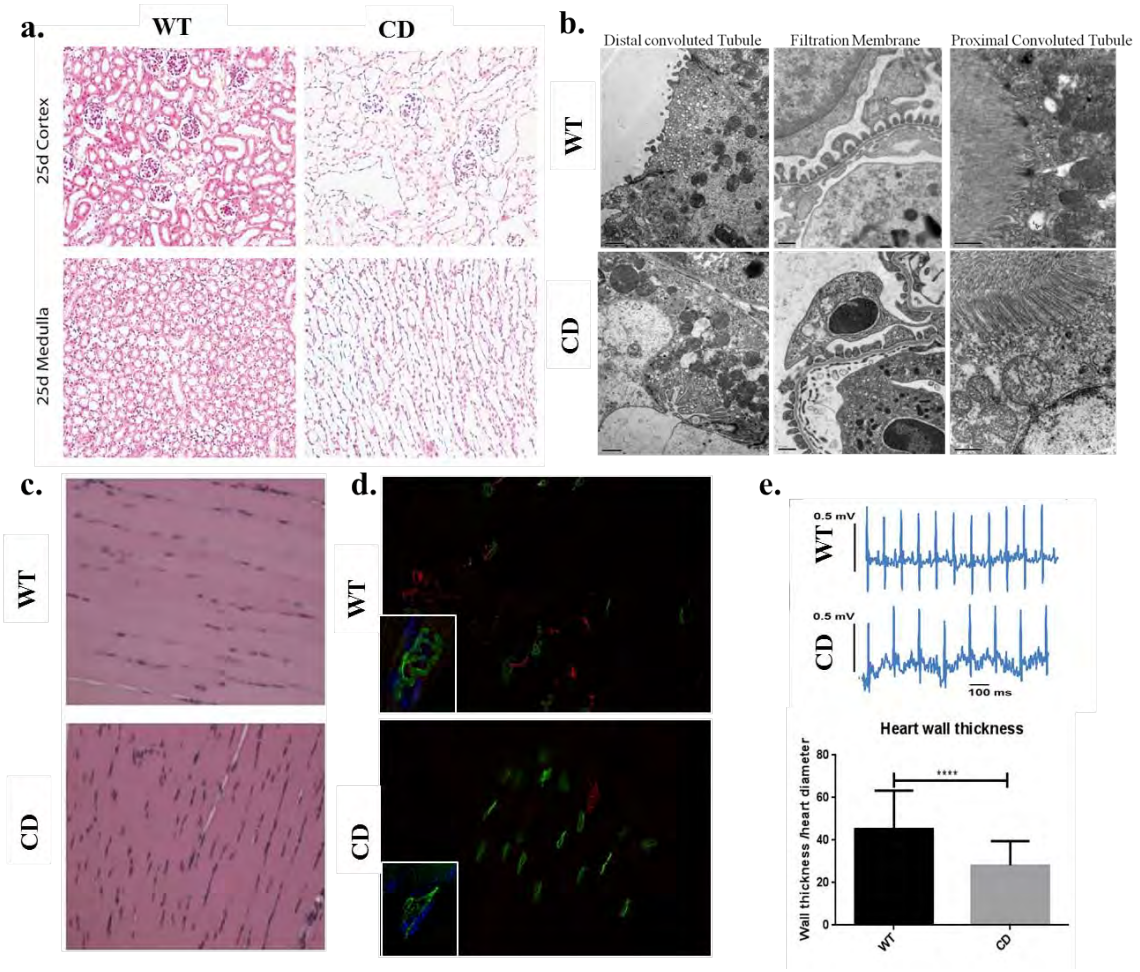

We then looked at peripheral tissues beginning with the kidney, which showed AspA levels even higher than the brain. Morphologically, H&E stain showed a significant difference in the lumen sizes of the kidney tubules [Figure 4.5a] and EM studies revealed apoptosing cells in the distal convoluted tubule, loosened filtration membranes and loosely structured villi in the proximal convoluted tubule [Figure 4.5b]. Since the miRBS vector detargeted therapeutic AspA expression from the muscle, heart and liver; we examined these organs in detail. Examination of the skeletal muscle histology showed that CD mice show more nucleation [Figure 4.5c]. Staining for the neuromuscular junction (NMJ) reveals that in CD mice, some NMJs show denervation [Figure 4.5d] and while a majority do not have the healthy pretzel shape but instead are collapsed [inset, Figure 4.5d].

We then looked at the heart for functional and morphological abnormalities [Figure 4.5e]. Electrocardiography (ECG) revealed bradycardia [Figure 4.5e, upper panel]. Closer examination of morphology revealed that the size of the heart was larger with respect to body weight [Figure 4.3b] and the heart walls were thinner in CD mice [Figure 4.5e, lower]. Also abnormalities in the vagus nerve [Figure 4.4a] could be linked to the bradycardia. We next examined the liver for structural abnormalities by H&E staining and tested serum for AST and ALT levels to check functions. The values though significantly different between the WT and CD mice fell within the normal range. In summary, the liver did not show any morphological or functional abnormalities [Figure 4.6a &b]. In addition to these organs we decided to examine the spleen because of its abnormally small size [Figure 4.3b]. Phenotyping of splenocytes by FACS revealed that

diseased mice have a significantly lower count of several immune cells including but not limited to the TCR, CD4 and CD8 cells [Figure 4.3c] and CFSE staining revealed that splenocytes of CD mice are unable to proliferate when challenged by CD28 [Figure 4.3d]. Hence, it appears that the immune system of CD mice is compromised. Additionally we examined the eyes for morphological changes by electron microscopy since blindness is one of the symptoms of CD patients and untreated mice have defective vision (Ahmed et al., 2013). EM analyses of the diseased mice showed disruption of the cellular matrix in several retinal layers [Figure 4.3e]. In CD mice, cells in the ganglion cells layer had a shrunken appearance while the inner plexiform layer showed an abundance of vacuoles. Cells were loosely arranged in the Outer Nuclear Layer. Regions like the Outer segment, transition cilia and the transition membrane externa showed apoptosing cells and disorganization.

NAA acts as an inflammatory agent to secondarily result in neurodegeneration

ICV administration of NAA gave rats seizures (Akimitsu et al., 2000), we decide to explore if NAA acts as an inflammatory agent. We performed in vitro studies on C57BL/6 bone marrow-derived macrophages that have been immortalized with CreJ2 retrovirus treating them with increasing concentrations of NAA. We found that 100mM NAA kills off the cells whereas lower doses of NAA does induce inflammatory genes most notably IL6 [Figure 4.7a]. Interestingly, AspA was upregulated in the macrophages presumably to maintain homeostasis. Whole brain homogenates also showed a similar trend [Figure 4.7b]. Moreover, since peripheral immune cells showed an abnormal phenotype [Figure 4.6c] we decided to explore the immunologically privileged brain for

Figure 4.6 Peripheral organs like spleen and eyes but not liver reveal morphological abnormalities in CD mice (a) Hematoxylin & Eosin staining of paraffin embedded liver shows no morphological abnormality (b) AST and ALT levels were determined using serum to determine functional abnormalities of liver. (c) FACS of splenocytes for TCR, CD8, CD4 and Treg markers (d) Splenocyte proliferation was monitored by estimating dilution of fluorescence of the CFSE dye over a period of 72 hours. Histograms of individual animals (n=4) were stacked. (e) Representative images from Electron Microscopy studies of the retinal layers of the eyes of WT and CD animals (n=3) Scale bars, 1μm.

Figure 4.6 Peripheral organs like spleen and eyes but not liver reveal morphological abnormalities in CD mice

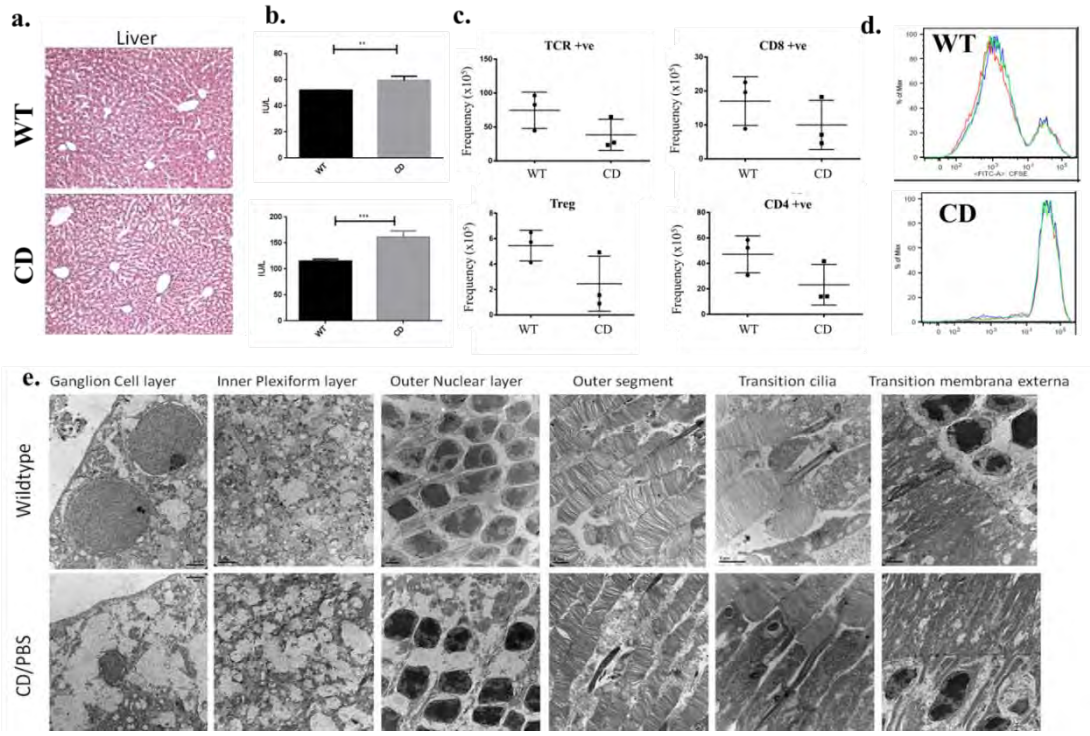

Figure 4.7 NAA mediates inflammation in the brain leading to microglia activation. (a) In vitro C57Bl/6 macrophages were treated with varying doses of NAA and assayed for expression of inflammatory genes and aspartoacylase by qRTPCR. (b) Brain homogenates of WT and CD were assayed for inflammatory genes (n=3). (c) Brain sections were stained for CD45RO and analyzed under light microscope.

Figure 4.7 NAA mediates inflammation in the brain leading to microglia activation.

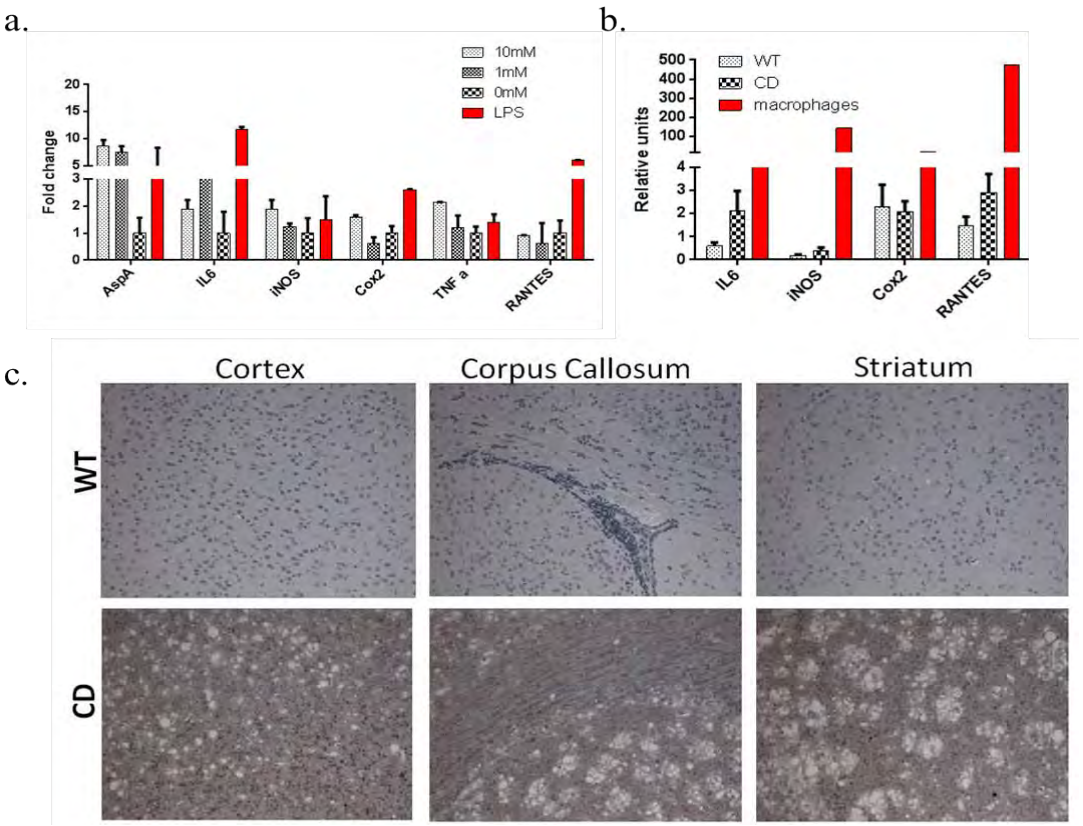

Figure 4.8 Examination of blood brain barrier in CD mice. (a) Animals were injected with Evans Blue dye alone or in combination with mannitol. After their extremities turned blue, animals were sacrificed, perfused with PBS and their brains were isolated and photographed. (b) Brain homogenates were assayed spectrophotometrically for presence of Evans Blue. (c) Liver was extracted and assayed similarly as a control for amounts of dye in the periphery. (d) Amount of Evans Blue in the brain was measured as a ratio of body weight. NS, not significant; **$P<0.01$.

Figure 4.8 Examination of blood brain barrier in CD mice.

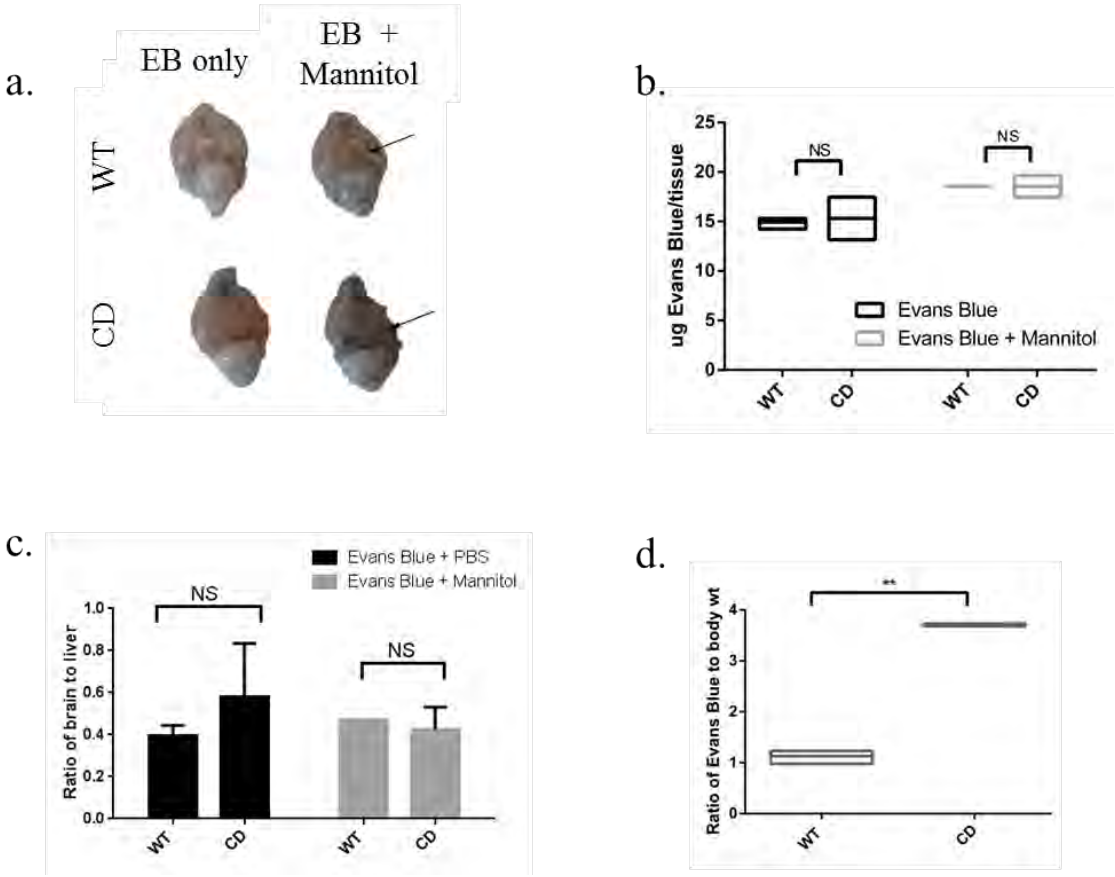

Figure 4.9 Involvement of caspases in CD pathogenesis. (a) Brain lysates were assayed for ATP consumption by Cell Titer Glo assay (n=5). (b) Brain homogenates were tested for presence of various caspases (n=3 in three experiments) (c) Brain sections were stained for cleaved caspase and microglia to test the presence of activated caspase in the corpus callosum. Scale 20µm. (d) Microglial cell culture isolated from CD mouse brains showed robust expression of cleaved caspase 3.

Figure 4.9 Involvement of caspases in CD pathogenesis.

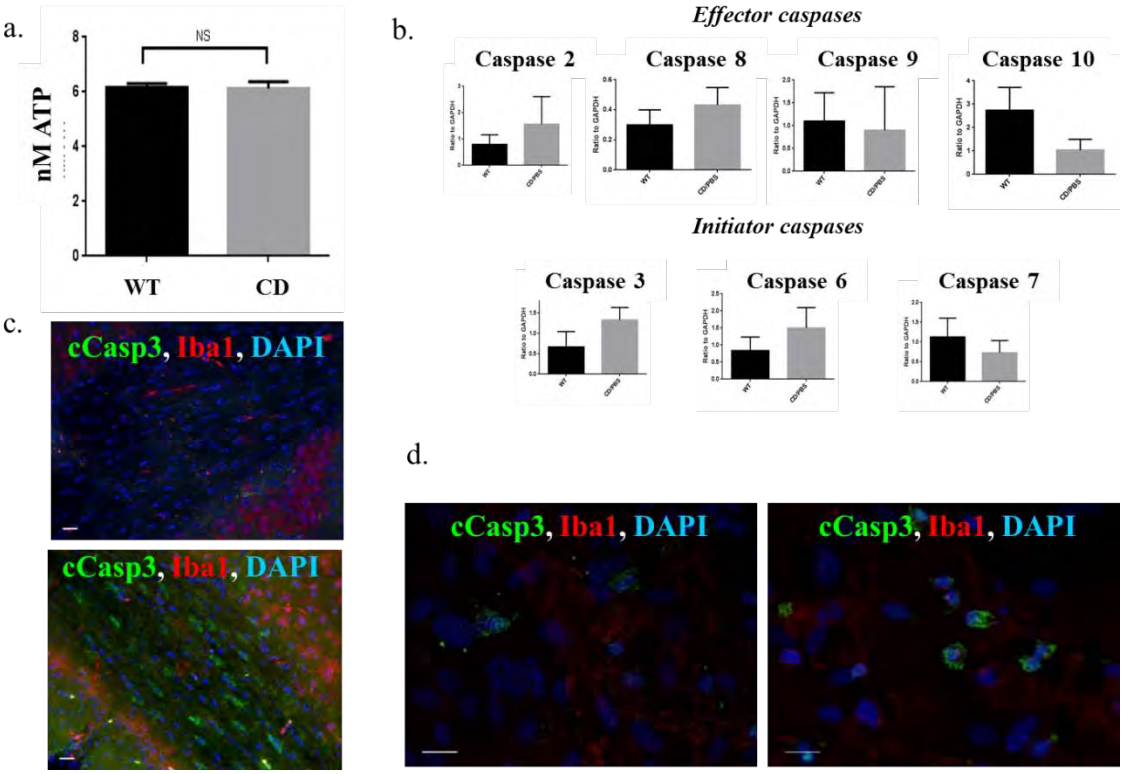

Figure 4.10 Behavior of *in vitro* neural cell cultures. (a) Immunofluorescence of *in vitro* primary cell cultures derived from WT mice to determine expression of aspartoacylase, AspA. (b) Electron Microscopy of oligodendrocyte cultures derived from WT and CD mice. Scale bars 1µm. (c) Electron microscopy of astrocyte culture of CD mice. Yellow arrows show centrosomes. Scale bars 0.5µm.

Figure 4.10 Behavior of *in vitro* neural cell cultures.

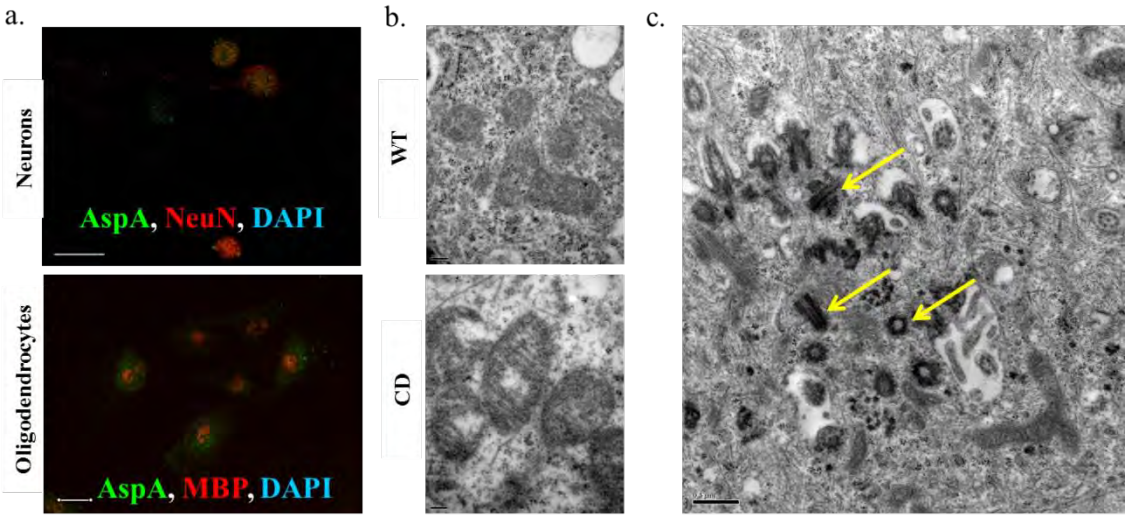

Figure 4.11 Malate-Aspartate Shuttle. Role of aspartate in generation of energy via production of NADH. NAD, nicotinamide adenine dinucleotide; NADH,reduced nicotinamide adenine dinucleotide, Cyt, cytosolic; Mt, mitochondrial.

Figure 4.11 Malate-Aspartate Shuttle.

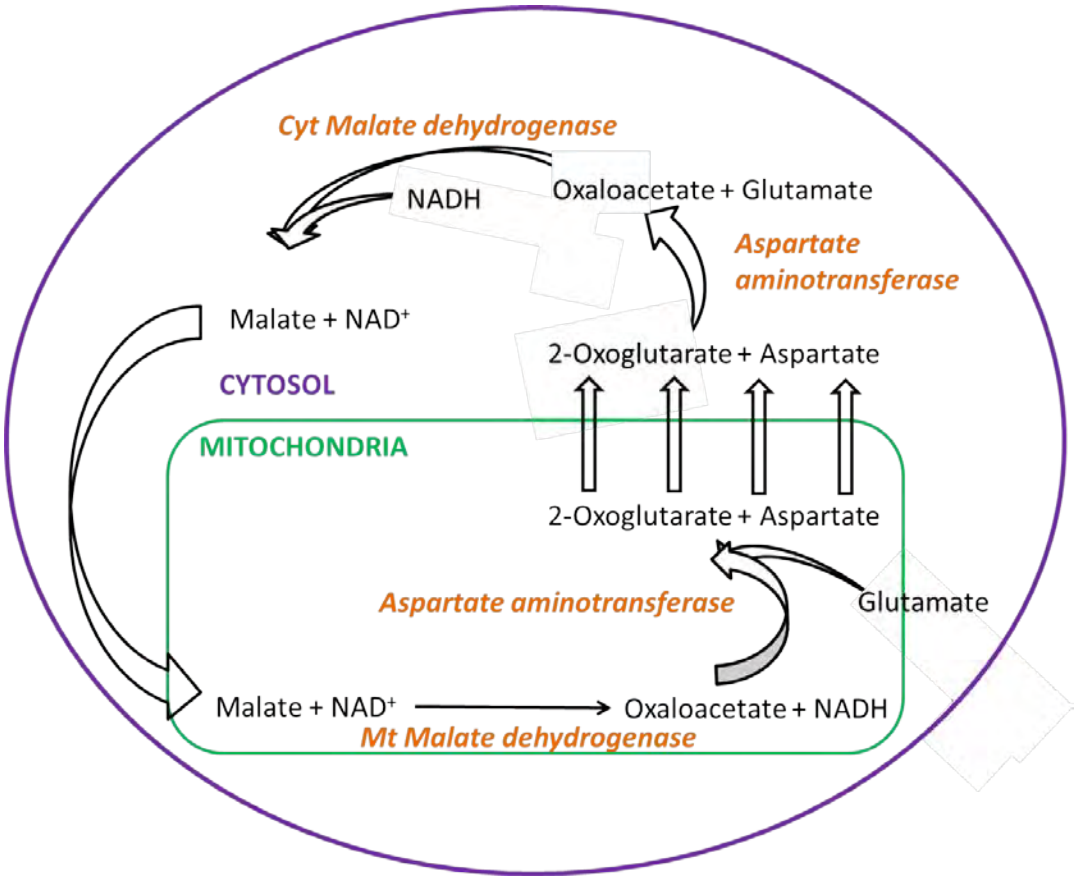

activated microglia using CD45RO staining (Gonzalez-Scarano and Baltuch, 1999). The rationale for this was based on the hypothesis that activated microglia can mediate tissue damage causing CNS inflammatory disorders leading to neurodegeneration. We found profuse signal in the CD brain that indicates that activated microglia are indeed present [Figure 4.7c] which may be responsible for the extensive neuroinflammation causing the vacuolation in the brain.

Blood Brain Barrier is not compromised at least at the onset of symptoms in CD mice

To further explore the molecular pathogenesis of CD, we tested CD mice for permeability of their Blood Brain Barrier using Evans Blue (EB) injections. Control mice were injected with saline or EB combined with mannitol pretreatment (3ml/100g) since mannitol reversibly opens the BBB. Results showed no difference in the BBB permeability by appearance of the brain in both WT and CD mice [Figure 4.8a]. Spectrophotometric readings from brain homogenates showed no significant difference in BBB permeability between WT and diseased animals [Figure 4.8b]. All mice showed similar levels of EB retention in the liver [Figure 4.8c] indicating that similar amounts of dye was present in circulation. The results indicate that the BBB is not disrupted at least in early pathogenesis of CD. Examination of EB retention in the brain with respect to body weight (Figure 4.8d) however indicated that there may be more to the story since diseased mice weigh almost one-third of their littermates (Ahmed et al., 2013).

Caspases are upregulated in CD mouse brains and in neural cell cultures

We also investigated if there was significant loss in cellular components of the brain with the white matter degeneration. Cell Titer Glo assay to measure amounts of

actively metabolizing cells by measuring ATP consumption also did not reveal significant differences [Figure 4.9a]. Since degeneration is a major feature in CD we investigated if apoptosis was significantly involved. Western blot of brain homogenates (n=3) did not show any significant upregulation in protein levels of either the initiator or the effector caspases [Figure 4.9b]. Brain homogenates, however, cannot represent differences in regional or transient caspase expression. Moreover activated microglia could be the source of such caspase expression. Hence, we performed immunofluorescence staining for cleaved caspase 3 and Iba1 in whole brain and primary cell cultures. We found robust expression of cleaved caspase 3 in microglia and the corpus callosum in the brain of CD mice [Figure 4.9c].

Behavior of primary neural cell cultures isolated from CD mice

Closer examination of neural cell types in culture revealed several interesting observations. First we saw expression of aspartoacylase by immunofluorescence in *in vitro* cultures of both neurons and oligodendrocytes isolated from WT mice [Figure 4.10a]. By electron microscopy we examined mitochondria in cultured oligodendrocytes and found that they were osmolyzed and damaged [Figure 4.10b] similar to that reported (Ahmed et al., 2013). Additionally astrocyte cultures from CD mice showed the presence of abnormal number of centrosomes [Figure 4.10c], that possibly indicates motility; however the implication of this is unknown.

Discussion

Intravenously administered CNS therapeutics requires administration of high doses to reach effective drug concentrations at CNS disease sites, resulting in a high systemic viral load and an increased manufacturing burden. The cogent next step in viral gene therapy targeting the CNS would be a more effective delivery method that lowers clinical risk-to-benefit ratio and reduces vector production costs without compromising efficiency of vector delivery. Based on our previous successful preclinical study in ameliorating CD (Ahmed et al., 2013), we used a 50-fold lower dose using intracerebroventricular injections. This would result in high CNS concentrations with minimal systemic exposure and toxicity and most importantly cause global CNS transduction.

As intravenous injections of rAAV9 had been efficient in correcting major CD symptoms (Ahmed et al., 2013), we primarily examined animals injected intracerebroventricularly using AAV9 [Figure 4.1]. In most cases there was no significant difference between the two methods of delivery; however, ICV injections showed remarkable rescue of edema in the brain [Figure 4.1e]. To our surprise, we found that ICV injected animals had a significantly different profile when it came to motor functions. In the first month following injection, their motor function performance was equivalent to the intravenous treated animals however this declined by 3 months of age [Figure 4.1f]. We closely examined if restriction for peripheral tissue had any effect so we assessed motor function for older animals injected with the miRNA-BS vector described earlier (Ahmed et al., 2013) [Figure 4.2] and found a similar result. This led us

to examine if peripheral tissues expressed AspA or showed gross differences [Figure 4.3b], suggesting that CD may not be corrected by restricting therapeutic vector expression to the CNS.

Aspartoacylase expression has previously been reported in the periphery including the kidney and several other organs; however, a detailed analysis was never performed (Mersmann et al., 2011; Surendran et al., 2006). Another study reported low bone mineral density in CD mice arising as a consequence of the genetic defect (Surendran et al., 2003) that would explain the emaciated appearance of the untreated mice. Our study sheds light on the importance of aspartoacylase in the periphery through a detailed analysis of several organs [Figures 4.5 & 4.6]. Interestingly, we found that there was lack of central nucleation but more nuclei in muscle fibers that could be related to denervation. This hypothesis seems to be plausible since in the neuromuscular junction (NMJ) staining by immunofluorescence we do see a lot of the CD NMJs lacking innervation. Moreover denervation could lead to smaller myofiber size, which in turn would appear as more crowded nuclei. The function of the malate aspartate shuttle could probably be affected by the deficiency of aspartoacylase derived aspartate. Since the shuttle would mainly function in gluconeogenesis, the organs involved would primarily be the liver. Though we don't see overt changes in the AST and ALT levels in the liver, the glycogen content might be worth a closer examination. Aspartoacylase was reported to be expressed in the sciatic nerve (Mersmann et al., 2011) hence we performed an extensive analysis on its morphology. Both X-ray diffraction and electron microscopy data confirmed that the deficiency of aspartoacylase indeed leads to morphological

differences [Figure 4.4]. The enteric nervous system has not been examined however the lowered glucose levels in the blood could indicate a role of aspartoacylase in glucose metabolism in the small intestine. This seems plausible since the small intestine shows high expression of aspartoacylase (Mersmann et al., 2011).It has been widely accepted that most CD pathology arises from deficiency of aspartoacylase; however, the damage perpetrated by the accumulated NAA cannot be underestimated. Studies have shown NAA administration to the rodent brain led to seizures (Akimitsu et al., 2000), which is a common symptom in CD patients (Beaudet, 2001). Additionally, the blood CDC revealed a disproportionate amount of granulocytes, indicating involvement of the immune system [Figure 4.3]. Splenocyte phenotyping by FACS suggests abnormalities in the bone marrow or even the thymus suggesting that production of lesser immune cells overall would lead to less mature immune cells in the spleen. Closer examination of the splenic architecture specifically the size of the pulp regions could shed light on the total proportions of immune cells. The lack of proliferation in CD splenocytes when challenged by CD28 indicates a lack of T cell response. These cells may be unable to proliferate due to a block in metabolism, perhaps in fatty acid synthesis in activated T cells. All these data indicate an involvement of the immune system that has never been reported before in the context of Canavan disease.

Since the brain is an immune-privileged organ, the only immune arm would be the resident macrophages- the microglia. This prompted us to examine if the accumulated NAA, in addition to generation of free radicals (Pederzolli et al., 2009), causes an upregulation of immune components secondarily resulting in white matter degeneration

and vacuolation. On external supplementation of NAA, interestingly we found an upregulation of the IL6 genes in WT macrophages. The results were similar in fresh brain homogenates of CD mice indicating that the immune response is another probable cause of the severe pathology in CD mice. Studies suggest an involvement of IL6 in the induction of autoimmunity (Iwanami et al., 2008) which opens up an interesting avenue of explanation for CD neuropathology. Accumulation of NAA may also cause nitric oxide toxicity in the brain by upregulation of inducible nitric oxide synthase (iNOS) in neurons and endothelia (Surendran and Kondapaka, 2005). Imbalance in NO levels may give rise to neurodegeneration (Surendran and Kondapaka, 2005). Upregulation of NAA inhibited catalase and glutathione peroxidase activities and increased hydrogen peroxide levels (Pederzolli et al., 2010) which suggest a potential role for inflammation. Oral administration of NAA in rats led to several symptoms similar to Canavan Disease (Delaney, 2010). Our data also suggest that excess NAA may activate microglia via an immune response that may result in vacuolization.

We would expect that the neuropathology and vacuolization would indicate a severe loss in cell numbers. To our surprise, we found that the cells present in the whole brain have comparable metabolic activities by quantifying the amount of ATP in brain lysates [Figure 4.9]. Though activated caspases were not evident in western blots of brain lysates [Figure 4.9b], immunofluorescence staining did show up massive upregulation of caspase 3 in the brain as well in primary neural cell culture [Figure 4.9b] indicating the involvement of apoptosis. The results can be reconciled since analysis of lysates might not detect localized or transient upregulation.

Another aspect that has been overlooked in the attempt to define CD pathogenesis is the characteristics of neural cells from CD mice. It may be argued that a proportion of stably transduced neuronal population may be enough to negate the toxicity which would probably explain why our previous preclinical therapy extended life to a great extent in spite of a single injection. The decline in quality of later life may indicate that the turnover of transduced glial cells reduces the overall aspartoacylase making "factories". Again, if neurons are only transduced population, the homeostasis of NAA metabolism may be affected. Since the functions of NAA have not been defined it is unknown how such a disturbance would affect the brain microenvironment. Hence we examined the individual characteristics of primary neural cultures. Neuronal cultures showed expression of aspartoacylase by immunofluorescence. Ultramicroscopic studies of oligodendrocytes showed abnormal mitochondria [Figure 4.10b] that resemble lysed mitochondria reported in the brain previously (Ahmed et al., 2013). Cell cultures of microglia derived from CD robustly expressed cleaved caspase 3 [Figure 4.9d], indicating their role in mediating apoptosis. Astrocytes showed the presence of multiple centrosomes [Figure 4.10c]; however, the significance of that is not known. As astrocytes are essential components of the blood brain barrier (BBB), and astrocytes may link spongy neurodegeneration and aspartoacylase deficiency, it was imperative for us to examine the BBB permeability of the CD mice more carefully. We did not find the BBB to be compromised in the CD mice at least at P20 when the pathology becomes more severe [Figure 4.8].

An important fact is that aspartate generated by the action of aspartoacylase has

very important implications in the energy metabolism in addition to it being a neurotransmitter (Cavallero et al., 2009). The aspartate-malate shuttle is an essential aspect of glucose metabolism in the cell [Figure 4.11]. Aspartate and glutamate are closely linked with each other through transaminase reactions (Cooms, 1997). Glutamine produced by astrocytes is used by neurons to produce glutamate in the glutamine-glutamate cycle (Newsholme et al., 2003). In astrocytes, the α-amino group of glutamate is transferred to oxaloacetate to yield aspartate by the catalysis of aspartate aminotransferase (Yudkoff et al., 1986). Aspartate aminotransferase [E.C 2.6.1.1] is involved in the aspartate-malate shuttle [Figure 4.11] that is essential in generating glucose and glutamate and occurs between the cytosol and mitochondria. Lack of aspartate may compromise the shuttle and lead to a decrease in glucose metabolism as observed in our serum biochemistry panel [Figure 4.3d]. Low blood glucose could also stem from issues in digestion that may possibly be caused by enzymatic defects or abnormalities in the intestine.

Increasingly, it seems that CD pathogenesis might not be confined to the CNS but may also involve pathogenesis of the peripheral organs which is also essential for future therapeutic strategies. A lower dose of vector does indeed alleviate the severity of symptoms but is not palliative, indicating the need for more powerful codon-optimized vectors and dose-escalation studies of the same to elucidate the best means of targeting disease models that can be translated to clinical therapeutics.

In conclusion, our study highlights the involvement of peripheral tissues in a primarily neurological disorder. We also suggest NAA-induced immune responses as a

likely mechanism for CD pathogenesis. In short our study points out new guidelines to be considered while designing newer and better therapeutics to target this fatal disease.

CHAPTER V: FINAL SUMMARY AND CONCLUDING REMARKS

The work in this Thesis investigates the development of an efficacious gene therapy strategy for the fatal pediatric autosomal recessive leukodystrophy Canavan disease. These studies first explore possible vectors to be used for such therapeutic applications and then translated them into preclinical applications in a bona-fide mouse model for the disease. The results of these investigations have a direct bearing in development of clinical therapeutics for afflicted patients. They also proffer a platform to investigate the molecular pathogenesis of the disease that will result in better and more efficacious palliative measures

Chapter II reports several rAAVs are capable of crossing the Blood Brain Barrier and transducing the CNS cells in both neonates as well as in adults. The ability of rAAVs to transduce amounts of neuronal cells in different regions may be relevant for treating neurological diseases such as spinal muscular atrophies (Suzuki et al., 2009) and neuronal ceroid lipofuscinoses (Hobert and Dawson, 2006). Transduction of astrocytes by rAAVs expressing secreted neurotrophic factors may be also beneficial for a number of neurodegenerative diseases such as Canavan disease (Kumar et al., 2006). Potential clinical application of intravascular rAAV-mediated gene delivery extends to the peripheral nervous system (Federici and Boulis, 2007). Efficient transduction of dorsal root ganglia may open new therapeutic possibilities for patients suffering from chronic pain (Beutler, 2010). From any of these perspectives, transduction patterns generated from our study may serve as initial proof-of-concept data for diverse neurological disorders. Our findings hold considerable clinical significance for gene therapy of CNS-

related disorders, especially for young patients. For a variety of neurological diseases, treatment during infancy will be necessary to prevent irreversible CNS injury.

rAAVrh.8 and rAAVrh.10 emerged as potent vectors with multiple strong areas of CNS transduction that can be developed into therapeutic strategies. Robust transduction throughout the spinal cord, brainstem, and cortex are characteristics desirable for treatment of disease with global CNS pathology like Canavan disease. Notably, rAAV9 displays similar transduction qualities in the spinal cord of adult mice by intravenous injection, as reported previously (Duque et al., 2009), although it ranked slightly below the performance of rAAVrh.8 in side-by side comparisons [Figures 2.6 & 2.7]. However, a direct comparison with previously published data is often complicated due to possible differences in vector production, dose, and quantification methods.

Canavan Disease (CD) falls in a category of diseases, which if treated, could have wide implications in developing therapeutics for a vast group of leukodystrophies and neurodegenerative diseases. Being a monogenic defect, CD is a perfect target for gene therapy, which could also be utilized as tools to tease out the underlying pathology of leukodystrophies and develop efficient therapeutics for them. Mouse models that show a less severe phenotype resembling infantile and juvenile CD patients could be used to determine disease progression. Additionally, the unique symptom of elevated NAA levels in CD also makes it a perfect disease model to study functions of NAA.

Chapter III and IV document the development of efficacious therapeutics for CD using the $AspA^{-/-}$ KO mouse model. The $AspA^{-/-}$ mouse model in SV129/Ev

background is a stringent preclinical model for the severest form of CD. In chapter III, investigations clearly demonstrated the feasibility of completely rescuing the early lethality, slowing down the disease progression, and extending the survival of CD mice as well as address off-target transgene expression in peripheral tissues using systemic delivery of rAAVs that can cross the BBB. The crucial role of AspA in myelination and early neurodevelopment as well as the feasibility of treating CD by CNS-targeted gene therapy using systemically delivered rAAVs is also highlighted. Chapter IV describes a more effective delivery method and lower vector dosage, reducing the clinical risk-to-benefit ratio and vector production costs. The study focuses on intracerebroventricular delivery as a possible improvement on delivery system to the CNS where global CNS delivery is achieved without affecting the peripheral tissues. The study however indicated that a systemic therapeutic measure is needed for effective alleviation of Canavan disease symptoms since the data indicated the involvement of peripheral tissues in a primarily CNS disorder. Additionally it also reports the probable activation of the immune system presumably caused by NAA accumulation secondarily causing vacuolation, a phenotype in the disease.

To achieve basic molecular understanding of CD pathogenesis, it is interesting to note that patients with mutations in the functionally similar aminoacylase I (hydrolyses N-acylated /N-acetylated amino acids (except L-aspartate)) have overlapping clinical features like encephalopathy, seizures, psychomotor dysfunction, hypotonia, and sensorineural hearing loss as well as excretion of N-acetylated amino acids in the urine. We report aspartoacylase expression in neurons both in the brain as well as in culture,

which was not reported before. From a cellular standpoint, to date, most of the expression and subcellular localization data for aspartoacylase have used a single RNA probe or single antibody which may fail to detect differences among aspartoacylase isoforms including aminoacylase I. An important element for translating observations from CD mice is coupling *in vivo* physiology and imaging in the mouse to functional neuroimaging in patients to help identify conserved neural circuit phenotypes and pave way to improve upon therapeutics.

In addition to existing therapeutic modalities, alternative means of treatment for CD could include partial silencing of the NAA biosynthetic enzyme AspNAT (Madhavarao et al., 2003) to control the NAA metabolism cycle. Additionally inhibition of NAA export from the neuronal mitochondria could markedly decrease NAA accumulation in interstitial spaces that probably causes osmotic dysregulation in the CNS. Pharmacological protection of oligodendrocytes against damage in demyelinating diseases could also be a promising avenue of treatment (Waksman, 1999). Intravenous delivery of rAAV9 (Ahmed SS, 2013) in the CD model suggests that lowering NAA levels in the brain probably led to alleviation of NAAduria as well as a decrease in edema indicating that the MWP theory could partially explain pathogenesis.

The utility of these newer AAVs is not confined to clinical application; systemic gene delivery to the CNS should also be useful as a convenient method to manipulate gene expression in the course of basic neuroscience research. Effective and stable transgene expression in the CNS by intravenous administration of rAAVs may be applied to establish somatic transgenic animal models, which is a potentially cheaper, faster, and

simpler method than conventional transgenesis. Somatic CNS gene knockdown animal models may also be created using the method described here (Siegel and Callaway, 2004). The field currently seems poised for more revolutionary progress with the advent of newer serotypes and advances in capsid evolution for rAAVs that are specific for different neural cell types and can cross the BBB. It is worthwhile to point out that the grouping we introduce should not be interpreted as if there are absolute boundaries between the groups, but rather, it is used as a means to facilitate the description of the large number of AAV serotypes tested and to provide a useful guide for selecting the most suitable vectors in future experimentation.

It should be noted however, in spite of newer serotypes there will still remain the issue of half-life of the transduced cells. All of these factors increasingly indicate the potential for combinatorial therapy strategies that could be translated to human patients.

BIBLIOGRAPHY

(2012). Minutes of the Recombinant DNA Advisory Committee, 12/4/12–5/12. In Recombinant DNA Advisory Committee (Bethesda, MD), pp. 9-10.

Abbott, N.J., Ronnback, L., and Hansson, E. (2006). Astrocyte-endothelial interactions at the blood-brain barrier. Nat Rev Neurosci *7*, 41-53.

Adachi, M., Schneck, L., Cara, J., and Volk, B.W. (1973). Spongy degeneration of the central nervous system (van Bogaert and Bertrand type; Canavan's disease). A review. Hum Pathol *4*, 331-347.

Adachi, M., Torii, J., Schneck, L., and Volk, B.W. (1972). Electron microscopic and enzyme histochemical studies of the cerebellum in spongy degeneration (van Bogaert and Bertrand type). Acta Neuropathol (Berl) *20*, 22-31.

Afione, S.A., Conrad, C.K., and Flotte, T.R. (1995). Gene therapy vectors as drug delivery systems. Clin Pharmacokinet *28*, 181-189.

Agrawal, D., Hawk, R., Avila, R.L., Inouye, H., and Kirschner, D.A. (2009). Internodal myelination during development quantitated using X-ray diffraction. J Struct Biol *168*, 521-526.

Ahmed SS, L.H., Cao C, Sikoglu EM, Denninger AR, Su Q, Eaton S, Liso Navarro AA, Xie J, Szucs S, Zhang H, Moore C, Kirschner DA, Seyfried TN, Flotte TR, Matalon R, Gao G (2013). A Single Intravenous rAAV Injection as Late as P20 Achieves Efficacious and Sustained CNS Gene Therapy in Canavan Mice. Mol Ther.

Ahmed, S.S., Li, H., Cao, C., Sikoglu, E.M., Denninger, A.R., Su, Q., Eaton, S., Liso Navarro, A.A., Xie, J., Szucs, S.*, et al.* (2013). A single intravenous rAAV injection as late as P20 achieves efficacious and sustained CNS Gene therapy in Canavan mice. Mol Ther *21*, 2136-2147.

Akimitsu T, K.K., Hanaya R, Iida K, Kiura Y, Arita K, Matsubayashi H, Ishihara K, Kitada K, Serikawa T, Sasa M. (2000). Epileptic seizures induced by N-acetyl-L-aspartate in rats: in vivo and in vitro studies. Brain Res *861*, 143-150.

Akimitsu, T., Kurisu, K., Hanaya, R., Iida, K., Kiura, Y., Arita, K., Matsubayashi, H., Ishihara, K., Kitada, K., Serikawa, T.*, et al.* (2000). Epileptic seizures induced by N-acetyl-L-aspartate in rats: in vivo and in vitro studies. Brain Res *861*, 143-150.

Albuquerque, C., Joseph, D.J., Choudhury, P., and MacDermott, A.B. (2009). Dissection, plating, and maintenance of cortical astrocyte cultures. Cold Spring Harb Protoc *2009*, pdb prot5273.

Ariyannur, P.S., Moffett, J.R., Manickam, P., Pattabiraman, N., Arun, P., Nitta, A., Nabeshima, T., Madhavarao, C.N., and Namboodiri, A.M. (2010). Methamphetamine-induced neuronal protein NAT8L is the NAA biosynthetic enzyme: implications for specialized acetyl coenzyme A metabolism in the CNS. Brain Res *1335*, 1-13.

Asokan, A., Schaffer, D.V., and Samulski, R.J. (2012). The AAV vector toolkit: poised at the clinical crossroads. Mol Ther *20*, 699-708.

Assadi, M., Janson, C., Wang, D.J., Goldfarb, O., Suri, N., Bilaniuk, L., and Leone, P. (2010). Lithium citrate reduces excessive intra-cerebral N-acetyl aspartate in Canavan disease. Eur J Paediatr Neurol *14*, 354-359.

Avila, R.L., Inouye, H., C., B.R., Yin, X., Trapp, B.D., Feltri, M.L., Wrabetz, L., and Kirschner, D.A. (2005). Structure and stability of internodal myelin in mouse models of hereditary neuropathy. J Neuropathol Exp Neurol *64*, 976-990.

Azzam, N.A., Bready, J.V., Vinters, H.V., and Cancilla, P.A. (1984). Spontaneous spongy degeneration of the mouse brain. Journal of neuropathology and experimental neurology *43*, 118-130.

Badens, C., Lacoste, C., Philip, N., Martini, N., Courrier, S., Giuliano, F., Verloes, A., Munnich, A., Leheup, B., Burglen, L.*, et al.* (2006). Mutations in PHD-like domain of the ATRX gene correlate with severe psychomotor impairment and severe urogenital abnormalities in patients with ATRX syndrome. Clin Genet *70*, 57-62.

Baek, R.C., Martin, D.R., Cox, N.R., and Seyfried, T.N. (2009). Comparative analysis of brain lipids in mice, cats, and humans with Sandhoff disease. Lipids *44*, 197-205.

Bartel, D.P. (2009). MicroRNAs: target recognition and regulatory functions. Cell *136*, 215-233.

Baslow, M. (1997). A review of phylogenetic and metabolic relationships between the acylamino acids, N-acetyl-L-aspartic acid and N-acetyl-L-histidine, in the vertebrate nervous system. J Neurochem *68*, 1335-1344.

Baslow, M.H. (1999). Molecular water pumps and the aetiology of Canavan disease: a case of the sorcerer's apprentice. J Inherit Metab Dis *22*, 99-101.

Baslow, M.H., Kitada, K., Suckow, R.F., Hungund, B.L., and Serikawa, T. (2002). The effects of lithium chloride and other substances on levels of brain N-acetyl-L-aspartic acid in Canavan disease-like rats. Neurochem Res *27*, 403-406.

Baslow, M.H., and Resnik, T.R. (1997). Canavan disease. Analysis of the nature of the metabolic lesions responsible for development of the observed clinical symptoms. J Mol Neurosci *9*, 109-125.

Baslow, M.H., and Yamada, S. (1997). Identification of N-acetylaspartate in the lens of the vertebrate eye: a new model for the investigation of the function of N-acetylated amino acids in vertebrates. Exp Eye Res *64*, 283-286.

Beaudet, A. (2001). Aspartoacylase deficiency (Canavan disease) In: Scriver CR, Beaudet AL, Sly WS, Valle D (eds). The metabolic and molecular bases of inherited disease, pp 5799–5805.

Beutler, A.S. (2010). AAV provides an alternative for gene therapy of the peripheral sensory nervous system. Mol Ther *18*, 670-673.

Bhakoo, K.K., Craig, T.J., and Styles, P. (2001). Developmental and regional distribution of aspartoacylase in rat brain tissue. J Neurochem *79*, 211-220.

Birken, D.L., and Oldendorf, W.H. (1989). N-acetyl-L-aspartic acid: a literature review of a compound prominent in 1H-NMR spectroscopic studies of brain. Neurosci Biobehav Rev *13*, 23-31.

Birnbaum, S.M., Levinton, L., Kingsley, R.B., and Greenstein, J.P. (1952). Specificity of amino acid acylases J Biol Chem *194*, 455-462.

Bradbury, M.W. (1985). The blood-brain barrier. Transport across the cerebral endothelium. Circulation research *57*, 213-222.

Brennecke, J., Stark, A., Russell, R.B., and Cohen, S.M. (2005). Principles of microRNA-target recognition. PLoS Biol *3*, e85.

Brown, B.D., and Naldini, L. (2009). Exploiting and antagonizing microRNA regulation for therapeutic and experimental applications. Nat Rev Genet *10*, 578-585.

Brown, B.D., Venneri, M.A., Zingale, A., Sergi Sergi, L., and Naldini, L. (2006). Endogenous microRNA regulation suppresses transgene expression in hematopoietic lineages and enables stable gene transfer. Nat Med *12*, 585-591.

Bruce AJ, B.M. (1995). Oxygen free radicals in rat limbic structures after kainate-induced seizures. Free Radic Biol Med *18*, 993-1002.

Calcedo, R., Vandenberghe, L.H., Gao, G., Lin, J., and Wilson, J.M. (2009). Worldwide epidemiology of neutralizing antibodies to adeno-associated viruses. The Journal of infectious diseases *199*, 381-390.

Canavan, M.M. (1931). Schilder's encephalitis periaxialis diffusa. Arch Neurol Psychiat *25*.

Cavallero, A., Marte, A., and Fedele, E. (2009). L-aspartate as an amino acid neurotransmitter: mechanisms of the depolarization-induced release from cerebrocortical synaptosomes. J Neurochem *110*, 924-934.

Cearley, C.N., Vandenberghe, L.H., Parente, M.K., Carnish, E.R., Wilson, J.M., and Wolfe, J.H. (2008). Expanded repertoire of AAV vector serotypes mediate unique patterns of transduction in mouse brain. Mol Ther *16*, 1710-1718.

Cearley, C.N., and Wolfe, J.H. (2006). Transduction characteristics of adeno-associated virus vectors expressing cap serotypes 7, 8, 9, and Rh10 in the mouse brain. Mol Ther *13*, 528-537.

Chakraborty, G., Mekala, P., Yahya, D., Wu, G., and Ledeen, R.W. (2001). Intraneuronal N-acetylaspartate supplies acetyl groups for myelin lipid synthesis: evidence for myelin-associated aspartoacylase. J Neurochem *78*, 736-745.

Chang YC, R.S., Rao JS (2009). Chronic administration of mood stabilizers upregulates BDNF and bcl-2 expression levels in rat frontal cortex. Neurochem Res *34*, 536-541.

Chen RW, C.D. (1999). Long term lithium treatment suppresses p53 and Bax expression but increases Bcl-2 expression. A prominent role in neuroprotection against excitotoxicity. J Biol Chem *274*, 6039-6042.

Chen, Y., Balasubramaniyan, V., Peng, J., Hurlock, E.C., Tallquist, M., Li, J., and Lu, Q.R. (2007). Isolation and culture of rat and mouse oligodendrocyte precursor cells. Nat Protoc *2*, 1044-1051.

Chomiak, T., and Hu, B. (2009). What is the optimal value of the g-ratio for myelinated fibers in the rat CNS? A theoretical approach. PLoS One *4*, e7754.

Chu, V., Otero, J.M., Lopez, O., Morgan, J.P., Amende, I., and Hampton, T.G. (2001). Method for non-invasively recording electrocardiograms in conscious mice. BMC physiology *1*, 6.

Cooms, M.W. (1997). Amino acid metabolism (New York, Wiley Liss).

Copray S, H.J., Sher F, Casaccia-Bonnefil P, Boddeke E (2009). Epigenetic mechanisms facilitating oligodendrocyte development, maturation, and aging. Glia *57*, 1579-1587.

Cotugno, G., Annunziata, P., Tessitore, A., O'Malley, T., Capalbo, A., Faella, A., Bartolomeo, R., O'Donnell, P., Wang, P., Russo, F.*, et al.* (2011). Long-term amelioration of feline Mucopolysaccharidosis VI after AAV-mediated liver gene transfer. Mol Ther *19*, 461-469.

D'Adamo AF Jr, G.L., Yatsu FM (1968). Acetyl transport mechanisms. Involvement of N-acetyl aspartic acid in de novo fatty acid biosynthesis in the developing rat brain. Exp Brain Res *5*, 267-273.

Davidson, B.L., and Breakefield, X.O. (2003). Viral vectors for gene delivery to the nervous system. Nat Rev Neurosci *4*, 353-364.

Davidson, B.L., Stein, C.S., Heth, J.A., Martins, I., Kotin, R.M., Derksen, T.A., Zabner, J., Ghodsi, A., and Chiorini, J.A. (2000). Recombinant adeno-associated virus type 2, 4, and 5 vectors: transduction of variant cell types and regions in the mammalian central nervous system. Proc Natl Acad Sci U S A *97*, 3428-3432.

Daya, S., and Berns, K.I. (2008). Gene therapy using adeno-associated virus vectors. Clin Microbiol Rev *21*, 583-593.

Delaney, B. (2010). Acute oral toxicity of N-acetyl-L-aspartic acid (NAA) in rats. Food and chemical toxicology : an international journal published for the British Industrial Biological Research Association *48*, 1761.

Di Pasquale, G., Davidson, B.L., Stein, C.S., Martins, I., Scudiero, D., Monks, A., and Chiorini, J.A. (2003). Identification of PDGFR as a receptor for AAV-5 transduction. Nat Med *9*, 1306-1312.

Duque, S., Joussemet, B., Riviere, C., Marais, T., Dubreil, L., Douar, A.M., Fyfe, J., Moullier, P., Colle, M.A., and Barkats, M. (2009). Intravenous administration of self-complementary AAV9 enables transgene delivery to adult motor neurons. Mol Ther *17*, 1187-1196.

During, M.J., Xu, R., Young, D., Kaplitt, M.G., Sherwin, R.S., and Leone, P. (1998). Peroral gene therapy of lactose intolerance using an adeno-associated virus vector. Nat Med *4*, 1131-1135.

Duvernoy, H.M., and Risold, P.Y. (2007). The circumventricular organs: an atlas of comparative anatomy and vascularization. Brain Res Rev *56*, 119-147.

Elpeleg, O.N., and Shaag, A. (1999). The spectrum of mutations of the aspartoacylase gene in Canavan disease in non-Jewish patients. J Inherit Metab Dis *22*, 531-534.

Escolar ML, P.M., Provenzale JM, Richards KC, Allison J, Wood S, Wenger DA, Pietryga D, Wall D, Champagne M, Morse R, Krivit W, Kurtzberg J. (2005). Transplantation of umbilical-cord blood in babies with infantile Krabbe's disease. N Engl J Med *352*, 2069-2081.

Falk, D.J., Mah, C.S., Soustek, M.S., Lee, K.Z., Elmallah, M.K., Cloutier, D.A., Fuller, D.D., and Byrne, B.J. (2013). Intrapleural administration of AAV9 improves neural and cardiorespiratory function in Pompe disease. Mol Ther *21*, 1661-1667.

Federici, T., and Boulis, N. (2007). Gene therapy for peripheral nervous system diseases. Curr Gene Ther *7*, 239-248.

Ferrari, F.K., Samulski, T., Shenk, T., and Samulski, R.J. (1996). Second-strand synthesis is a rate-limiting step for efficient transduction by recombinant adeno-associated virus vectors. J Virol *70*, 3227-3234.

Fisher, K.J., Gao, G.P., Weitzman, M.D., DeMatteo, R., Burda, J.F., and Wilson, J.M. (1996). Transduction with recombinant adeno-associated virus for gene therapy is limited by leading-strand synthesis. J Virol *70*, 520-532.

Flotte, T.R., Afione, S.A., Conrad, C., McGrath, S.A., Solow, R., Oka, H., Zeitlin, P.L., Guggino, W.B., and Carter, B.J. (1993). Stable in vivo expression of the cystic fibrosis transmembrane conductance regulator with an adeno-associated virus vector. Proc Natl Acad Sci U S A *90*, 10613-10617.

Folch, J., Lees, M., and Sloane Stanley, G.H. (1957). A simple method for the isolation and purification of total lipides from animal tissues. Journal of Biological Chemistry *226*, 497-509.

Foust, K.D., Nurre, E., Montgomery, C.L., Hernandez, A., Chan, C.M., and Kaspar, B.K. (2009). Intravascular AAV9 preferentially targets neonatal neurons and adult astrocytes. Nat Biotechnol *27*, 59-65.

Foust, K.D., Wang, X., McGovern, V.L., Braun, L., Bevan, A.K., Haidet, A.M., Le, T.T., Morales, P.R., Rich, M.M., Burghes, A.H., *et al.* (2010). Rescue of the spinal muscular atrophy phenotype in a mouse model by early postnatal delivery of SMN. Nat Biotechnol *28*, 271-274.

Francis, J., Markov, V., and Leone, P. (2013). Dietary triheptanoin rescues oligodendrocyte loss, dysmyelination and motor function in the nur7 mouse model of Canavan disease. J Inherit Metab Dis.

Fu, H., Muenzer, J., Samulski, R.J., Breese, G., Sifford, J., Zeng, X., and McCarty, D.M. (2003). Self-complementary adeno-associated virus serotype 2 vector: global distribution and broad dispersion of AAV-mediated transgene expression in mouse brain. Mol Ther *8*, 911-917.

Gagliardi, C., and Bunnell, B.A. (2009). Large animal models of neurological disorders for gene therapy. ILAR J *50*, 128-143.

Gao, G., Vandenberghe, L.H., Alvira, M.R., Lu, Y., Calcedo, R., Zhou, X., and Wilson, J.M. (2004). Clades of Adeno-associated viruses are widely disseminated in human tissues. J Virol *78*, 6381-6388.

Gao, G.P., Alvira, M.R., Wang, L., Calcedo, R., Johnston, J., and Wilson, J.M. (2002). Novel adeno-associated viruses from rhesus monkeys as vectors for human gene therapy. Proc Natl Acad Sci U S A *99*, 11854-11859.

Gasmi, M., Brandon, E.P., Herzog, C.D., Wilson, A., Bishop, K.M., Hofer, E.K., Cunningham, J.J., Printz, M.A., Kordower, J.H., and Bartus, R.T. (2007). AAV2-mediated delivery of human neurturin to the rat nigrostriatal system: long-term efficacy and tolerability of CERE-120 for Parkinson's disease. Neurobiology of disease *27*, 67-76.

Gibbons, R.J., and Higgs, D.R. (2000). Molecular-clinical spectrum of the ATR-X syndrome. Am J Med Genet *97*, 204-212.

Goldstein, F.B. (1976). Amidohydrolases of brain; enzymatic hydrolysis of N-acetyl-l-aspartate and other N-acyl-L-Amino acids. J Neurochem *26*, 45-49.

Gonzalez-Scarano, F., and Baltuch, G. (1999). Microglia as mediators of inflammatory and degenerative diseases. Annual review of neuroscience *22*, 219-240.

Gray, S.J., Matagne, V., Bachaboina, L., Yadav, S., Ojeda, S.R., and Samulski, R.J. (2011). Preclinical differences of intravascular AAV9 delivery to neurons and glia: a comparative study of adult mice and nonhuman primates. Mol Ther *19*, 1058-1069.

Grimm, D., and Kay, M.A. (2003). From virus evolution to vector revolution: use of naturally occurring serotypes of adeno-associated virus (AAV) as novel vectors for human gene therapy. Curr Gene Ther *3*, 281-304.

Grimm, D., Pandey, K., Nakai, H., Storm, T.A., and Kay, M.A. (2006). Liver transduction with recombinant adeno-associated virus is primarily restricted by capsid serotype not vector genotype. J Virol *80*, 426-439.

Grodd, W., Krägeloh-Mann, I., Petersen, D., Trefz, F.K., and Harzer, K. (1990). In vivo assessment of N-acetylaspartate in brain in spongy degeneration (Canavan disease) by proton spectroscopy. Lancet *336*, 437-438.

Guy, J., Qi, X., Muzyczka, N., and Hauswirth, W.W. (1999). Reporter expression persists 1 year after adeno-associated virus-mediated gene transfer to the optic nerve. Arch Ophthalmol *117*, 929-937.

Hagen, G., and Bjerkas, I. (1990). Spongy degeneration of white matter in the central nervous system of silver foxes (Vulpes vulpes). Veterinary pathology *27*, 187-193.

Hagen, G., Blakemore, W.F., and Bjerkas, I. (1990). Ultrastructural findings in spongy degeneration of white matter in silver foxes (Vulpes vulpes). A naturally occurring demyelinating disease with oligodendrocyte vacuolation. Acta neuropathologica *80*, 590-596.

Hauser, E.C., Kasperzyk, J.L., d'Azzo, A., and Seyfried, T.N. (2004). Inheritance of lysosomal acid beta-galactosidase activity and gangliosides in crosses of DBA/2J and knockout mice. Biochemical Genetics *42*, 241-257.

Hermonat PL, M.N. (1984). Use of adeno-associated virus as a mammalian DNA cloning vector: transduction of neomycin resistance into mammalian tissue culture cells. Proc Natl Acad Sci U S A *81*, 6466-6470.

Hershfield, J.R., Madhavarao, C.N., Moffett, J.R., Benjamins, J.A., Garbern, J.Y., and Namboodiri, A. (2006). Aspartoacylase is a regulated nuclear-cytoplasmic enzyme. FASEB J *20*, 2139-2141.

Hershfield, J.R., Pattabiraman, N., Madhavarao, C.N., and Namboodiri, M.A. (2007). Mutational analysis of aspartoacylase: implications for Canavan disease. Brain Res *1148*, 1-14.

Hinderer, C., Bell, P., Gurda, B.L., Wang, Q., Louboutin, J.P., Zhu, Y., Bagel, J., O'Donnell, P., Sikora, T., Ruane, T.*, et al.* (2014). Intrathecal Gene Therapy Corrects CNS Pathology in a Feline Model of Mucopolysaccharidosis I. Mol Ther.

Hioki, H., Kameda, H., Nakamura, H., Okunomiya, T., Ohira, K., Nakamura, K., Kuroda, M., Furuta, T., and Kaneko, T. (2007). Efficient gene transduction of neurons by lentivirus with enhanced neuron-specific promoters. Gene Ther *14*, 872-882.

Hirano, A. (1981). Structure of normal central myelinated fibers. Adv Neurol *31*, 51-68.

Hobert, J.A., and Dawson, G. (2006). Neuronal ceroid lipofuscinoses therapeutic strategies: past, present and future. Biochim Biophys Acta *1762*, 945-953.

Huang, Y.S., and Richter, J.D. (2007). Analysis of mRNA translation in cultured hippocampal neurons. Methods in enzymology *431*, 143-162.

Hunt, A., and Burne, R. (1995). Medical and nursing problems of children with neurodegenerative disease. Palliative medicine *9*, 19-26.

Hwu, W.L., Muramatsu, S., Tseng, S.H., Tzen, K.Y., Lee, N.C., Chien, Y.H., Snyder, R.O., Byrne, B.J., Tai, C.H., and Wu, R.M. (2012). Gene therapy for aromatic L-amino acid decarboxylase deficiency. Sci Transl Med *4*, 134ra161.

Iwanami, K., Matsumoto, I., Tanaka-Watanabe, Y., Inoue, A., Mihara, M., Ohsugi, Y., Mamura, M., Goto, D., Ito, S., Tsutsumi, A.*, et al.* (2008). Crucial role of the interleukin-6/interleukin-17 cytokine axis in the induction of arthritis by glucose-6-phosphate isomerase. Arthritis and rheumatism *58*, 754-763.

Janelidze, S., Nordstrom, U., Kugler, S., and Brundin, P. (2014). Pre-existing immunity to adeno-associated virus (AAV)2 limits transgene expression following intracerebral AAV2-based gene delivery in a 6-hydroxydopamine model of Parkinson's disease. J Gene Med *16*, 300-308.

Janson, C., McPhee, S., Bilaniuk, L., Haselgrove, J., Testaiuti, M., Freese, A., Wang, D.J., Shera, D., Hurh, P., Rupin, J., *et al.* (2002). Clinical protocol. Gene therapy of Canavan disease: AAV-2 vector for neurosurgical delivery of aspartoacylase gene (ASPA) to the human brain. Hum Gene Ther *13*, 1391-1412.

Janzer, R.C., and Raff, M.C. (1987). Astrocytes induce blood-brain barrier properties in endothelial cells. Nature *325*, 253-257.

Jiang, H., Lillicrap, D., Patarroyo-White, S., Liu, T., Qian, X., Scallan, C.D., Powell, S., Keller, T., McMurray, M., Labelle, A., *et al.* (2006). Multiyear therapeutic benefit of AAV serotypes 2, 6, and 8 delivering factor VIII to hemophilia A mice and dogs. Blood *108*, 107-115.

Kaplitt, M.G., Feigin, A., Tang, C., Fitzsimons, H.L., Mattis, P., Lawlor, P.A., Bland, R.J., Young, D., Strybing, K., Eidelberg, D., *et al.* (2007). Safety and tolerability of gene therapy with an adeno-associated virus (AAV) borne GAD gene for Parkinson's disease: an open label, phase I trial. Lancet *369*, 2097-2105.

Kaplitt, M.G., Leone, P., Samulski, R.J., Xiao, X., Pfaff, D.W., O'Malley, K.L., and During, M.J. (1994). Long-term gene expression and phenotypic correction using adeno-associated virus vectors in the mammalian brain. Nat Genet *8*, 148-154.

Kasperzyk, J.L., El-Abbadi, M.M., Hauser, E.C., D'Azzo, A., Platt, F.M., and Seyfried, T.N. (2004). N-butyldeoxygalactonojirimycin reduces neonatal brain ganglioside content in a mouse model of GM1 gangliosidosis. J Neurochem *89*, 645-653.

Kaul, R., Casanova, J., Johnson, A.B., Tang, P., and Matalon, R. (1991). Purification, characterization, and localization of aspartoacylase from bovine brain. J Neurochem *56*, 129-135.

Kaul, R., Gao, G.P., Aloya, M., Balamurugan, K., Petrosky, A., Michals, K., and Matalon, R. (1994). Canavan disease: mutations among Jewish and non-Jewish patients. Am J Hum Genet *55*, 34-41.

Kaul, R., Gao, G.P., Balamurugan, K., and Matalon, R. (1993). Cloning of the human aspartoacylase cDNA and a common missense mutation in Canavan disease. Nat Genet *5*, 118-123.

Kessing LV, S.L., Forman JL, Andersen PK. (2008). Lithium treatment and risk of dementia. Arch Gen Psychiatry *65*, 1331-1335.

Kim, J.Y., Grunke, S.D., Levites, Y., Golde, T.E., and Jankowsky, J.L. (2014). Intracerebroventricular viral injection of the neonatal mouse brain for persistent and widespread neuronal transduction. J Vis Exp.

Kirmani, B.F., Jacobowitz, D.M., Kallarakal, A.T., and Namboodiri, M.A. (2002). Aspartoacylase is restricted primarily to myelin synthesizing cells in the CNS: therapeutic implications for Canavan disease. Brain Res Mol Brain Res *107*, 176-182.

Kitada, K., Akimitsu, T., Shigematsu, Y., Kondo, A., Maihara, T., Yokoi, N., Kuramoto, T., Sasa, M., and Serikawa, T. (2000). Accumulation of N-acetyl-L-aspartate in the brain of the tremor rat, a mutant exhibiting absence-like seizure and spongiform degeneration in the central nervous system. J Neurochem *74*, 2512-2519.

Kleiter, M., Hogler, S., Kneissl, S., Url, A., and Leschnik, M. (2011). Spongy degeneration with cerebellar ataxia in Malinois puppies: a hereditary autosomal recessive disorder? Journal of veterinary internal medicine / American College of Veterinary Internal Medicine *25*, 490-496.

Klugmann, M., Leichtlein, C.B., Symes, C.W., Serikawa, T., Young, D., and During, M.J. (2005). Restoration of aspartoacylase activity in CNS neurons does not ameliorate motor deficits and demyelination in a model of Canavan disease. Mol Ther *11*, 745-753.

Klugmann, M., Symes, C.W., Klaussner, B.K., Leichtlein, C.B., Serikawa, T., Young, D., and During, M.J. (2003). Identification and distribution of aspartoacylase in the postnatal rat brain. Neuroreport *14*, 1837-1840.

Kumar, S., Biancotti, J.C., Matalon, R., and de Vellis, J. (2009). Lack of aspartoacylase activity disrupts survival and differentiation of neural progenitors and oligodendrocytes in a mouse model of Canavan disease. J Neurosci Res *87*, 3415-3427.

Kumar, S., Mattan, N.S., and de Vellis, J. (2006). Canavan disease: a white matter disorder. Ment Retard Dev Disabil Res Rev *12*, 157-165.

Le Coq, J., An, H.J., Lebrilla, C., and Viola, R.E. (2006). Characterization of human aspartoacylase: the brain enzyme responsible for Canavan disease. Biochemistry *45*, 5878-5884.

Lee DH, P.G. (2007). Mutagenesis induced by the nitric oxide donor sodium nitroprusside in mouse cells. Mutagenesis *22*, 63-67.

Leone, P., Janson, C.G., Bilaniuk, L., Wang, Z., Sorgi, F., Huang, L., Matalon, R., Kaul, R., Zeng, Z., Freese, A., *et al.* (2000). Aspartoacylase gene transfer to the mammalian central nervous system with therapeutic implications for Canavan disease. Ann Neurol *48*, 27-38.

Leone, P., Shera, D., McPhee, S.W., Francis, J.S., Kolodny, E.H., Bilaniuk, L.T., Wang, D.J., Assadi, M., Goldfarb, O., Goldman, H., *et al.* (2012). Long-term follow-up after gene therapy for canavan disease. Sci Transl Med *4*.

Lin W, P.B. (2009). Endoplasmic reticulum stress in disorders of myelinating cells. Nat Neurosci *12*, 379-385.

Macala, L.J., Yu, R.K., and Ando, S. (1983). Analysis of brain lipids by high performance thin-layer chromatography and densitometry. Journal of Lipid Research *24*, 1243-1250.

Madhavarao, C.N., Arun, P., Anikster, Y., Mog, S.R., Staretz-Chacham, O., Moffett, J.R., Grunberg, N.E., Gahl, W.A., and Namboodiri, A.M. (2009). Glyceryl triacetate for Canavan disease: a low-dose trial in infants and evaluation of a higher dose for toxicity in the tremor rat model. J Inherit Metab Dis *32*, 640-650.

Madhavarao, C.N., Arun, P., Moffett, J.R., Szucs, S., Surendran, S., Matalon, R., Garbern, J., Hristova, D., Johnson, A., Jiang, W., *et al.* (2005). Defective N-acetylaspartate catabolism reduces brain acetate levels and myelin lipid synthesis in Canavan's disease. Proc Natl Acad Sci *102*, 5221-5226.

Madhavarao, C.N., Chinopoulos, C., Chandrasekaran, K., and Namboodiri, M.A. (2003). Characterization of the N-acetylaspartate biosynthetic enzyme from rat brain. J Neurochem *86*, 824-835.

Madhavarao, C.N., Moffett, J.R., Moore, R.A., Viola, R.E., Namboodiri, M.A., and Jacobowitz, D.M. (2004). Immunohistochemical localization of aspartoacylase in the rat central nervous system. J Comp Neurol *472*, 318-329.

Manfredsson, F.P., and Mandel, R.J. (2010). Development of gene therapy for neurological disorders. Discovery medicine *9*, 204-211.

Manfredsson, F.P., Rising, A.C., and Mandel, R.J. (2009). AAV9: a potential blood-brain barrier buster. Mol Ther *17*, 403-405.

Matalon, R. (1997). Canavan disease: diagnosis and molecular analysis. Genet Test *1*, 21-25.

Matalon, R., Kaul, R., and Michals, K. (1993). Canavan disease: biochemical and molecular studies. J Inherit Metab Dis *16*, 744-752.

Matalon, R., and Michals-Matalon, K. (1999). Biochemistry and molecular biology of Canavan disease. Neurochem Res *24*, 507-513.

Matalon, R., Michals, K., Sebesta, D., Deanching, M., Gashkoff, P., and Casanova, J. (1988). Aspartoacylase deficiency and N-acetylaspartic aciduria in patients with Canavan disease. Am J Med Genet *29*, 463-471.

Matalon, R., Rady, P.L., Platt, K.A., Skinner, H.B., Quast, M.J., Campbell, G.A., Matalon, K., Ceci, J.D., Tyring, S.K., Nehls, M.*, et al.* (2000). Knock-out mouse for Canavan disease: a model for gene transfer to the central nervous system. J Gene Med *2*, 165-175.

Matalon, R.M., and Michals-Matalon, K. (2000). Spongy degeneration of the brain, Canavan disease: biochemical and molecular findings. Front Biosci *5*, D307-311.

Mayor, H.D., Jamison, R.M., Jordan, L.E., and Melnick, J.L. (1965). Structure and Composition of a Small Particle Prepared from a Simian Adenovirus. J Bacteriol *90*, 235-242.

McCarty, D.M. (2008). Self-complementary AAV vectors; advances and applications. Mol Ther *16*, 1648-1656.

McCarty, D.M., Fu, H., Monahan, P.E., Toulson, C.E., Naik, P., and Samulski, R.J. (2003). Adeno-associated virus terminal repeat (TR) mutant generates self-complementary vectors to overcome the rate-limiting step to transduction in vivo. Gene Ther *10*, 2112-2118.

McPhee, S.W., Francis, J., Janson, C.G., Serikawa, T., Hyland, K., Ong, E.O., Raghavan, S.S., Freese, A., and Leone, P. (2005). Effects of AAV-2-mediated aspartoacylase gene transfer in the tremor rat model of Canavan disease. Brain Res Mol Brain Res *135*, 112-121.

Mehta, V., and Namboodiri, M.A.A. (1995). N-Acetylaspartate as an acetyl source in the nervous system. Mol Brain Res *31*, 151-157.

Mersmann, N., Tkachev, D., Jelinek, R., Röth, P., Möbius, W., Ruhwedel, T., Rühle, S., Weber-Fahr, W., Sartorius, A., and Klugmann, M. (2011). Aspartoacylase-lacZ knockin mice: an engineered model of Canavan disease. PLoS One *6*, e2033.

Mingozzi, F., and High, K.A. (2007). Immune responses to AAV in clinical trials. Curr Gene Ther *7*, 316-324.

Mingozzi, F., and High, K.A. (2011). Immune responses to AAV in clinical trials. Curr Gene Ther *11*, 321-330.

Mizuguchi, K., Hoshino, H., Hamaguchi, H., and Kubota, M. (2009). [Long term clinical course of Canavan disease--a rare Japanese case]. No To Hattatsu *41*, 353-356.

Mondino M, B.J., Saoud M. (2013). N-acetyl-aspartate level is decreased in the prefrontal cortex in subjects at-risk for schizophrenia. Front Psychiatry.

Muramatsu, S., Fujimoto, K., Kato, S., Mizukami, H., Asari, S., Ikeguchi, K., Kawakami, T., Urabe, M., Kume, A., Sato, T.*, et al.* (2010). A phase I study of aromatic L-amino acid decarboxylase gene therapy for Parkinson's disease. Mol Ther *18*, 1731-1735.

Nakai, H., Fuess, S., Storm, T.A., Muramatsu, S., Nara, Y., and Kay, M.A. (2005). Unrestricted hepatocyte transduction with adeno-associated virus serotype 8 vectors in mice. J Virol *79*, 214-224.

Nakai, H., Thomas, C.E., Storm, T.A., Fuess, S., Powell, S., Wright, J.F., and Kay, M.A. (2002). A limited number of transducible hepatocytes restricts a wide-range linear vector dose response in recombinant adeno-associated virus-mediated liver transduction. J Virol *76*, 11343-11349.

Namboodiri, A.M., Moffett, J.R., Arun, P., Mathew, R., Namboodiri, S., Potti, A., Hershfield, J., Kirmani, B., Jacobowitz, D.M., and Madhavarao, C.N. (2006). Defective myelin lipid synthesis as a pathogenic mechanism of Canavan disease. Adv Exp Med Biol *576*, 145-163; discussion 361-143.

Newsholme, P., Procopio, J., Lima, M.M., Pithon-Curi, T.C., and Curi, R. (2003). Glutamine and glutamate--their central role in cell metabolism and function. Cell biochemistry and function *21*, 1-9.

Novotny EJ Jr, H.J., Rothman Dl (1999). Cerebral amino acids and metabolites in aminoacylase II deficiencies: alterations with dietary therapy. Mol Chem Neuropathol.

O'Donnell T, R.S., Nakashima TT, Hanstock CC, Ulrich M, Silverstone PH. (2000). Chronic lithium and sodium valproate both decrease the concentration of myo-inositol and increase the concentration of inositol monophosphates in rat brain. Brain Res *880*.

O'Mahony, A.M., Godinho, B.M., Cryan, J.F., and O'Driscoll, C.M. (2013). Non-viral nanosystems for gene and small interfering RNA delivery to the central nervous system: formulating the solution. J Pharm Sci *102*, 3469-3484.

O. Bluml, S., Seymour, K.., Philippart, M., Matalon, R., and Ross, B. (1998). Elevated Brain Water in Canavan Disease: Impact of a Diuretic Therapy. . Intl Soc Magn Res.

Obermaier, G., Kretzschmar, H.A., Hafner, A., Heubeck, D., and Dahme, E. (1995). Spongiform central nervous system myelinopathy in African dwarf goats. Journal of comparative pathology *113*, 357-372.

Opie, S.R., Warrington, K.H., Jr., Agbandje-McKenna, M., Zolotukhin, S., and Muzyczka, N. (2003). Identification of amino acid residues in the capsid proteins of adeno-associated virus type 2 that contribute to heparan sulfate proteoglycan binding. J Virol *77*, 6995-7006.

Pacak, C.A., Mah, C.S., Thattaliyath, B.D., Conlon, T.J., Lewis, M.A., Cloutier, D.E., Zolotukhin, I., Tarantal, A.F., and Byrne, B.J. (2006). Recombinant adeno-associated virus serotype 9 leads to preferential cardiac transduction in vivo. Circulation research *99*, e3-9.

Pardridge, W.M. (2002). Drug and gene targeting to the brain with molecular Trojan horses. Nature reviews Drug discovery *1*, 131-139.

Passini, M.A., and Wolfe, J.H. (2001). Widespread gene delivery and structure-specific patterns of expression in the brain after intraventricular injections of neonatal mice with an adeno-associated virus vector. J Virol *75*, 12382-12392.

Patel, M. (2004). Mitochondrial dysfunction and oxidative stress: cause and consequence of epileptic seizures. Free Radic Biol Med *37*, 1951-1962.

Pederzolli CD, M.C., Scapin F, Rockenbach FJ, Sgaravatti AM, Sgarbi MB, Wyse AT, Wannmacher CM, Wajner M, Dutra-Filho CS (2007). N-acetylaspartic acid promotes oxidative stress in cerebral cortex of rats. Int J Dev Neurosci *25*, 317-324.

Pederzolli, C.D., Rockenbach, F.J., Zanin, F.R., Henn, N.T., Romagna, E.C., Sgaravatti, A.M., Wyse, A.T., Wannmacher, C.M., Wajner, M., de Mattos Dutra, A.*, et al.* (2009).

Intracerebroventricular administration of N-acetylaspartic acid impairs antioxidant defenses and promotes protein oxidation in cerebral cortex of rats. Metabolic brain disease *24*, 283-298.

Pioro, E.P., Wang, Y., Moore, J.K., Ng, T.C., Trapp, B.D., Klinkosz, B., and Mitsumoto, H. (1998). Neuronal pathology in the wobbler mouse brain revealed by in vivo proton magnetic resonance spectroscopy and immunocytochemistry. . Neuroreport *14*, 3041-3046.

Pruchnic, R., Cao, B., Peterson, Z.Q., Xiao, X., Li, J., Samulski, R.J., Epperly, M., and Huard, J. (2000). The use of adeno-associated virus to circumvent the maturation-dependent viral transduction of muscle fibers. Hum Gene Ther *11*, 521-536.

Rabinowitz, J.E., Rolling, F., Li, C., Conrath, H., Xiao, W., Xiao, X., and Samulski, R.J. (2002). Cross-packaging of a single adeno-associated virus (AAV) type 2 vector genome into multiple AAV serotypes enables transduction with broad specificity. J Virol *76*, 791-801.

Rahim, A.A., Wong, A.M., Hoefer, K., Buckley, S.M., Mattar, C.N., Cheng, S.H., Chan, J.K., Cooper, J.D., and Waddington, S.N. (2011). Intravenous administration of AAV2/9 to the fetal and neonatal mouse leads to differential targeting of CNS cell types and extensive transduction of the nervous system. FASEB J *25*, 3505-3518.

Ruitenberg, M.J., Eggers, R., Boer, G.J., and Verhaagen, J. (2002). Adeno- associated viral vectors as agents for gene delivery: Application in disorders and trauma of the central nervous system. Methods *28*, 182–194.

Sager TN, F.-J.A., Hansen AJ. (1997). Transient elevation of interstitial N-acetylaspartate in reversible global brain ischemia. J Neurochem *68*, 675-682.

Saher, G., Brügger, B., Lappe-Siefke, C., Möbius, W., Tozawa, R., Wehr, M.C., Wieland, F., Ishibashi, S., and Nave, K.A. (2005). High cholesterol level is essential for myelin membrane growth. Nat Neurosc *8*, 468-475.

Samuel S, K.R., Jayavelu T, Chinnakkannu P (2005). Protein oxidative damage in arsenic induced rat brain: influence of DL-a-lipoic acid. Toxicol Lett *155*, 27-34.

Samulski RJ, S.M., Muzyczka N, Friedmann T, ed. (1999). Adeno Associated Viral Vectors: The Development of Human Gene Therapy (NY, Cold Spring Harbor Press).

Segel R, A.Y., Zevin S, Steinberg A, Gahl WA, Fisher D, Staretz-Chacham O, Zimran A, Altarescu G. (2011). A safety trial of high dose glyceryl triacetate for Canavan disease. Mol Genet Metab *103*, 203-206.

Seki, T., Matsubayashi, H., Amano, T., Kitada, K., Serikawa, T., Sakai, N., and Sasa, M. (2002). Adenoviral gene transfer of aspartoacylase into the tremor rat, a genetic model of epilepsy, as a trial of gene therapy for inherited epileptic disorder. Neurosci Lett *328*, 249-252.

Seyfried, T.N., Glaser, G.H., and Yu, R.K. (1978). Cerebral, cerebellar, and brain stem gangliosides in mice susceptible to audiogenic seizures. J Neurochem *31*, 21-27.

Siegel, R.M., and Callaway, E.M. (2004). Francis Crick's legacy for neuroscience: between the alpha and the Omega. PLoS Biol *2*, e419.

Sipo, I., Fechner, H., Pinkert, S., Suckau, L., Wang, X., Weger, S., and Poller, W. (2007). Differential internalization and nuclear uncoating of self-complementary adeno-associated virus pseudotype vectors as determinants of cardiac cell transduction. Gene Ther *14*, 1319-1329.

Snyder, R.O., Miao, C.H., Patijn, G.A., Spratt, S.K., Danos, O., Nagy, D., Gown, A.M., Winther, B., Meuse, L., Cohen, L.K.*, et al.* (1997). Persistent and therapeutic concentrations of human factor IX in mice after hepatic gene transfer of recombinant AAV vectors. Nat Genet *16*, 270-276.

Solsona MD, F.L., Boquet EM, Andrés JL. (2012). Lithium citrate as treatment of Canavan disease. Clin Neuropharmacol *35*, 150-151.

Spange S, W.T., Heinzel T, Krämer OH (2009). Acetylation of non-histone proteins modulates cellular signalling at multiple levels. Int J Biochem Cell Biol *41*, 185-198.

Steen RG, O.R. (2005). Abnormally high levels of brain N-acetylaspartate in children with sickle cell disease. AJNR Am J Neuroradiol *26*, 463-468.

Stenson PD, B.E., Mort M, Phillips AD, Shiel JA, Thomas NS, Abeysinghe S, Krawczak M, Cooper DN (2003). Human Gene Mutation Database (HGMD): 2003 update. Human Mutation *21*, 577–581.

Stoica, L., Ahmed, S.S., Gao, G., and Sena-Esteves, M. (2013). Gene transfer to the CNS using recombinant adeno-associated virus. Curr Protoc Microbiol *Chapter 14*, Unit14D 15.

Sun, X., Lu, Y., Bish, L.T., Calcedo, R., Wilson, J.M., and Gao, G. (2010). Molecular analysis of vector genome structures after liver transduction by conventional and self-complementary adeno-associated viral serotype vectors in murine and nonhuman primate models. Hum Gene Ther *21*, 750-761.

Surendran, S. (2009). Upregulation of N-acetylaspartic acid alters inflammation, transcription and contractile associated protein levels in the stomach and smooth muscle contractility. Mol Biol Rep *36*, 201-206.

Surendran, S., and Kondapaka, S.B. (2005). Altered expression of neuronal nitric oxide synthase in the duodenum longitudinal muscle-myenteric plexus of obesity induced diabetes mouse: implications on enteric neurodegeneration. Biochemical and biophysical research communications *338*, 919-922.

Surendran, S., Matalon, K.M., Szucs, S., Tyring, S.K., and Matalon, R. (2003). Metabolic changes in the knockout mouse for Canavan's disease: implications for patients with Canavan's disease. Journal of child neurology *18*, 611-615.

Surendran, S., Matalon, R., and Tyring, S.K. (2006). Upregulation of aspartoacylase activity in the duodenum of obesity induced diabetes mouse: implications on diabetic neuropathy. Biochemical and biophysical research communications *345*, 973-975.

Suzuki, K., Kastuno, M., Banno, H., and Sobue, G. (2009). Pathogenesis-targeting therapeutics for spinal and bulbar muscular atrophy (SBMA). Neuropathology *29*, 509-516.

Svennerholm, L. (1957). Quantitative estimation of gangliosides in senile human brains. Acta Soc Med Ups *62*, 1-16.

Tallan, H.H., Moore, S., and Stein, W.H. (1956). N-Acetyl-L-aspartic acid in brain. J Biol Chem *219*, 257-264.

Taylor DL, D.S., Obrenovitch TP, Doheny MH, Patsalos PN, Clark JB, Symon L. (1995). Investigation into the role of N-acetylaspartate in cerebral osmoregulation. J Neurochem *65*, 275-281.

Thomas, C.E., Storm, T.A., Huang, Z., and Kay, M.A. (2004). Rapid uncoating of vector genomes is the key to efficient liver transduction with pseudotyped adeno-associated virus vectors. J Virol *78*, 3110-3122.

Traeger, E.C., and Rapin, I. (1998). The clinical course of Canavan disease. Pediatr Neurol *18*, 207-212.

Traka, M., Wollmann, R.L., Cerda, S.R., Dugas, J., Barres, B.A., and Popko, B. (2008). Nur7 is a nonsense mutation in the mouse aspartoacylase gene that causes spongy degeneration of the CNS. J Neurosci *28*, 11537-11549.

Tsacopoulos M, M.P. (1996). Metabolic coupling between glia and neurons. J Neurosci *16*, 877-885.

Tsai, G., and Coyle., J. (1995). N-acetylaspartate in neuropsychiatric disorders. Prog Neurobiol *46*, 531-540.

Tsai G, G.D., Chang RW, Flood J, Baer L, Coyle JT (1998). Markers of glutamatergic neurotransmission and oxidative stress associated with tardive dyskinesia. Am J Psychiatry *155*, 1207-1213.

Unalp, A., Altiok, E., Uran, N., Ozturk, A., and Yuksel, S. (2008). Novel mutation of aspartoacylase gene in a Turkish patient with Canavan disease. J Trop Pediatr *54*, 208-210.

Urbaniak Hunter, K., Yarbrough, C., and Ciacci, J. (2010). Gene- and cell-based approaches for neurodegenerative disease. Adv Exp Med Biol *671*, 117-130.

Van Bogaert L, B.I. (1949). Sur une idiotie familiale avec dégénérescence spongieuse de nevraxe. Acta Neurol Belg.

Vandenberghe, L.H., Wilson, J.M., and Gao, G. (2009). Tailoring the AAV vector capsid for gene therapy. Gene Ther *16*, 311-319.

Waksman, B. (1999). Demyelinating disease: evolution of a paradigm. Neurochem Res *24*, 491-495.

Wang, J., Leone, P., Wu, G., Francis, J.S., Li, H., Jain, M.R., Serikawa, T., and Ledeen, R.W. (2009). Myelin lipid abnormalities in the aspartoacylase-deficient tremor rat. Neurochem Res *34*, 138-148.

Wang, X.S., Qing, K., Ponnazhagan, S., and Srivastava, A. (1997). Adeno-associated virus type 2 DNA replication in vivo: mutation analyses of the D sequence in viral inverted terminal repeats. J Virol *71*, 3077-3082.

Wang, Z., Zhu, T., Qiao, C., Zhou, L., Wang, B., Zhang, J., Chen, C., Li, J., and X., X. (2005). Adeno-associated virus serotype 8 efficiently delivers genes to muscle and heart. Nat Biotechnol *23*, 321-328.

Wolburg, H., and Paulus, W. (2010). Choroid plexus: biology and pathology. Acta neuropathologica *119*, 75-88.

Xie, J., Ameres, S.L., Friedline, R., Hung, J.H., Zhang, Y., Xie, Q., Zhong, L., Su, Q., He, R., Li, M.*, et al.* (2012). Long-term, efficient inhibition of microRNA function in mice using rAAV vectors. Nat Methods *9*, 403-409.

Xie, J., Xie, Q., Zhang, H., Ameres, S.L., Hung, J.H., Su, Q., He, R., Mu, X., Seher Ahmed, S., Park, S.*, et al.* (2010). MicroRNA-regulated, Systemically Delivered rAAV9: A Step Closer to CNS-restricted Transgene Expression. Mol Ther.

Yang, B., Li, S., Wang, H., Guo, Y., Gessler, D.J., Cao, C., Su, Q., Kramer, J., Zhong, L., Ahmed, S.S.*, et al.* (2014). Global CNS transduction of adult mice by intravenously delivered rAAVrh.8 and rAAVrh.10 and nonhuman primates by rAAVrh.10. Mol Ther *22*, 1299-1309.

Yudkoff, M., Nissim, I., Hummeler, K., Medow, M., and Pleasure, D. (1986). Utilization of [15N]glutamate by cultured astrocytes. The Biochemical journal *234*, 185-192.

Zabner, J., Seiler, M., Walters, R., Kotin, R.M., Fulgeras, W., Davidson, B.L., and Chiorini, J.A. (2000). Adeno-associated virus type 5 (AAV5) but not AAV2 binds to the apical surfaces of airway epithelia and facilitates gene transfer. J Virol *74*, 3852-3858.

Zachary, J.F., and O'Brien, D.P. (1985). Spongy degeneration of the central nervous system in two canine littermates. Veterinary pathology *22*, 561-571.

Zano, S., Malik, R., Szucs, S., Matalon, R., and Viola, R.E. (2010). Modification of aspartoacylase for potential use in enzyme replacement therapy for the treatment of Canavan disease. Mol Genet Metab.

Zeng, B.J., Pastores, G.M., Leone, P., Raghavan, S., Wang, Z.H., Ribeiro, L.A., Torres, P., Ong, E., and Kolodny, E.H. (2006a). Mutation analysis of the aspartoacylase gene in non-Jewish patients with Canavan disease. Adv Exp Med Biol *576*, 165-173; discussion 361-163.

Zeng, B.J., Wang, Z.H., Torres, P.A., Pastores, G.M., Leone, P., Raghavan, S.S., and Kolodny, E.H. (2006b). Rapid detection of three large novel deletions of the

aspartoacylase gene in non-Jewish patients with Canavan disease. Mol Genet Metab *89*, 156-163.

Zhang, H., Liu, X., and Gu, X. (2010). Two novel missense mutations in the aspartoacylase gene in a Chinese patient with congenital Canavan disease. Brain Dev *32*, 879-882.

Zhang, H., Yang, B., Mu, X., Ahmed, S.S., Su, Q., He, R., Wang, H., Mueller, C., Sena-Esteves, M., Brown, R.*, et al.* (2011). Several rAAV vectors efficiently cross the blood-brain barrier and transduce neurons and astrocytes in the neonatal mouse central nervous system. Mol Ther *8*, 1440-1448.

Zincarelli, C., Soltys, S., Rengo, G., and Rabinowitz, J.E. (2008). Analysis of AAV serotypes 1-9 mediated gene expression and tropism in mice after systemic injection. Mol Ther *16*, 1073-1080.

Zlokovic, B. (2008). The blood-brain barrier in health and chronic neurodegenerative disorders. Neuron *57*, 178-201.